Self-assembled monolayers to create novel surfaces utilising peptides identified by phage display for in vitro study of cancer stem cells

Clare O'Malley

School of Engineering and Materials Science

Completed under the supervision of

Dr. Helena S. Azevedo & Professor Ian C. Mackenzie

Submitted in partial fulfilment of the requirements of the Degree of Doctor of Philosophy

September 2018

Statement of originality

I, Clare O'Malley, confirm that the research included within this thesis is my own work or that where it has been carried out in collaboration with, or supported by others, that this is duly acknowledged below and my contribution indicated. Previously published material is also acknowledged below.

I attest that I have exercised reasonable care to ensure that the work is original, and does not to the best of my knowledge break any UK law, infringe any third party's copyright or other Intellectual Property Right, or contain any confidential material.

I accept that the College has the right to use plagiarism detection software to check the electronic version of the thesis.

I confirm that this thesis has not been previously submitted for the award of a degree by this or any other university.

Signature:

Date: 21st September 2018

Details of collaboration and publications:

[QCM-D data was collected in collaboration with Dr João Borges at the University of Aveiro]

ACKNOWLEDGMENTS

During the course of this PhD project there have been many hurdles and unexpected turns which have tested my resolve and would have been insurmountable without the support and guidance from my family, friends, and colleagues.

Firstly I would like to express my appreciation for the guidance received from Dr Helena Azevedo, whose input throughout the process kept the project moving forward. Her feedback and encouragement during the final stages of writing the thesis was invaluable.

I am grateful to Professor Ian Mackenzie for his supervision, advice on all things cancer stem cell-related, and desire to support my work in any way he could.

I would like to thank the past and present members of the MHAtriCell Group for their advice, technical support, and for creating the working environment that has enabled me to complete my PhD. I would particularly like to thank Dominic Collis and Elham Radvar for their friendship as we tackled the task of conducting our research. I wish you the best of luck in your chosen future careers.

I would also like to thank the Mackenzie lab for their questions and comments at group meetings which aided my progression. I especially thank Dr Adrian Biddle for his assistance with flow cytometry and cancer cell culture.

I want to acknowledge the help and expert advice I received with cell imaging and experimental design from Dr Luke Gammon. As well as Dr Gary Warnes, Flow cytometry core facility manager, for performing the FACS which was pivotal to this project.

I would like to thank Dr João Borges, from the University of Aveiro, for his contribution to chapter III, performing further QCM-D experiments and modelling of the results.

I also express my gratitude to Dr Ahuva Nissim and Professor David Wareham, who both passed on precious technical knowledge and advice regarding phage display, in addition to allowing me to work within their laboratories.

To all my friends who have humoured my inability to go an entire evening without talking about the experiments I was working on and have been there in the final stages to provide perspective, and remind me of what I have achieved.

I thank The Queen Mary Institute of Bioengineering and the Engineering and Physical Sciences Research Council for financial support through my PhD studentship (Award number 1502316).

I want to thank my family for their interest and belief. With a special thanks to my sister, for consistently helping me to figure out the best solution.

Finally, I want to express just how grateful I am to my parents for their unconditional support, without which I wouldn't be where I am today, about to embark on the next stage of my career having completed, one of the greatest achievements of my life.

SELF-ASSEMBLED MONOLAYERS TO CREATE NOVEL SURFACES UTILISING PEPTIDES IDENTIFIED BY PHAGE DISPLAY FOR IN VITRO STUDY OF CANCER STEM CELLS

Abstract

Systematic analyses of global cancer rates suggest the annual number of head and neck cancer (HNC) cases is approaching 1 million and in England 5-year survival rates are remain around 50%. This is due to metastasis and recurrence which are thought to be driven by a subset of cells within the tumour with stem cell-like properties, so-called cancer stem cells (CSCs). Within HNC further sub-populations of CSCs with a mesenchymal phenotype have been identified. To better understand the role of these epithelial-to-mesenchymal transition (EMT) cells in cancer progression *in vitro* models are used. One rapid way of creating a system with a controlled surface environment for studying cell behaviour is to use self-assembled monolayers (SAMs). Here we use a peptide-based SAM to immobilise hyaluronic acid (HA), which plays a role in HNC progression, to create and characterise a model surface for studying the interaction with cells *in vitro*. This surface can support the culture of cancer cells and, when compared to existing methods of HA immobilisation, has different properties, including roughness and hydrophobicity and was seen to influence cell migration. *In vitro* use of HA-inspired glycopolymers was also assessed for their ability to mimic HA's effects on cancer cell behaviour, with a view to reducing the use of animal-derived HA. In parallel studies phage display was used to identify a peptide which showed enhanced binding to the EMT subset of CSCs. This peptide can then be used in the previously established SAM system to create a surface with the potential to probe cancer cell behaviour in a well-defined surface. Looking ahead this surface could be used for crude enrichment of the EMT fraction and determining the peptide's cell surface binding partner could provide an additional marker for FACS-based isolation of this population.

TABLE OF CONTENTS

LIST OF ABBREVIATIONS

A	
ABC	ATP-binding cassette
Ac-Pep-1	Acetylated Pep-1
ALDH	Aldehyde dehydrogenase
AM	Acetoxymethyl
AML	Acute myeloid leukaemia
APC	Allophycocyanin
APN	Aminopeptidase N
B	
BSA	Bovine serum albumin
C	
CAP	Chondrocyte-affinity peptide
CD(XX)	Cluster of differentiation (XX)
CD44s	Standard isoform of CD44
CD44v	Variant isoform of CD44
CPP	Cell-penetrating peptides
CRIP1	Cysteine-rich intestinal protein 1
CS	Chondroitin sulfate
CSC	Cancer stem cell
CTC	Circulating tumour cell
D	
DAPI	4',6-diamidino-2-phenylindole
DCM	Dichloromethane
DMF	Dimethylformamide
E	
E. coli	Escherichia coli
ECM	Extracellular matrix
EDC	1-Ethyl-3-(3-dimethylaminopropyl)carbodiimide
EDCI	N-(3-Dimethylaminopropyl)-N'-ethylcarbodiimide hydrochloride

EDTA	Ethylenediaminetetraacetic acid
EGFR	Epidermal growth factor receptor
ELISA	Enzyme-linked immunosorbent assay
Em	Emission
EMT	Epithelial to mesenchymal transition
EpCAM	Epithelial cell adhesion molecule
ESA	Epithelial specific antigen
ESC	Embryonic stem cell
ESI-MS	Electrospray ionisation – mass spectrometry
EthD-1	Ethidium homodimer-1
Ex	Excitation
F	
F’	F-factor
FACS	Fluorescence activated cell sorting
FCS	Foetal calf serum
FDA	Food and drug administration
FITC	Fluorescein isothiocyanates
Fmoc	9-fluorenylmethoxycarbonyl
Fn	Fibronectin
FSC	Forward scattered light
FT-IR	Fourier-transformed infrared spectroscopy
G	
GAG	Glycosaminoglycan
GBM	Glioblastoma multiforme
GFP	Green fluorescent protein
GlcA	D-glucuronic acid
GlcNAc	N-Acetyl-D-glucosamine
GLP-1RA	Glucagon-like peptide-1 receptor agonists
GO	Gemtuzumab ozogamicin
GPC	Gel permeation chromatography

H

HA-	Hyaluronic acid
HA-	
TxRd	Texas red tagged HA
HER2	Human epidermal growth factor receptor 2
HMW	High molecular weight
HNC	Head and neck cancer
HNSCC	Head and neck squamous cell carcinoma
HOBt	1-hydroxybenzotriazole hydrate DIC - N,N'-diisopropylcarbodiimide
HPLC	High-performance liquid chromatography
HRP	Horseradish peroxidase
HS-	
Pep-1	Thiolated Pep-1

I

IFNα	Interferon-α
IHBP4	Intracellular hyaluronan-binding protein 4
IPTG	Isopropyl-β-D-thiogalactopyranoside

L

LB	Luria Broth
LMW	Low molecular weight
LYVE-1	Lymphatic Vessel Endothelial Hyaluronan Receptor

M

MBHA	4-methylbenzhydrylamine
MES	2-(N-Morpholino)ethanesulfonic acid
MET	Mesenchymal to epithelial transition
MMW	Medium molecular weight
MW	Molecular weight

N

NEB	New England BioLabs
NMR	Nuclear magnetic resonance

O

OD_{600}	Ocular density at 600 nm
P	
PBS	Phosphate buffered saline
PBST	Phosphate buffered saline with tween
PDL	Poly-D-lysine
PDMS	Polydimethylsiloxane
PE	Phycoerythrin
PEG	Polyethylene glycol
Pfu	Plaque-forming units
PLC	Phospholipase C
PLGA	Poly(d,l-lactic acid-co-glycolic acid)
PLL	Poly-L-lysine
PPI	Protein-protein interactions
PSB	Polystyrene surface-binding
Q	
QCM-D	Quartz crystal microbalance with dissipation
R	
RAFT	Reversible Addition Fragmentation Chain-Transfer
S	
SAM	Self-assembled monolayer
SSC	Side-scattered light
T	
TBS	Tris-buffered saline
Tet	Tetracycline
Tet^R	Tetracycline resistance
TFA	Trifluoroacetic acid
TMB	3,3’,5,5’-Tetramethylbenzidine
U	
UDP	Uridine diphosphate
W	
WT	Wild-type

X

Xgal	5-bromo-4-chloro-3-indolyl-β-D-galactopyranoside

Other

μCP -	Micro-contact printing

LIST OF FIGURES

LIST OF TABLES

SECTION 1: INTRODUCTION

Background

The study of cancers in vitro has provided a plethora of insights on the initiation, growth, progression, response to treatment, and recurrence which had led to vast improvements in cancer treatment and overall survival rates. However, there are still significant gaps in our understanding of cancer and how environmental cues are transduced to affect a response, such as altered gene transcription, migration, or proliferation. To effectively probe the response of cells to individual stimuli it is essential to have a well-defined culture environment. The use of self-assembled monolayers (SAMs) for controlling tissue culture conditions has been highly effective. Their benefits are manifold, spontaneous assembly, a rapid and simple fabrication process, and modification of the free end to display a range of functionalities. These factors make SAMs an accessible, highly tuneable tool for in vitro cell culture studies.

Functionalisation of surfaces through incorporation of peptides into SAMs provides a platform for studying the interactions of cell surface proteins and functional protein domains, such as those from extracellular matrix proteins. Through manipulation of the assembly process, surfaces can also be formed which exhibit dual functionality for creating more complex systems. The overall benefit of utilising SAMs in this way is the production of customizable cell culture environments in a controlled and defined manner.

Identification of peptide sequences which are biologically important and that play a key role in progression or modulation of disease can be a challenging and time consuming process. Phage display is a technique which provides a platform for the high-throughput screening of many interactions, for the purpose of this work the focus will be protein-protein interactions. The physical linkage between the modified phage genome and the encoded fusion protein displayed on the viral coat enables isolation of the DNA sequence based on the binding properties of the peptide. The technique has successfully been used to select peptide-binders to recombinant proteins as well as to more complex targets such as cancer cells. An additional desirable feature of phage display is the ability to pan against complex mixtures of biological samples or cells to select for binders without the need to isolate and purify a precise target.

The advent of automated peptide synthesis now means that isolated binding peptides

can now be synthesised, for a comparatively lower cost over a much shorter time frame, a matter of hours for sequences with less than 20 amino acids. Synthesised peptides can then be characterised further in vitro and developed for downstream applications, including cell-targeting, drug delivery, or as in vitro reagents.

Research objectives

The overall aims of this PhD work were:

i. To develop a simple platform for studying in vitro the interactions of phage display-derived peptides with relevant biomacromolecules and cells.

ii. To then apply this platform for the immobilisation of extracellular matrix components) to create model surfaces for investigating the response of head and neck cancer cells.

iii. To investigate in *vitro* the potential of hyaluronic acid-based glycopolymers to influence stem behaviours on head and neck cancer cells.

iv. To establish a whole-cell phage display protocol to identify a novel peptide sequence that is able to specifically bind to head and neck cancer stem cells.

The work within chapter IV sets out the development of a self-assembled monolayer system and demonstration of its ability to immobilise hyaluronic acid. It also begins to investigate the application of the platform in the in vitro cell culture of head and neck cancer stem cells.

Chapter V deals with the development of a phage display protocol to select for peptide sequences that could be modified in the same way as the Pep-1 peptide used in chapter IV to create a self-assembling peptide surface.

The investigation of the effects of hyaluronic acid-inspired glycopolymers on head and neck cancer cells is contained within chapter VI. Here initial studies are performed which lay the ground work for exploring the option of using synthetic glycopolymers in place of natural glycosaminoglycans in the platform outlined in chapter IV.

Chapter I - Introduction

1. Head and neck cancer

Over the past decade, the incidence of head and neck cancer (HNC) has been steadily increasing, from 600,000 cases worldwide in the year 2000 to almost 1 million in 2012.[1] The average 5-year survival rate is still only 58%.[2] Current treatment of HNC involves surgical intervention, radiotherapy, or chemotherapy, or combinations of all three.[3]

1.1. Cancer stem cells

Many solid tumours have been shown to contain a subpopulation of cells with stem cell-like qualities.[4] These so-called cancer stem cells (CSCs) can both self-renew and display a plasticity which enables them to differentiate into each of the cell types found within a tumour, thus generating heterogeneity.[5] For head and neck squamous cell carcinoma (HNSCC) a tumour stem-like cell population was first identified by Prince et al.,[6] who found that Cluster of Differentiation 44 positive ($CD44^+$) cells, isolated from human head and neck tumours, had significantly higher rates of tumour formation when implanted into immunocompromised mice when compared with CD44- cells from the same tumour. When analysed by flow cytometry, the tumours that grew gave rise to cell with a range of CD44 expression, indicating that tumour heterogeneity was restored.

1.1.1. *In vitro* culture of head and neck squamous cell carcinoma (HNSCC) cell lines

Maintenance of adult stem cells relies on asymmetrical division where the stem cell gives rise to an identical stem cell, as well as a transit amplifying cell which will ultimately differentiate. This same hierarchy is also seen within cancer stem cells, and, as with epidermal cells, when HNSCC cell lines are cultured *in vitro* distinct colony morphologies are seen.[7] There are three colony morphologies, paraclone, holoclone, and meroclone. Paraclone colonies are irregular in shape and cells are loosely packed; holoclone colonies are round with tightly packed cells and meroclones have features in-between the two.[8] In HNSCC cell lines, holoclone-derived cells can give rise to all colony types and show higher levels of proliferation and clonogenicity compared to paraclone-derived cells. Looking at stem cell-related markers, holoclone colonies exhibited greater staining for stem cell-related markers whereas paraclone colonies showed positive staining for early markers of differentiation.[7] Thus holoclone formation can be used as an indicator of

stem-ness.

1.1.2. Cancer stem cells and treatment

Several studies have demonstrated that CSCs, like normal adult stem cells, have an increased resistance to conventional cancer treatments when compared to the bulk tumour.[9] Reduced sensitivity of CSCs to current treatments may contribute to the low 5-year survival rate still seen in HNCs. While standard treatments, radiotherapy, chemotherapy and surgery, or a combination of these, can drastically reduce the size of the tumour, any remaining CSCs, are able, through self-renewal and differentiation to repopulate the tumour and re-establish heterogeneity. This also occurs where CSCs have metastasised and initiated secondary tumours at distal sites.[10] In HNSCC specifically, it has been shown that the CSC population exhibits reduced apoptosis in response to chemotherapy drugs, such as cisplatin and etopiside, as well as to radiation treatment when compared to cells which did not express high levels CD44.[11,12] It is also seen that cells which exhibit cisplatin resistance have higher expression levels of stem cell markers Oct4 and Nanog, alongside greater migration capacity and clonogenicity, again suggesting a link between stem properties and chemo-resistance.[13] They may also be more effective at evading anti-tumour immunity, as experiments demonstrate $CD44^+$ cells have greater ability to inhibit T cell proliferation and to induce Treg production when compared to $CD44^-$ cells from the same human HNSCC cell line Gun-1.[14] With these characteristics in mind, the current school of thought implicates CSCs as drivers of tumour growth, reoccurrence, and metastasis.[15]

1.1.3. Targeted therapeutics

Having an important role in disease progression, CSCs have been considered as an interesting option for targeted therapies to help to meet the current need in HNSCC treatment. Traditional treatment of cancer by radiotherapy and chemotherapy has several unwanted and unpleasant side effects, which are due to the broad-brush nature of their mechanisms. Radiotherapy is applied as a highly-focused beam to minimise exposure and damage to healthy cells. Chemotherapy is administered either intravenously or in tablet form and because of the systemic nature of these delivery methods; off-target side effects are seen in healthy fast-dividing tissues. Reducing the number of chemotherapy or radiotherapy treatment cycles needed

through adjuvant therapies, especially those that are targeted, is expected to improve patient quality of life during and after treatment.[4,5] In addition, the rate of recurrence would also be reduced due to a greater elimination of CSCs.

Targeted cancer therapy is a rapidly expanding field and through coupling a chemotherapeutic agent to a cancer-specific targeting molecule, such as an antibody or a peptide, improvements in drug delivery have been seen *in vivo*. For example, in mouse xenograft models of breast cancer, coupling doxorubicin to peptides known to specifically bind tumour vasculature resulted in increased survival and reduced tumour volume, compared with free drug alone.[16] The first antibody-targeted chemotherapeutic approved for clinical use was gemtuzumab ozogamicin (GO), a humanised anti-CD33 antibody. Despite initial concerns over levels of toxicity, subsequent and ongoing clinical trials have demonstrated that in conjunction with other treatments GO can improve relapse rates and event-free survival in patients with acute myeloid leukaemia (AML), and has since be approved Food and Drug Administration (FDA) for use in the United States.[17–20]

To develop targeted therapies, identification of a cell surface marker unique to the cells of interest is required. In the case of HNC, CD44v6 has been used as a target, in a phase 1 clinical trial. Riechelmann *et al.*[21] used a monoclonal antibody, conjugated to a chemotherapeutic, against CD44v6 to direct the drug to the CD44v6 expressing HNSCCs. On binding to CD44v6, receptor internalization is triggered and the drug is metabolised and activated within the cell. The use of a therapy that is only active when inside the target cell allows for a systemic delivery system, where all tissues are exposed to the drug, while only those expressing the target marker are affected. While this trial demonstrated that it was possible to accurately deliver treatment to cells based on their expression of CD44v6, several side effects were seen, particularly within normal epithelia, due to their expression of CD44v6.[22] The complexity of the expression profile of CD44 and its variant isoforms, coupled with the off-target side effects seen in the above trial, leaves room for the identification of an additional specific marker of HNSCC CSCs.

1.2. Epithelial to mesenchymal transition

Epithelial-to-mesenchymal transition (EMT) is a process that has been implicated in cancer migration and metastasis, as well as in therapeutic resistance.[10] During

development, EMT is a vital process in formation of the mesoderm, where epithelial cells undergo a change in gene expression, acquire a mesenchymal phenotype and migrate away from the epithelial layer from which they originated.[23] It is also an important process in wound healing, where the EMT programme can be triggered by inflammation at the site of injury, and enables keratinocytes at the edge of the wound to become motile and advance into the wound and initiate re-epithelialisation through the reverse process of mesenchymal-to-epithelial transition (MET).[24] Characteristically, epithelial cells show cell polarity, cell-cell adhesions and low motility. These characteristics are lost during EMT and cells acquire a mesenchymal phenotype defined by increased motility, invasion and resistance to apoptosis.[25]

These processes are also associated with the progression of cancer, and within HNC, a subset of CSCs has been identified, which appears to have undergone EMT and have a more mesenchymal phenotype. The so-called EMT subpopulation in HNSCC can be isolated using fluorescence activated cell sorting (FACS) by looking at cell surface expression of CD44 and Epithelial Cell Adhesion molecule (EpCAM, also known as epithelial specific antigen, ESA). EMT cells are $CD44^{high}/EpCAM^{low}$ compared to epithelial (Epi) CSCs which show a $CD44^{high}/EpCAM^{high}$ expression profile (Figure 1).[26] EpCAM is a transmembrane protein with a primary role in epithelial cell-cell adhesion, and mRNA levels are elevated in HNSCC and EpCAM expression is used as a marker of cancer cells.[27,28]

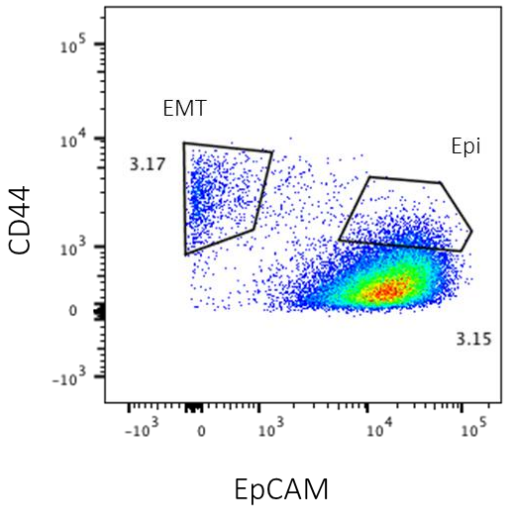

Figure 1: **Flow cytometry scatter plot,** showing the distinct CD44/EpCAM expression profile of EMT and Epi populations within the LuC4 cell line, which are used in the experiments throughout the thesis.

These CD44^{high}/ESA^{low} cells have a morphology and behaviours distinct from CD44^{high}/ESA^{high} cells, they have higher expression of EMT-related genes, such as Twist, Snail and Vimentin, as well as lower expression of epithelial-specific genes, including E Cadherin, Involucrin, and Calgranulin B.[26] Some EMT cells can switch between mesenchymal and epithelial phenotypes, and supports the hypothesis that these CSCs are involved in tumour metastasis, when they undergo EMT, migrate out of the tumour and to reach secondary sites where they return to an epithelial phenotype, via MET, and generate secondary tumours with the same heterogeneity as primary tumour.[29]

Combinations of therapies can be used to increase the effect of a single therapy, for example radiation therapy can be enhanced by co-treatment with cetuximab. However, in HNSCC cell lines, which upregulate EMT-associated genes, this effect is negated.[30] This association of a more migratory and treatment-resistant phenotype, with the upregulation of EMT-related genes and down regulation of epithelial specific genes, has been observed in several tumour types,[31,32] corroborating the hypothesis that cells which have undergone EMT may play a pivotal role in understanding and improving the treatment of cancers.

Identification of additional specific markers of the EMT subpopulation of cancer cells would provide useful tools to improve effective isolation of EMT cells, either alone or in

combination with the existing marker panel. This would allow more extensive *in vivo* studies to further characterise these cells and to elucidate fully their role in cancer progression, resistance to treatment, and recurrence. Such markers and specific cell-binding molecules, would also have a potential to be translated into a clinical setting for *in vivo* detection, as a diagnostic device, or as a targeting molecule for therapy.

1.3. CD44

As mentioned previously, CD44 is used as a marker of CSCs and is a potential therapeutic target. CD44 is a widely expressed transmembrane receptor encoded by a single gene, consisting of 20 exons (Figure 2). Exons 6 to 15 (or v1- v10) can be alternatively spliced to give rise to multiple CD44 isoforms.[33,34] The standard isoform (CD44s) is the smallest and does not contain any of the variable exons. CD44 gene products that contain the alternately spliced exons are referred to as 'variant' isoforms (CD44v). Variant exons are found in the extracellular portion of the CD44 molecule, between the plasma membrane and the amino-terminal domain (Figure 2).

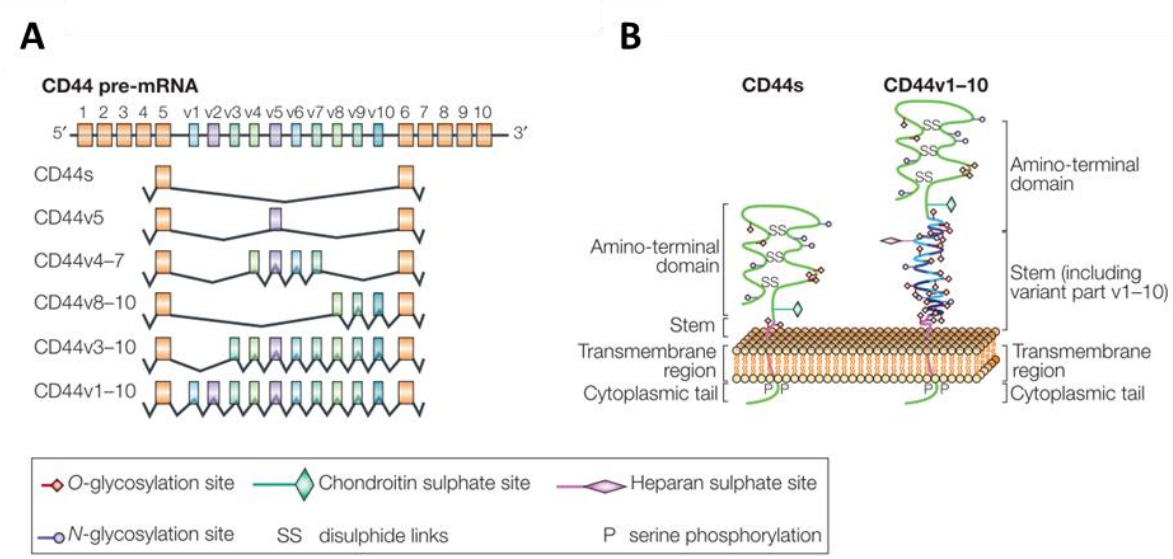

Figure 2: **CD44 exons and structure.** (A) The 20 exons which make up the CD44 protein, those present in all CD44 isoforms are depicted in orange and those subject to alternative splicing in either green, blue, or purple. Below are known variant isoforms. (B) A comparison of the structure of the standard isoform and the largest isoform containing all variant exons. The presence of variant exons extends the stem region, while the hyaluronic acid binding site containing amino-terminal domain remains unaffected (Adapted from Ponta *et al.* 2003). [208]

1.3.1. Variant isoform expression

Distinct patterns of CD44 isoform expression are seen across tissue and cell types,[35] these alternatively spliced exons are susceptible to a range of post translational modifications, which can influence its downstream function through interactions with other receptors of signalling molecules.[36] For example, v3 –containing CD44 receptors contain the Ser-Gly-X-Gly motif, proposed as a glycosaminoglycan (GAG) attachment site, and are modified with heparin sulfate which facilitates specific growth factor binding.[37,38] Furthermore CD44 splice variants, including v10, contain an additional HA-binding motif B-(X_7)-B where B is either R or K and X7 contains no acidic residues and at least one basic amino acid. This has been shown to enhance chondroitin sulfate (CS) dependent cell-cell adhesion.[39]

When CD44-expressing epithelial cells are induced to undergo EMT, a switch in isoform expression can be seen, from CD44v to CD44s. In addition, knock down of CD44 by shRNA prevented cells from going through EMT, which was recovered by the introduction of CD44s but not CD44v isoforms.[40] This demonstrated a requirement for CD44s expression for epithelial cells to transition to a mesenchymal phenotype. CD44s is also seen to protect against cell death which supports the role for EMT cancer cells in tumour recurrence.[40] Additionally, there is experimental evidence that variant isoforms of CD44 have an additional role in tumour progression and metastasis.[41–43]

In HNSCC cell lines, the fraction of CSCs which have undergone EMT show preferential expression of CD44s, compared to the CSCs with an epithelial phenotype which predominantly express CD44v isoforms.[44]

1.3.2. CD44 and role in HNSCC

Current literature looking at the role CD44 plays in HNSCC specifically, demonstrates the relevance of CD44 as a prognostic marker, as well as its active role in several cell-signalling pathways through which it exerts its effects on tumour behaviour.

In terms of CD44 expression status, and its use as an indicator of disease prognosis, a retrospective analysis of CD44 expression in biopsies of early stage cancers, taken prior to treatment, showed that higher levels of both CD44 mRNA and general protein, was

correlated with recurrence following radiotherapy.[45] Initial studies have also suggested that levels of CD44 present in patient saliva can be used as a predictor of HNSCC when used in combination with total saliva protein levels and clinical factors.[46] Taken together, these results indicate that higher levels of CD44 are seen in HNSCC, and yet higher levels seem to be associated with cancer and its progression.

FACS sorted $CD44^{high}$ cells show increased resistance to treatment with cisplatin and docetaxel, with the $CD44^{high}/EpCAM^{low}$ population having an even greater resistance. Induction of the $CD44^{high}/EpCAM^{low}$ phenotype through the upregulation of transcription factor Snail also resulted in reduced sensitivity to cisplatin and docetaxel, as well as increased ATP-binding cassette (ABC) drug transporter expression.[47] Further to this, knockdown of CD44 results in increased cisplatin sensitivity, again corroborating the functional role of CD44 in HNSCC treatment resistance.[42]

Additionally, it has been demonstrated that chemical and siRNA-mediated down regulation of CD44 results in reduced proliferation and expression of stem-cell markers Oct4, Nanog, and Sox2, as well as a loss of clonogenicity, sphere forming ability, and an upregulation of markers of epithelial differentiation.[48,49] These results indicate that CD44 is required for maintenance of stem cell properties. Correlation has also been observed between expression of stem cell-markers and resistance to cisplatin.[50]

1.3.3. CD44 and HA

The majority of CD44s functions within HNSCC, such as proliferation, migration, and gene expression, have been linked with its interaction with hyaluronan, a component of the extracellular matrix (ECM) discussed in more detail below.[51] Hyaluronan, also known as hyaluronic acid (HA), binds to CD44 at its amino-terminal domain through interactions with 8 key amino acids.[52] HA binding can induce interaction with or stabilisation of signalling complexes to affect downstream responses.[51]

HA's ability to increase cell migration is consistently reported and this effect is abrogated when CD44-HA interactions are disrupted, either by anti-CD44 antibodies which physically inhibit binding,[53] or by knockdown of CD44 by siRNA.[42] Further investigation of CD44-dependent cell migration in HNSCC highlights a role for CD44 association with epidermal growth factor receptor (EGFR), immunoblots of cell lysates obtained following

treatment with HA show co-immunoprecipitation of CD44 with EGFR. This physical linkage between the two receptors,[53] is mediated by leukemia-associated RhoGEF (LARG).[54] EGFR-mediated signalling is also increased on HA binding to CD44 and use of EGFR inhibitors stops cell migration,[53] and this effect on cell motility has been shown to be mediated by protein kinase C, phospholipase C (PLC) and RhoA signalling.[55–57]

Signalling pathways and interactions of CD44-HA with EGFR have been implicated in drug resistance. Cisplatin resistance of HNSCC cells was abolished by treatment with both EGFR and ERK inhibitors independently,[53] inhibition of PLC was also able to reduce CD44-HA induced cisplatin resistance,[56] as did Rho and PI-3 kinase inhibitors.[57] In addition to these signalling cascades, CD44-HA binding is implicated in cancer therapy resistance through regulation of ABC drug transporters, where HA depletion is seen to correlate with reduced drug transporter expression.[58,59]

A potential way to exploit the CD44-HA interaction would be to use HA as a targeting molecule to deliver payloads. HA has been used to deliver metal nanoparticles to CD44-expressing cells, which when exposed to an alternating magnetic field generated an increase in temperature that induced apoptosis.[60]

From these results, it is clear that CD44-HA interactions have an important role in initiating a range of signalling pathways that are able to increase HNSCC cells motility and therapy resistance, thus supporting tumour progression.

2. Hyaluronic Acid

Hyaluronic acid is a GAG comprised of two alternating sugars, D-glucuronic acid and N-acetyl-D-glucosamine. These sugars contain several hydrophilic carboxyl, hydroxyl and acetamido groups which are responsible for HA's high water solubility.[61] Additionally, axial hydrogen atoms create hydrophobic patch domains along the molecule which play an important role in the way HA chains interact with each other in solution.[62]

2.1. Biological importance

HA is widely expressed throughout the body making up a large component of the ECM in many tissues. Unlike other members of the GAG family, such as chondroitin sulphate or heparin sulphate, HA is non-sulphated and has a unique set of viscoelastic properties. The presence of hydrophilic and hydrophobic regions, allows HA to form a mesh-like network

when in water, where the hydrophobic domains interact with each other. As part of the ECM, this behaviour and mesh formation confers resilience to tissues. When external pressure is applied to the HA network an internal swelling pressure is created through mutual repulsion between carboxyl groups and this allows the HA to spring back into its original shape once the pressure is released.[63] These viscoelastic properties are responsible for HA's function in the vitreous humour,[64] and within synovial fluid and articular cartilage.[65]

Since its isolation from bovine vitreous humour,[66] HA has been widely studied and applied to both translational and basic science perspectives. It has been successfully applied in the clinic, as a treatment for osteoarthritis,[67] in ophthalmic surgeries and in augmentation procedures as dermal fillers.[68] HA levels are also being investigated as potential biomarkers; its serum levels can help to monitor disease progression in cases of liver fibrosis [69] and is also used as a biomarker for cancers of the including bladder,[70] prostate,[71] breast,[72] and head and neck.[73]

There is extensive evidence for the role of HA in many biological processes which are executed through interactions with its main receptors, receptor for hyaluronan-mediated motility (RHAMM, also known as CD168),[74] lymphatic vessel endothelial hyaluronan receptor (LYVE-1),[75] intracellular hyaluronan-binding protein 4 (IHBP4),[76] and CD44 (discussed in the context of HNSCC above). In addition to its contribution to migration and drug resistance, HA is seen to be involved in angiogenesis,[77] inflammation,[78] and would healing.[79]

2.2. Molecular weight

As a result of its polysaccharide nature HA exists within a range of molecular weights (MWs), but HA chains are typically of high molecular weight, usually 1000 kDa and above.[80] However, enzymatic digestion by hyaluronidases results in the production of low MW HA, 20 kDa to 800 Da,[81] which can have remarkably different effects both *in vitro* and *in vivo*. The size of HA chains is broadly divided into 4 categories; high MW (HMW) >1000 kDa, medium MW (MMW) 250-1000 kDa, low MW (LMW) 10-250 kDa, and oligo-HA <10 kDa.[80]

A review of research papers which have investigated the MW of HA present in different

tissues determined that HMW HA tends to be found in healthy tissues and LMW HA is broadly seen in disease.[80] Oligo-HA is angiogenic in endothelial cells (ECs), whereas HMW HA inhibits EC proliferation and migration, and therefore angiogenesis.[79] Broadly speaking, LMW HA is a pro-inflammatory molecule and HMW HA can be immunosuppressive,[78] this effect is particularly evident in rheumatoid arthritis. [82,83] However, in the current literature, there are still conflicting opinions as to the exact role of varying MWs of HA (comprehensively reviewed by Monslow *et al*).[80]

2.3. Immobilisation on surfaces

Due to the pivotal role of HA in many cellular processes, especially cancer progression, numerous strategies have been developed to immobilise HA on surfaces, aiming to study its effects in a 2D *in vitro* environment. These approaches often require the chemical modification of native HA with several different molecules, and can include biotinylation to allow immobilisation by streptavidin,[84,85] conjugation to dopamine for co-immobilisation,[86,87] thiolation to enable tethering to gold,[88] and azidation to allow crosslinking and stabilisation of HA films formed by spin-coating.[89] Functionalisation of surfaces with epoxy, amine, or hydroxyl groups is required to allow covalent attachment of HA.[90–93] For example, 11-mercapto-1-undecanol can be used to form self-assembled monolayers (SAMs) which bind to gold through S-Au interaction resulting in the display of hydroxyl groups. These can be modified further with epoxy groups which can undergo ring opening to covalently bind HA via its hydroxyl groups.[90]

Such modifications can be problematic as chemicals used for crosslinking, such as glutaraldehyde, can be toxic to cells.[94] The degree of crosslinking can also be detrimental to cell survival and influence cell functions.[95] They may also interfere with the native properties of HA. For example, both thiolation and biotinylation have been shown to inhibit HA degradation by hyaluronidases, and influence its conformation once immobilised.[85,96] Altered presentation of macromolecules has been shown to affect cell adhesion and highlights the sensitivity of mammalian cells to their culture environment and the importance of creating well-defined surfaces for *in vitro* studies of cell behaviour.[97,98]

Combining SAMs with phage display is a useful tool for fabrication of functionalised culture surfaces with precise properties and the ability to interact with cells to influence

their behaviour.

3. Phage display

Phage display is a technique involving rounds of affinity selection of large libraries of genetically modified bacteriophage displaying a fusion protein on its surface against a target. Since being developed by Smith in 1985,[99] it has undergone continuous optimisation to become a valuable platform across a range of fields, including consensus sequence identification for drug development,[100] selecting sequences to maintain stem cells in culture for tissue engineering and regenerative medicine,[101] and isolation of antibodies to use as blood-typing reagents.[102] Phage display takes advantage of the relatively straightforward genetic modification of bacteriophage (phage) such that a fusion protein, or peptide, is expressed and displayed on the surface of the mature phage. This leaves the inserted protein free to interact with its environment. Libraries of modified phage can then be screened for binders against a whole range of different target molecules, including proteins,[103] DNA,[104] cell surface receptors,[105] whole cells,[106] and *in vivo* targets.[107] The technique has successfully been used to identify numerous high affinity, target-specific antibodies, antibody fragments and peptides, as well as short binding motifs, such as Lys-Pro-Pro (LPP) and Thr/Ser-Ala-Arg (T/SAR).[100] The way in which libraries are constructed, and an attractive feature of phage display, is the physical linkage between the genotype of the phage and its phenotype, with the encoded molecule displayed on its surface.

3.1. Applications of phage display

Phage display has a diverse range of applications and, depending on the experimental set up, can be used to answer many research questions, including identifying novel ligands for known receptors, determining the sequence of an epitope, or selecting specific cell-targeting molecules. The use of phage display has evolved from being a technique primarily used in biological sciences to one that is now used across materials sciences and beyond. The success of the technique lies in part, with the creativeness of the researchers developing the protocols. Most applications of phage display fall into the category of epitope mapping or identification of novel target-binders and these applications are discussed below. However, for the most part this review will focus on the use of phage display for the discovery of novel binders.

3.1.1. Epitope mapping

Epitope mapping enables the identification of the critical binding regions of proteins and antibodies, as well as the minimal sequence required for their functionality. There are many strategies which use phage display to achieve this, using either gene fragment, cDNA or genomic expression libraries.[108]

Phage libraries with restricted diversity, such as gene-fragment libraries, are useful tools where binding sites or epitopes are to be characterised within a particular protein or antibody. Gene fragment libraries take the cDNA of the target protein and, through random digestion of the sequence using DNase 1, phage libraries consisting of peptides covering the whole amino acid sequence of the protein can be generated. This strategy has been successfully used to map additional epitopes of the bluetongue virus outer capsid protein VP5[109] and to identify novel epitopes in the sp100 nuclear PBC autoantigen.[110]

Entire cDNA or genomic libraries can also be used to construct genomic expression phage libraries and identify epitopes within the genome. These libraries are, by nature, larger than gene-fragment libraries and are a useful tool in identifying the most immunogenic epitopes and for vaccine development. Libraries constructed from the genome of *Staphylococcus epidermidis* have also been utilised to isolate the bacterial protein responsible for fibrinogen-binding and the location of the binding site within the protein.[111] Such libraries can be screened against complex mixtures, such as patent sera, and peptides which bind to clinically relevant components of the sera will be selected for.[112]

Crucially, methods using cDNA allow the identification of functional proteins that are encoded by genomic material and therefore sequences identified exist *in vivo* and are not simply mimics. The use of random peptide libraries for epitope mapping has reported several useful mimotopes, such as those mimicking house dust mite-specific antibodies [113] and an antibody-binding region of HIV-1 protein gp120.[114] Both the linear B-cell epitope of the Classical swine fever virus' E2 protein and a linear epitope of the anthrax toxin lethal factor were also mapped using a commercially available random peptide library and the sequences identified used to determine the role of each residue in epitope function.[115,116] These examples have utilised monoclonal antibodies (mAb) in the panning

steps, but polyclonal antibodies have also been able to identify epitopes within a random peptide libraries.[117,118]

Further to this, random peptide libraries have been successfully used to determine key amino acids within an antibody-binding domain of the glycoprotein D of herpes simplex virus type 1 and, when synthesised, the selected peptide could be used to immunise mice against the herpes simplex virus type 1.[119]

For comparing genomic or gene-fragment libraries with random peptide libraries for epitope mapping, gene-based libraries have the benefit of selecting sequences which are present in vivo while random peptide libraries may only identify similar consensus sequences. Additionally, random peptide libraries are limited when investigating larger epitopes, as libraries of 6 or 7 amino acids might not be long enough to cover the minimal binding sequence. Conversely, larger 12-, or 15-mer fusions may not have all amino acid sequence combinations represented due to limitations on how many phages can be contained within a library.[120]

However, with the emergence of commercially available random peptide libraries and the need to generate a new fragment library for each target, while random libraries can be screened against multiple unrelated targets, random libraries may provide the simplest way for researchers to carry out epitope mapping using phage display.

3.1.2. Protein-protein interactions

Both peptide and antibody phage libraries have demonstrated usefulness in screening for novel target-binders and identifying important protein-protein interactions (PPIs) playing essential roles in signal transduction and many cellular functions and behaviours. There is a wide interest in identifying new peptide sequences and antibodies or antibody fragments which bind to target molecules. Whether it is for targeted drug delivery, to form reagents for molecular biology, for *in vitro* characterisation of cell populations, or to induce the directed differentiation of stem cells for regenerative medicine.

Antibody libraries, constructed from either Ig isotopes, antigen-binding (Fab) fragments, single-chain variable fragments (scFv) or single domain antibodies (sdAb) display large exogenous sequences providing ample surface area for interacting with the target being

panned against. Peptide libraries tend to display a much shorter sequence and successful panning has been done with libraries between 6 and 43 amino acid peptides. Commercial libraries are commonly between 7 and 12 amino acids, which obviously presents a smaller surface to interact with the target. It is known that the number of amino acids required for specific binding varies across different interactions. Typically, antibodies require a grouping of 6 amino acids to recognise and bind antigens.[121] Major histocompatibility complex proteins recognize sequences of 12 -16 residues.[122] In the case of fibronectin, only 3 amino acids, arginine-glycine-aspartic acid (RGD), are required for integrin binding.[123] The ability of binding to be mediated by such a small number of amino acids suggests that phage display libraries constructed from short, 7-12 amino acid fusions, are of sufficient size to identify sequences capable of specific target binding.

Highly specific binders have been found using recombinant or purified target molecules. However, for some targets, recombinant versions are of limited value. For example, membrane bound proteins or transmembrane receptors contain hydrophobic domains which, in vivo, are inserted into the lipid bilayer. When recombinantly expressed, some proteins form aggregates or fold incorrectly, this presents a problem when trying to identify functional ligands where conformation is key for binding. The flexibility of phage display means that this problem can be avoided by panning against cells modified to stably express a known target protein. For example, the successful transfection of CHO cells with a human recombinant VPAC1 was used to select binders from a peptide library.[105] It is also possible to select phage clones against cell targets without a known marker on the cell surface. These 'fishing' experiments have been used to find peptide sequences that can specifically target hepatocarcinoma and breast cancer cells.[124,125] This highlights the potential of phage display in cell identification and targeted therapeutics.

3.1.3. Protein-target interactions

In addition to probing PPIs, phage display has also been applied to investigating the interaction of the displayed fusion proteins with non-protein targets, such as inorganic (metals, minerals), biological (tissues, proteins, and polysaccharides) and synthetic materials (tissue culture surfaces).

Matsubara *et al*. (1999)[126] identified 3 phage clones which could bind to their target ganglioside monosialoganglioside galactose, a glycolipid that is present on the cell surface and a known receptor of cholera toxin. Sequences which can bind camptothecin (CPT), a small molecule inhibitor of topoismerase, have been successfully identified,[127] and protein-DNA interactions have also been probed through the expression of zinc-fingers as a fusion protein on the phage surface. Random mutation of the amino acid sequence followed by panning on the DNA target resulted in the identification of the crucial residues involved in making protein-DNA contacts.[104]

Further to non-protein cellular targets, several groups have used phage display to identify clones which bind to surfaces of materials. Metal surfaces that have been used as targets include silver, platinum, titanium, aluminum, and gold, and sequences identified have been used to initiate nucleation of metal crystals or to guide the growth of nanowires.[128] These studies provide a useful insight into how proteins interact with surfaces and information gained can potentially be used to optimize experimental systems where metal surfaces are used as substrates for the attachment of peptides, proteins, or cells.

Polymers have also been targeted to isolate binding sequences. This is of interest as a significant number of panning experiments are carried out in plastic dishes, wells, or tubes. Knowledge of known plastic-binders enables researches to identify any such selected sequences in their experiments and exclude them from subsequent experiments and analysis. Submission of the identified sequences to databases such as SAROTUP provides a searchable tool to determine which clones may be target-unrelated. Plastic binding sequences can also be used to immobilise molecules on a plastic surface.[129,130]

3.2. Panning strategy

The basic phage display protocol for identification of target-binding clones involves immobilisation of the target, purified protein or cell type, followed by incubation with a diverse phage library. Any unbound phages are removed by washing and bound phages can then be eluted, either non-specifically using a high or low pH, or by using a known ligand for the target. This process, known as biopanning or affinity selection, is followed by amplification of eluted phages using an appropriate bacterial strain and once purified these phages can then be used in further rounds of panning. Typically, biopanning is

carried out 3 or 4 times and is combined with rounds of negative selection to reduce the number of non-specific phages from the pool, such as those binding the plastic of the dish.

There have been several iterations of this basic method each tailored to the type of target. Below the key features and some of the binders identified by the most common panning strategies are described.

3.2.1. Recombinant target immobilisation

When using a specific protein, virus, or toxin, which can be recombinantly expressed, the simplest way of immobilising the target is to allow it to adsorb onto a 96-well plate by incubation of the purified target in an appropriate buffer. This protocol has been used to find peptides that bind to HA.[131] The peptide identified, named Pep-1, has been used for several downstream applications. Through biotinylation of Pep-1 and detection by FITC-labelled streptavidin it has been utilised as a reagent for *in situ* staining of HA in tissue sections of human foreskin.[132] It has also been used to immobilise HA on the surface of contact lenses and improve longevity of lens hydration. [133] Pep-1 can further be used as an *in vitro* reagent to inhibit HA-receptor binding to elucidate a role for HA in T cell proliferation.[134]

Another strategy for panning is to use target molecules with affinity tags to immobilize the target, or to allow the library to be incubated with the target in solution before capture onto a solid matrix. Using a tag reduces any changes in conformation induced by adsorption to a surface and enables all faces, and therefore epitopes, of the target to be accessible to the phages, maximising the probability of identifying a binder.

The strong and specific interaction between biotin and streptavidin can be exploited. Biotinylation of the target molecule enables immobilisation on a streptavidin-coated plate or beads. This method has been successful in isolating peptides which bind Troponin I, a biomarker for heart disease, with nano-molar affinity.[103] However, biotinylation of recombinant proteins is a multi-step process and can denature the protein, meaning it is not suitable for use with all potential targets. Additionally, using this technique, elution of bound phage is achieved using a low pH or bacteria can be added directly to wells containing the phage-target complexes. Both these methods use non-specific elution,

and there are likely to be a larger number of non-specific background phage clones taken into future rounds of panning.[108] To eliminate this problem, Koide et al. (2009)[135] developed a system which allows eversible affinity capture on a streptavidin-coated surface.

Several alternative reagents can be used for affinity capture protocols including maltose-binding protein (MBP) and amylose, glutathione S-transferase (GST) and glutathione, or polyhistidine with chelated nickel beads. Antibody targets can be captured by protein A or protein G beads,[136] and His-tagging of EphB receptors has been used to select peptides which can discriminate between the different classes of receptor and, in some cases, block ephrin binding.[137]

3.2.2. Whole cell panning

Panning on membrane bound proteins and cell-surface receptors can be challenging, because hydrophobic domains within the protein can aggregate when not inserted in the cell membrane, or complex tertiary or quaternary structures may not be formed correctly. In these situations, phages that are isolated as binders by panning experiments may not interact with the native target in the same way. In the case of transmembrane proteins, phages recognising intracellular domains not accessible *in situ* will have limited use for targeted treatments or cell staining without permeabilising the cells.

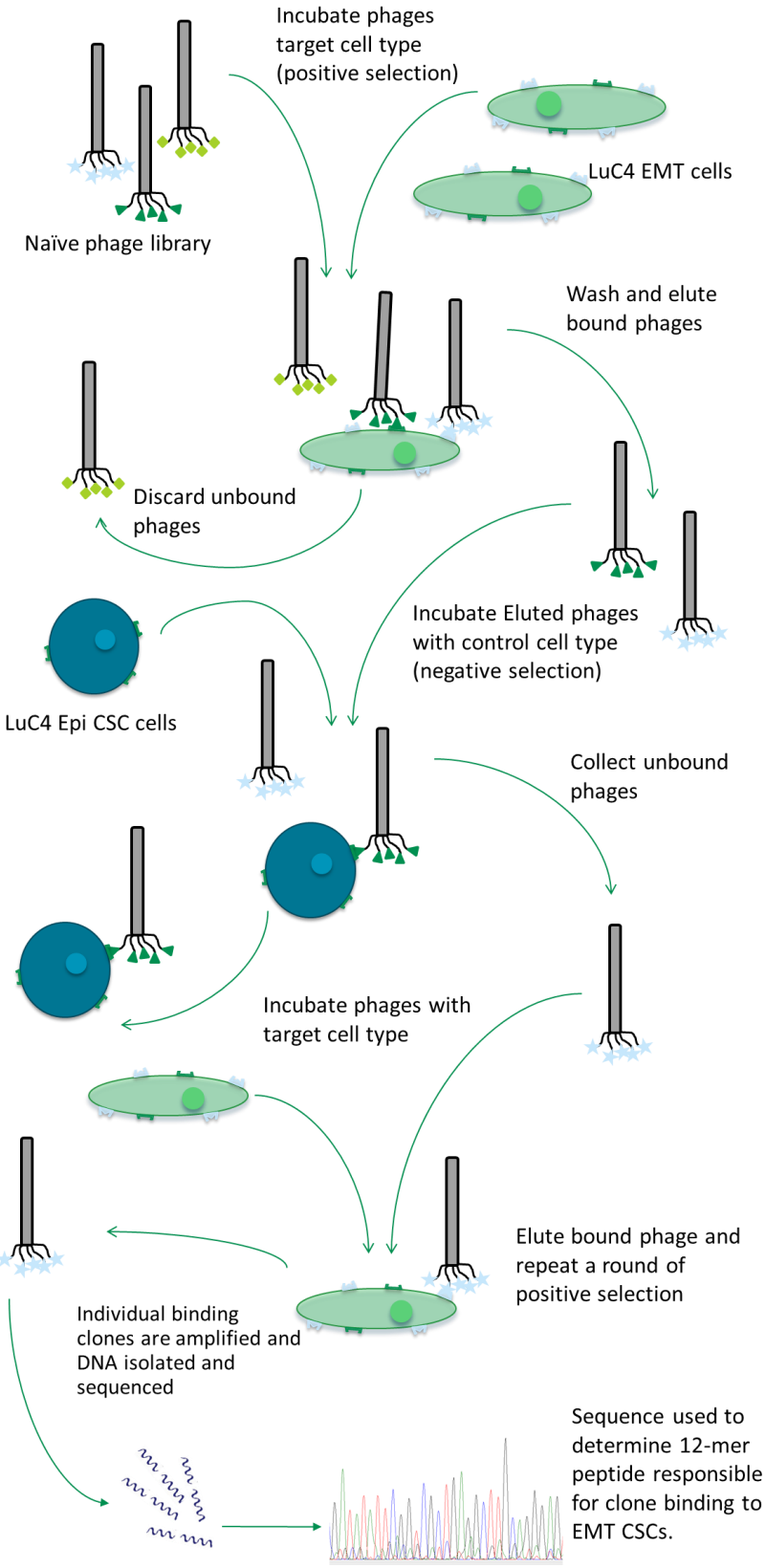

Figure 3: Whole cell panning schematic. A potential workflow of biopanning, including rounds of positive and negative selection, on target and non-target cells respectively, with subsequent sequencing of identified phages.

Panning libraries against whole cells, either in suspension or as a monolayer, can circumvent these limitations. However, the sheer number of potential binding sites, either lipids, proteins or carbohydrates, on the cell surface can lead to large numbers of different phage clones being selected as a result of either specific or non-specific binding. If the chosen target has a known ligand, this can be used for the elution of phages which are bound to an overlapping region on the target, ensuring the majority of recovered phages were target-associated. Where there is no known ligand, or to select a phage with high binding affinity, rounds of negative selection can be used to deplete the phage pool of sequences which do not bind the target.[138] For example, incubating the library with a cell type that does not express the target to sequester phages which bind to ubiquitous cell surface molecules before carrying out positive selection (Figure 3). This strategy had been used to identify antibodies which bind human blood group antigens as well as human autoantibodies against the thyroid.[139,140]

There are still limitations associated with this approach using whole cells for affinity selection. Each round of negative selection removes only a fraction of the non-specific phages and can also remove target-binding phages from the pool, as well as reducing library diversity. Combining positive and negative selection is another approach which can be used. The library is incubated with both target-positive and target-negative cells at the same time, where the negative cells are in an excess to absorb non-target-specific phages. To isolate the target cell-bound phages, the cell types need to be separated. This can be done by fluorescence activated cell sorting (FACS), which requires and existing marker for the target cell population. Alternatively, magnetically activated cell sorting can be used where target cells are labelled with magnetic beads before mixing with negative cells. A magnetic field can then be applied to a column to pull out the labelled cells.[102]

3.2.3. Biopanning and rapid analysis of selective interactive ligands

Biopanning and rapid analysis of selective interactive ligands (BRASIL) was pioneered by Giordano et al., (2001)[141] and uses differential centrifugation and organic phase separation to isolate phages bound to cell targets. Briefly, cells are incubated with a phage library in suspension and this suspension is then transferred onto the surface of an organic phase consisting of a mixture phthalates. Following centrifugation of these two layers, to pellet the cells and any bound phages, the tube is snap-frozen and the tube cut

to recover the cells which are transferred to a fresh tube. Removing the pellet by cutting the tube reduces the risk of unbound phages in the aqueous layer cross-contaminating recovered phages. Amplification and purification of cell-binding phages can then be carried out in an appropriate bacterial strain in the same manner as other biopanning methods. To date, there are 98 original research articles citing the used of the BRASIL method for separation of target-binding phages.

The AWYPLPPA peptide was isolated from random peptide library as a sequence which specifically binds hepatocellular carcinoma (HCC) cell line with a high metastatic potential compared to a cell line which exhibits low levels of migration. In the first round, the library was incubated with cells of low metastatic potential to preclear the library and the unbound phages remaining in the aqueous layer were then used to pan against the HCC cells to isolate cell-binding peptides.[142] Combining this method with traditional cell-bound phage isolation as a more stringent final washing step, Derda et al., (2010)[101] were able to isolate peptides which support the growth of embryonal carcinoma cells and maintain their pluripotent state. Further examples of cell-binding peptide sequences can be found in the comprehensive review of using peptide libraries to select for cell-binding peptides by Gray & Brown.[143]

3.2.4. *In vivo* panning

The principle behind conducting phage display *in vivo* involves injecting the library into a host animal and allowing phages to circulate before washing the cardiovascular system, harvesting the tissue or organ of interest and collecting the clones which have accumulated locally. Using this simple strategy, and allowing the injected peptide library to circulate for 6 minutes across 3 rounds of selection, Yao et al. (2005)[144] were able to identify 2 peptides which targeted the vasculature of the pancreas. Enriched libraries can also aid selection. For example, using a mouse model of islet cell carcinoma Joyce et al. (2003)[145] identified three peptides which home to the tumour vasculature. They conducted initial rounds of panning *ex vivo* on cells isolated form the mouse model, to enrich for target cell-binding clones, before *in vivo* selection was carried out.

Most *in vivo* studies have used animal models where the animal is sacrificed following selection. While this method has generated many useful peptides and antibody fragments, the quality of these molecules will be limited by how good the model is or by

interspecies differences. The first study conducted in humans[146] used a cyclic peptide library injected intravenously which was allowed to circulate for 15 minutes. Biopsies were then taken from multiple sites including the skin, bone marrow, fat and skeletal muscle. Analysis of the recovered phages and their inserts revealed several peptides containing a three amino acid motif within each tissue type. Using online databases, it was seen that some of the sequences identified are found in human proteins, demonstrating the potential for this method to select for biologically relevant sequences. Further to this, a peptide mimic of interleukin-11 (IL-11) isolated from the prostate sample was shown to display the same staining pattern as an antibody against the IL-11 receptor on tissue sections and in vitro experiments showed that peptide binding to the IL-11 receptor was inhibited by addition of the natural ligand, demonstrating the specificity of the interaction.

Panning in living human cancer patients with both peptide and scFv libraries has also been conducted, where following intravenous infusion of libraries and circulation for 30 minutes superficial tumour nodules were removed and phages recovered. Again, sequences collected contained motifs that are present in human proteins, and binding studies suggested that the presence of phages in the tumour was not due to random accumulation. Importantly, this study also demonstrated no allergic response to the infusion of the phage libraries in patients which means *in vivo* phage display in humans may be a viable option for the selection of patient specific tumour-targeting peptides and antibody fragments.[147]

3.3. Limitations

Biopanning provides a platform for high throughput screening of phage libraries for interaction with a target of choice, be it DNA, proteins, or cells. However there some inherent limitations that must be considered when designing a protocol.

3.3.1. Selection bias

One consideration is loss of library diversity through the amplification process. While reduced library diversity is a desired outcome from the rounds of panning, as only target-binding phages are selected to enter the next round, amplification of phages in bacteria imposes another selection pressure on the pool. As a result, phage clones with no specific

interaction with the target, but which have a replicative advantage, such as increased growth rate or infectivity, will be overrepresented in the library following amplification (Reviewed Derda et al., 2011).[148]

To eliminate the binding-independent reduction of diversity, it is possible to select for target-binders without including an amplification step. Combining differential centrifugation with a single round of panning on colorectal cancer cells with a Fab phage library, generated by immunizing mice with three colorectal cancer cell lines, resulted in 51-90% of recovered clones giving a positive result in the enzyme-linked immunosorbent assay (ELISA).[149] A similar method was also used for selecting polyclonal Fab fragments against either Cryptosporidium parvum glycoproteins or a C. parvum oocyst/sporozoite preparation where 50-73% of the recovered phages were specific for the antigen.[150] Combining phage display with next generation sequencing also appears to provide a promising method for reducing panning and amplification rounds while still identifying high affinity clones.[151]

Amplifying each recovered phage clone in isolation would also minimise selection bias, as this would remove the competition between different clones during the amplification process. In practice this can be challenging, however, Derda et al. (2010)[152] used a microfluidic system to generate consistent sized droplets in which individual phage clones could be amplified uniformly, thus removing amplification-induced selection bias.

3.3.2. Clone Specificity

For both antibody and peptide phage display, not all identified phage clones are true binders of their target. Clones which bind non-specifically to the target or the plastic of tubes or wells used to carry out each round of selection will be eluted with specific phages when a low pH elution is used or when panning against cells unbound phages can become trapped with the pellet during washing steps.

There are several ways to assess target-specificity. The use of online databases is a quick way to determine if potential binders contain known plastic-binding motifs or have been previously identified as conferring a replicative advantage to the phage (reviewed Vodnik et al., 2011).[153] It is also possible to see if sequences obtained from panning experiments

have been found as binders for other targets within the literature or if they correspond to portions of human proteins. However, such online data bases are reliant on researchers continually submitting their sequences and updating the catalogue as more work is done.

The use of online databases, outlined in Table 1, to check if identified binders contain target-unrelated binding motifs, or if they have been identified in other studies, requires the sequence of the DNA insert of selected phages to be known. While extracting and sequencing the phage DNA is not particularly difficult, it can be time-consuming and expensive, depending on the number of clones being investigated. A phage-binding ELISA allows the specificity of individual clones or clone pools to be assessed without the sequence needing to be known. If an antibody against the target molecule is available plates can be coated with selected phage clones and incubated with a solution of the target, the appropriate enzyme-linked antibody can then be used to determine binding. If there is no available antibody for the target, or the exact molecule is unknown, a phage capture ELISA can be used. The target is immobilised and then incubated with phage clones. An antibody which recognises the bacteriophage can then be used to indicate binding. It is often beneficial to test the entire phage pool that is recovered from panning to ensure that there is some binding capacity before clones are amplified and tested by ELISA individually.

Where individual clones are used, those that give a positive signal can be analysed further and their binding assessed more quantitatively using, for example, competition assays.

3.4. Library Construction

Phage display libraries can be constructed using many different bacteriophage strains with a range of fusion sites available for the insertion of DNA sequences. The most commonly used phages include M13 and fd filamentous phages, the T4 and T7 lytic phages as well as λ phage.

The exact structure of a bacteriophage differs between types, however, they all possess a coat or capsid protein which can display the fusion product in a way which does not interfere with the normal phage life cycle. It is possible for the fusion proteins to be displayed at different sites depending on where the DNA fragments are ligated, the

location of the fusion can also influence the number of times the fusion is expressed, as well as impose constraints on the peptide or antibody being displayed. In the case of filamentous bacteriophage, they have an elongated shape consisting of different coat proteins, encasing the single stranded DNA (Figure 4). The most common sites for display are as fusions to the amino terminal of pIII or pVIII coat proteins. There are approximately 2700 copies of the pVIII protein on each phage, which means inserting new genetic material at the pVIII gene site can result in a level of high display.[154] However fusions of large sequences at this site are not well tolerated.[59] The pIII site is compatible with larger fusions and can support both multivalent and monovalent display.

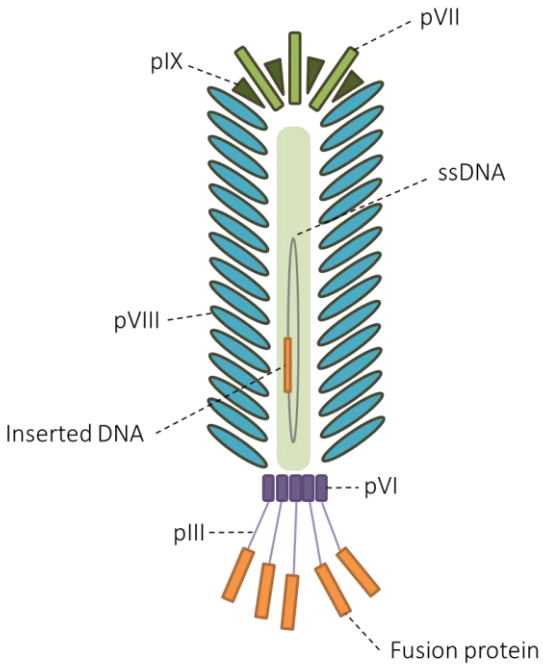

Figure 4: Diagram of M13 bacteriophage structure. Showing the distribution of coat proteins pIII, pVI, pVII, pVIII, and pIX. The fusion protein, encoded by the inserted DNA sequence, is displayed at the N-terminal of the pIII coat protein. In this diagram multivalent display is shown.

Several phage libraries also incorporate antibiotic resistance and screening mechanisms, such as α-complementation of β-galactosidase for blue/white screening, to help prevent and identify cross-contamination or enrichment of wild-type phage.

Random peptide libraries, including 7-mer, 12-mer and cyclic libraries are commercially available from New England Biolabs, making peptide phage display accessible to a wider range of researchers. Bio-Rad also offers commercially available Fab fragment libraries

such as Human Combinatorial Antibody Libraries (HuCAL) which represent over 95% of human antibody diversity. Customised libraries can also be purchased from companies, such as Creative Biolabs or Antibody Design Laboratories, which allows scientists to use more specific antibody or cDNA libraries without having to construct their own.

3.4.1. Phage vs phagemid

When using filamentous phage to construct a library, either a phage or phagemid system can be used. In a phage system, the cDNA comprising the library is incorporated into the bacteriophage genome using restriction enzymes and ligases to ensure the DNA fragment is inserted at the required location. The first use of bacteriophage to display a polypeptide as a fusion protein on its surface was reported by Smith, et al. in 1985,[99] where BamHI was used to generate a fragment of Eco R1 endonuclease for insertion into the genome of a f1 phage.

A phagemid system uses a Ff-phage-derived expression vector, the so called phagemid and this plasmid consists of the DNA sequence of the protein to be displayed, the required sequences for bacterial replication and the origin of replication and packaging signal of the strain of bacteriophage being used. The phagemid alone is unable to complete the full phage lifecycle and requires co-infection with helper phage to do so. The helper phage provides the bacteriophage proteins missing from the phagemid and allows packaging of the fusion protein into complete phage which can then be secreted by the bacterium.

Two key differences between using phagemids or phages are the ability of the phagemid to accommodate larger inserts and the control over the number of times the fusion protein is displayed. Monovalent display of antibody libraries in a M13 phagemid system has assisted the selection of high affinity binders, where a multivalent system may also select for binders with a lower affinity, but which interact with the multiple targets on display.[155] A comparison using the two library types, phage an phagemid, demonstrates the specific benefits of each system; multivalent display by a scFv phage library yields a higher number of different binding clones being identified in each round of panning, while the same library in a phagemid system identified fewer antigen-binding antibodies with higher affinity binding.[156]

3.4.2. Antibody libraries

Antibody libraries can be generated from the cDNA isolated from either naïve or immunised donor antibody producing cells, while large naïve libraries can be used to identify target-binding antibodies.[157] There are benefits to using immune libraries. Immunisation of animals with the target antigen, or using human donors who have already been exposed to the antigen of interest, allows for the enrichment of antibodies which are target related within the library and can lead to the selection of high affinity antibodies, for even complex targets such as human cancer cells.[149] One drawback of immune libraries is the requirement to generate a new library for each new target antigen to be investigated.

An additional consideration is the use of scFv or Fab libraries. Fab fragments demonstrate higher stability and a reduced tendency to form multimers compared to scFv molecules, but broadly have lower expression levels in *E. Coli*. On the other hand, scFv are smaller and may be a more useful tool in downstream applications. Additionally, their library production can be simpler than that of Fab fragments.[108]

Semi-synthetic antibody libraries offer another method of generating a library with high diversity and sequences not found *in vivo*. Using polymerase chain reaction (PCR) techniques, amino acid substitutions or sequence insertions can be made in the complimentary determining region (CDR) of an antibody.[158] Typically, these changes are made in the heavy chain of CDR3 as it contributes substantially to antigen binding and its function is not dependent on conformation.[159]

3.4.3. Sub-libraries

Once target binding clones have been identified and the sequences determined, it is possible to construct a sub-library to enhance its affinity for the target. For example, semi-synthetic antibody libraries can also be generated based on antigen-binding antibody fragments previously identified by phage display.

With random peptide libraries, this can be done by the random mutation of the identified sequence through error prone PCR or site directed mutagenesis. It has been used to gain a more accurate picture of the consensus sequence which recognises the human Mab b12.[160]

Caloxin 1b1, a peptide inhibitor of a Ca+ pump found in the coronary artery was modified by random mutagenesis to generate a new peptide phage display library. Further panning lead to the identification of a more selective secondary peptide with a 20-fold increase in affinity. This new peptide, caloxin 1c2, was also seen to elicit physiological effects *in vitro.*[161] Peptide sub-libraries have also been generated based on biologically important *in vivo* sequences to select peptides with the capacity to bind to multiple receptor targets,[162] demonstrating their use in combination with rational design.

3.5. Properties of ligands (peptides or antibodies) from phage display libraries

3.5.1. Size

Peptide libraries display smaller fusion products compared to antibody display libraries, but both are of sufficient size to identify specific binders. The size of the displayed protein can influence experimental set up and, to an extent, may limit the sequences identified; it also has important implications for use of target-binders in downstream applications.

Smaller molecules can diffuse further and, in the context of drug delivery, peptides could provide improved tissue penetration when compared to antibodies or antibody fragments. The average molecular weight of an amino acid is 110 Da and a peptide identified through phage display using a 12-mer library would have a molecular weight around 1300 Da whereas antibody fragments have molecular weights ranging from 12 to 160 kDa for single antibody domain to a normal antibody, respectively (Figure 5).

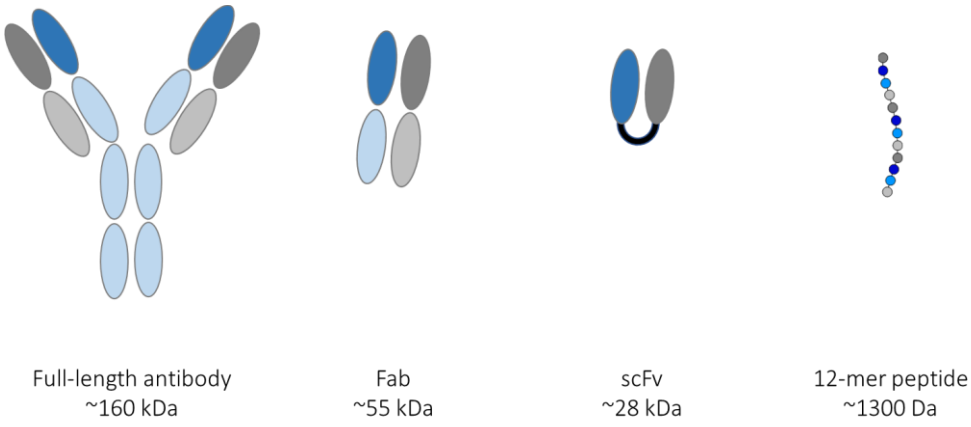

Figure 5: **Relative sizes of ligands generated from phage display libraries.** Ranging from an antibody, typically the largest, to short peptide sequences.

The iRGD peptide identified as tumour homing peptide by panning of *ex vivo* tumours

with one round of *in vivo* selection with a cyclic 7-mer library on the T7 phage, is seen to travel out of the tumour vasculature and into the tumour tissue when injected intravenously and allowed to circulate.[163] The consensus sequence R/K-X-X-R/K has been observed in many phage display-derived peptides and is a requirement at the C-terminal for these peptides to penetrate the targeted tissue.[164]

The use of Fab fragments compared to intact monoclonal antibodies has also been shown to enhance penetration into tumour spheroids and the smaller Fab molecules are able to give a more homogeneous coverage,[165] although other factors such as binding affinity and kinetics may have a greater influence on targeted tissue penetration.

3.5.2. Binding affinity

Antibody-antigen interactions are known to exhibit high affinity and specificity *in vivo*. This is demonstrated through their use as in vitro reagents for cell staining and *in vivo* as therapeutics but there are still limitations. Experimental observations showed that antibody distribution within a tumour is heterogeneous when administered intravenously and this leads to the binding-site barrier hypothesis.[166] Modeling antibody-antigen binding suggests that, along with size, one important factor in the binding-site barrier hypothesis is the affinity with which the antibody binds to the antigen. A higher affinity slows the diffusion into the center of the tumour.[166,167] Utilising Fab fragments, which bind though monovalent interactions, in place of monoclonal antibodies, can reduce binding affinity therefore improving infiltration. Good tissue penetration is particularly important when antibodies, their fragments or peptides, are being used as targeting molecules for drug delivery to ensure that cells throughout the target tissue receive the payload.

Cyclisation of peptides has been seen to alter peptide characteristics, resulting in increased stability, cell penetration and reduced systemic clearance across a range of applications (Reviewed Cardote & Ciulli, 2016).[168] Studies which manipulate the conformation of displayed peptides to form cyclic libraries have shown that higher affinity binders can be selected.[169] Cyclic peptides can be achieved by including pairs of cysteines for the formation of disulfide bridges, or through chemical modification of the library. A comparison of peptide libraries containing sequences with either a single leading cysteine or a pair of flanking cysteines found that the cyclic peptide library identified higher affinity

binders.[170]

3.5.3. *In vivo* properties

When choosing between using an antibody or peptide based phage library, an important consideration is how the purified binder will behave in its intended downstream application. For example, if the antibody, antibody fragment or peptide, is to be conjugated to a drug or an imaging agent and used to target specific tissues *in vivo* then non-specific uptake and half-life will influence success.

Panning strategies which include at least one *in vivo* round can enrich for clones which bind the target while also identifying, and eliminating, those which accumulate in non-target organs. This can be done by recovering phages from organs where high levels of drug would cause off-target toxicity, such as the liver, kidneys or bone marrow, and comparing these sequences to those retrieved from the target organ. Any sequences which feature highly in phages isolated from off-target organs can then be discounted from the target organ phage pool.[171]

A potential drawback of using small peptides, Fab or scFv fragments with molecular weights below ~50 kDa, is that they often exhibit a short half-life *in vivo* due to rapid clearance from the blood by the kidneys. A short half-life can be seen as a limitation as it can mean low levels of accumulation at the target site. However, longer half-lives can also increase unwanted toxicity. For applications in imaging, where probes such as fluorophores, contrast agents, are coupled to the targeting ligand, half-lives which are too long can result in reduced contrast images.[172] In the case of both peptides and antibody fragments, half-life can be modulated through chemical modification. PEGylation of antibody fragments can be used to increase half-life due, in part, to increased molecular weight as the complexes are not filtered out of circulation by the kidney.[173]

When using antibodies and their fragments as diagnostic tools or therapies, there is a risk of immune-related adverse events, where non-human phage libraries have been used, but the resulting binders can be humanized to reduce their immunogenicity. However, doing this, by CDR grafting, framework fine tuning or other methods, can reduce antigen binding affinity.[108] Owing to their smaller size, synthesized peptides identified by phage

display tend to have a lower level of immunogenicity and higher concentrations may be required to elicit an immune response.[122]

3.5.4. Internalisation

For use in targeted drug delivery, or as a therapeutic agent themselves, internalisation of peptides and antibodies can either be required for their function or enhance their effect.[174] Around 10% of FDA approved drugs require metabolism by the body to be converted into the active form.[175] In the context of targeted therapeutics, it is beneficial for any homing molecule to be easily internalised by target cells.

Whole cell panning experiments can be set up to maximise the proportion of phage clones isolated which can undergo cell internalisation. After incubation with the library, phages bound to the surface can be eluted using a non-specific elution buffer, intact cells can then be dissociated, pelleted and lysed to free any internalised clones. Further modification of the phage genome has also been used to identify internalised clones, insertion of a reporter gene, such as green fluorescence protein (GFP), allows cells containing phage can be visualised and separated from those which have not taken up phage.[176]

Using a library designed around the Tat transduction domain, peptides which could cross the cell membrane were identified. Panning was carried out on a human epidermoid carcinoma cell line where cell surface-bound clones were removed by repeated washes and internalised phages were recovered from cell lysates. Synthesis of the isolated peptide sequences and labelling with fluorescein isothiocyanate (FITC) allowed assessment of the amount of cellular uptake when compared to the parent peptide sequence.[177]

3.5.5. Production and modifications

Recent advances in peptide synthesis technologies enable the synthesis of identified target-binding peptides at a relatively low cost and with a short turnaround time. They can be purified by reverse-phase high performance liquid chromatography (HPLC) methods. To generate desired Fab and scFv molecules, expression can be carried out in either bacteria or yeast systems and purified using optimised conditions for the fragment. For example, Fab fragments can be purified using Protein G affinity chromatography or

other protocols using protein G due to the presence of a constant region.[108]

Once antibody fragments or peptides have been made, there are multiple options for chemical modifications to enhance their function in their downstream applications. Both antibodies and peptides can be conjugated to fluorophores for use in imaging or as *in vitro* reagents as well as to drugs, such as chemotherapeutics, while preserving their target-binding homing function [178–180] Doxorubicin coupling to tumour-targeting peptides using carbodiimide chemistry saw improved survival compared with doxorubicin treatment alone in mouse models of breast cancer.[16]

To further increase the suitability of peptides for use as therapeutics, a number of modifications can be made. Improved cellular uptake can be achieved by conjugation to known cell penetrating peptides, [181] while incorporation of D- and non-natural amino acids into peptide sequences has the potential to reduce susceptibility to cleavage by proteases *in vivo* resulting in an increased half-life.[182]

3.6. Successes of phage display

Utilising combinations of panning strategies, modification and conjugations such as cyclisation, fluorescent labelling, biotinylation, or PEGylation highlighted above, phage display has produced several successful approved therapies and reagents with even more in the pipeline.

The first fully humanized antibody approved by the FDA, adalimumab, was identified by phage display with panning against tumour necrosis factor alpha (TNFα), with a binding affinity of 15 nM.[183] Since its initial licensing for the treatment of rheumatoid arthritis, it has also been approved for treating Crohn's disease, psoriasis and several other inflammatory diseases. Its success is highlighted by its position as the bestselling drug of 2016.[184]

There are many phage display-derived antibodies currently in clinical development, as therapies in their own right or as conjugates. An example of an antibody drug conjugate (ADC) currently in phase 1 clinical trials is BAY 1129980, which consists of an auristatin (an inhibitor of cell division) derivative coupled to a monoclonal antibody against the cell surface protein C4.4A, which serves as an indicator of metastatic potential in cancers. The antibody was generated from a recombinant antibody gene library panned against

biotinylated C4.4A which was then captured on magnetic streptavidin-coated beads. *In vivo* studies treating non-small cell lung carcinoma models demonstrate that BAY 1129980 is able to inhibit tumour growth, indicating its potential for use in the clinic.[180]

Screening of a scFv library against interleukin-12 (Il-12) and subsequent targeted mutagenesis of the identified fragment to improve binding resulted in the isolation and development of briakinumab. There have been several clinical trials assessing its use to treat multiple sclerosis, Crohn's disease and psoriasis.[185] However, development has since been discontinued for all three indications. This demonstrates that while phage display is an excellent tool for identifying candidates for therapy they are still at risk of the same stumbling blocks as any other new therapeutic.

In comparison to the use of antibodies, peptide based therapeutics is much younger, but rapidly expanding field, with a number of exciting candidates undergoing clinical trials. Bicycle Therapeutics is a biotechnology company which uses phage display based platforms to identify target-binding peptides and these can then be converted to bicyclic peptides using chemical scaffolds. Using this strategy, several drug candidates have been identified and are at various stages of development, from discovery through to clinical trials. BT1718, a Membrane Type 1 Matrix Metalloproteinase-targeting bicyclic peptide coupled to the MD1 toxin, has entered first time in human phase I/IIa trial following its success in xenograft models which is due to be completed in 2022 (ClinicalTrials.gov, 2018).

Wu et al. (2015)[186] provide an elegant example of how *in vitro* panning on a colorectal cancer cell line using a random peptide library was able to identify several phage clones which specifically home to tumour tissue in xenograft models. They identified the best target-binder and coupled it to polyethylene glycol- 1,2-Distearoyl-sn-glycero-3-phosphoethanolamine (DSPE) to incorporate it into lipid nano-particles encasing anticancer drugs. Inclusion of the peptide resulted in enhanced cellular uptake of the nano-particles accompanied by increased cytotoxicity in target cells *in vitro* and in *in vivo* xenografts treatment reduced tumour size beyond the reduction seen with non-targeted liposomes. While these results present a potential candidate for enhanced treatment of colorectal cancer in humans, Wu and colleagues were also able to identify the binding partner of the pHCT74 peptide on the cell surface as α-enolase, which could be a useful

marker to further characterise cell properties *in vitro*. The pattern of immunohistochemistry staining of tumour and non-target organ sections also demonstrated the potential of these peptides for use as diagnostic reagents.

Peptide phage display has also proven to be a useful tool for identifying ligands for difficult to target intracellular signaling molecules, such as β-catenin, an intracellular protein involved in both cell adhesion and regulation of gene transcription, where dysregulated β-catenin function is associated with several cancers. Due to its multiple roles, finding an inhibitor which only acts to interfere with disease function has been challenging. Through the use of chemically constrained peptide phage display libraries, several potential candidates for inhibitors have been identified, although studies to investigate *in vitro* function are still required.[187]

4. Self-assembled Monolayers (SAMs)

Self-assembled monolayers are an organised arrangement of molecules that are able to form spontaneously on solid surfaces via chemisorption [188] Most commonly SAMs are formed using alkanethiols, where the HS- group has an affinity for metals, such as gold and silver. [189] Typically, Au is the chosen surface for alkanethiol SAM formation for cell based studies and this interaction has been well characterised, with molecule spacing seen to be 0.5 nm and aligned molecules assemble at a 30° angle which give the optimal van der Waals forces between each chain.[188] SAM formation can also be applied to a range of substrates utilising different functional groups, many of which have uses in cell culture or important clinical applications. For example stainless steel (reviewed [190]) titanium,[191] silicon,[192]and glass[193] have all been used as surfaces for SAM formation, and in the case of glass used successfully to create mixed peptides SAMs which induced the expression of chondrogenic markers by human articular chondrocytes when used as a culture surface.

4.1. Functionalisation of SAMs

Another advantage to using alkanethiols for SAM formation is the ability to functionalise the alkyl chain at its opposite end. This allows control over, and optimisation of, the properties of the SAM for use in its intended application. At the most basic level, functionalisation can alter the charge or hydrophobicity of a surface (Figure 6),[194,195]

present a range of chemical groups which can be used to further modify the SAM,[87] or to create more complex systems using molecules such as peptides.

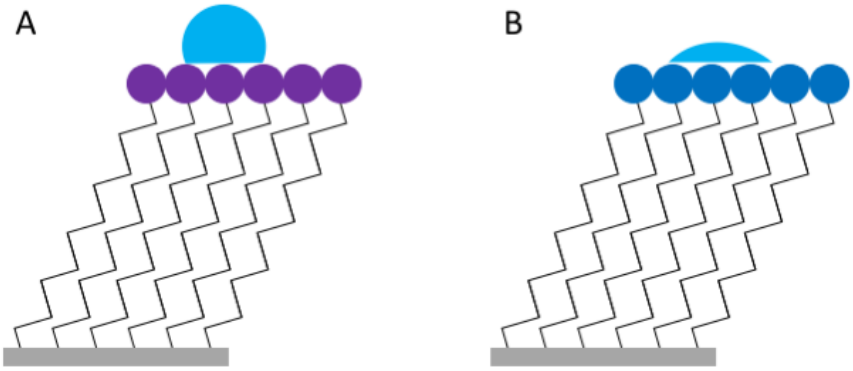

Figure 6: **Self-assembled monolayers with different surface properties as a result of the terminal group.** Hydrophobic surface created by alkanethiols containing groups such as CH_3 (A) and more hydrophilic surfaces formed by alkanethiols with functional groups including OH, COOH, and NH_2(B).

4.1.1. Functionalised surfaces for cell culture

SAMs provide a simple way to fabricate well-defined substrates to control and investigate cell behaviour. These surface modifications can be made in a way which is nontoxic to cells, making them a particularly attractive option as a research tool for *in vitro* cell culture. The effect of changing surface hydrophobicity has been studied by several groups and it is generally accepted that hydrophilic surfaces tend to promote cell binding while a hydrophobic surface will reduce cell adhesion.

As mentioned, the terminal group on a SAM can be altered and the effects of a range of functional groups on cells in culture can then be investigated. The most commonly studied groups, in terms of cell culture, are hydroxyl (-OH), carboxyl acid (-COOH), amino ($-NH_2$), methyl ($-CH_3$) and mercapto (-SH). Increased proliferation and cell migration has been documented with $-NH_2$ and -COOH modifications, while the opposite was seen when -OH and -SH terminal groups were used.[194,196,197]

Functionalisation of alkanethiols with peptides provides a platform to study the effects

of peptide sequences, which may be derived from known binding sites from ligands or by phage display, on cell behaviour. This strategy has been successfully employed to influence cell adhesion, support proliferation, and direct differentiation or even maintain pluripotency of stem cells.[194–196,198,199] Using the cell-binding amino acid motif, arginine - glycine - aspartate (RGD), initially identified in fibronectin (Fn) and subsequently in additional ECM proteins, Roberts *et al.*[200] were able to assess the function of the RGD sequence and demonstrate that it is sufficient to mediate cellular attachment to the SAM substrate.

Due to the ease and speed with which they can be created, SAMs can also be applied to high-throughput screening of peptide-cell interactions to identify surfaces able to elicit the desired effect on cells in culture.[201] Using this approach, in combination with phage display to identify candidate peptides binding embryonic stem cells (ESCs), Derda *et al.*[202] were able to fabricate two peptide-SAMs to which ESCs adhered and which supported their proliferation and maintained pluripotency.

The ability to fabricate well defined and ordered surfaces is increasingly important for the regulated production of *in vitro*-expanded pluripotent, multipotent, or differentiated cells for cell-based therapies. SAMs can provide a rapid and simple method to achieve this and can eliminate the need for animal-derived products, or feeder cells,[203] to support cell proliferation or differentiation.

4.1.2. SAMs for adsorption of biological molecules

Manipulation of surface properties through the application of SAMs can also be used to alter the adsorption of macromolecules. In the case of Fn, an ECM protein involved in integrin binding, conformational changes in the way the protein is displayed can be induced by using SAMs with different functional groups. Alkanethiol SAMs displaying -OH, -COOH and -NH_2 groups caused a significant difference in the binding between Fn adsorbed and an anti-Fn antibody.[97] Subsequent studies revealed that culture on adsorbed Fn caused an upregulation of osteoblast specific genes, matrix mineralisation and increased enzyme activity on -OH and -NH_2, whereas -COOH functionalised SAMs did not, demonstrating that surface chemistry can influence complex cellular functions.[198]

In addition to the chemical modification and covalent immobilisation of HA, thiol reactive surfaces have been reacted with a cysteine-containing HA-binding peptide, termed HABpep, which is then able to bind and immobilise unmodified HA.[133] This strategy has been applied to immobilise HA both on contact lenses and cartilage, while the use of covalent bonds required for the peptide immobilisation exclude this method from being considered self-assembly. It does demonstrate, however, that HA-binding peptides can be used to immobilise native HA. It opens the possibility of functionalising alkanethiols, or other self-assembling molecules, with HA-binding peptides as a means of non-covalently modifying a surface with HA.

4.2. Patterning of self-assembled monolayers

Another useful property of SAMs is the ability to restrict their formation to discreet areas. Selectively covering a surface with a SAM, or multiple SAMs, with differential cell-binding properties, can be used to restrict cell growth on desired areas. Being able to spatially control the binding of proteins and cells is particularly useful in several fields including, biosensors, tissue engineering and in the automatisation of cell screening studies.

There are several methods for creating patterned surfaces with SAMs; once a monolayer is formed micromachining can be used to remove the gold and therefore creating channels or areas where the SAM is no longer present. However, there are limitations to using this technique, mainly that it is a slow process.[204] A method which is now more commonly used for substrate patterning is micro-contact printing (μCP), where a polydimethylsiloxane (PDMS) stamp can be 'inked' with the required alkanethiolates to form the SAM and then these transferred onto the gold surface.[204] In the case of alkanethiolates on a gold surface, this happens within seconds, meaning the complete process is much quicker and the amount of SAM spreading seen is minimal.[205]

More complex patterned substrates can be created by using micro-contact printing to deposit a SAM functionalised with one peptide or chemical terminal group and then immerse the surface in a solution with a different functionalisation. The result is distinct areas of the substrate with different surface chemistries and properties, such as SAMs resistant to protein binding and those which promote it.[206] This can then be applied to a range of cell studies to define areas of cell growth,[205] and can aid the use of automated

microscopes for medium to high-throughput screening. Alternatively, creating channels of cell permissive surfaces can be used to model complex cell structures for potential use in organ-on-chip platforms.[207]

4.3. SAM stability

When engineering a surface for cell-based applications, as described above, an important consideration is the environment in which the SAM will be used and how they will interact. By modifying the sequence or components of the molecules used to create a SAM the half-life of resulting monolayers can be tuned. As an example, μCP of glycol-terminated alkane thiols have been developed which have a substantially increased lifespan of at least 35 days, during which time they are able to support the culture of cells *in vitro.*[208] Systems have also been established where SAM-surfaces can be regenerated following their initial use. SAMs used to create a biosensing surface show retained function and sensitivity for anywhere between 25 and 50 cycles of use and restoration.[209,210] Re-use of such surfaces allows preservation of reagents and will ultimately reduce the cost of these materials. Similarly, SAMs with applications in cell culture can also be utilised repeatedly for cell culture. By employing a simple regeneration step, following removal of cells using trypsin, the surfaces can retain their integrity to be used for up to 15 rounds of subsequent culture.[211] These works highlight the capability of SAMs to function as a stable surface and an increasingly affordable technology for cell culture applications.

SECTION 2: EXPERIMENTAL

Chapter II - Materials and Methods

1. HA-binding peptide identified by phage display (Pep-1)

Pep-1 is a 12-amino acid peptide which was identified by Mummert et al.[131] as a HA-binder through phage display using the New England Biolabs random peptide library. Since first being published, several studies have demonstrated the utility of Pep-1 for blocking HA-cell interactions via the cell surface receptor CD44,[131] and inhibiting the downstream function of HA[212] as well as in situ detection of HA.[132,213] Pep-1's sequence is GAHWQFNALTVR (Figure 7).

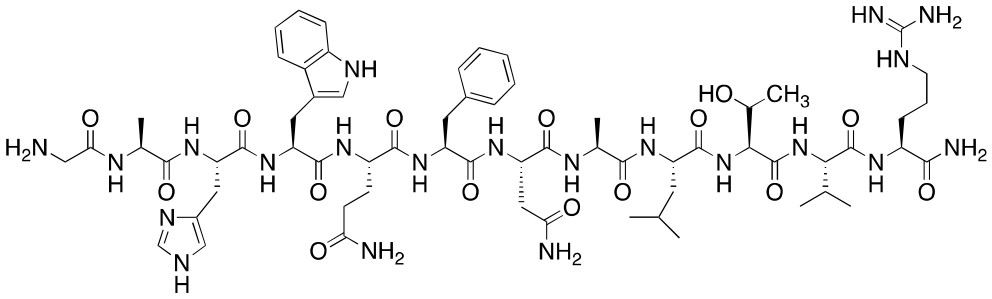

Figure 7: **Structure of Pep-1.** Created with ChemDraw.

The Pep-1 used in this work was synthesised, modified and purified, by Mr Dominic Collis from MHAtricel group, as described below.

1.1. Peptide synthesis

Peptide synthesis, either in a liquid- or solid-phase format, enables the production of useful biological molecules ranging in size from a few amino acids to much larger proteins. Chemical synthesis avoids the need for genetic modification of host organisms, such as bacteria to produce recombinant proteins, which is beneficial for peptides to be used *in vivo.* The Pep-1 peptide used for this thesis was synthesised on the Liberty Blue automated microwave peptide synthesiser (CEM, UK), using solid-phase peptide synthesis with 9-fluorenylmethoxycarbonyl (Fmoc) chemistry.[214] In this method, 4-methylbenzhydrylamine (MBHA) rink amide resin is used to tether the first amino acid at its C-terminal, subsequent protected amino acids are added to its N-terminal via their C-terminal through a condensation reaction forming an amide bond (Figure 8). The Fmoc group protecting the N-terminal is base-labile and when used in combination with acid-labile protecting groups on amino acid side chains allows effective orthogonal growth of

the peptide. The deprotection of the N-terminal under basic conditions, using 20% piperidine in dimethylformamide (DMF), does not affect protection of the R groups and ensures the newly free amine group is the only available site for the carboxyl group of the next amino acid to react with. As the growing peptide is attached to a solid support, and is insoluble, it is possible to wash and filter excess reagents and unwanted by-products out after each round of deprotection and coupling. Once the desired peptide sequence is achieved and the final N-terminal deprotection is complete, the peptide can be capped or coupled to another molecule, such as an alkyl tail or a fluorophore, before being cleaved from the resin. The acidic cleavage conditions for the resin also allow the simultaneous deprotection of amino acid side-chains.

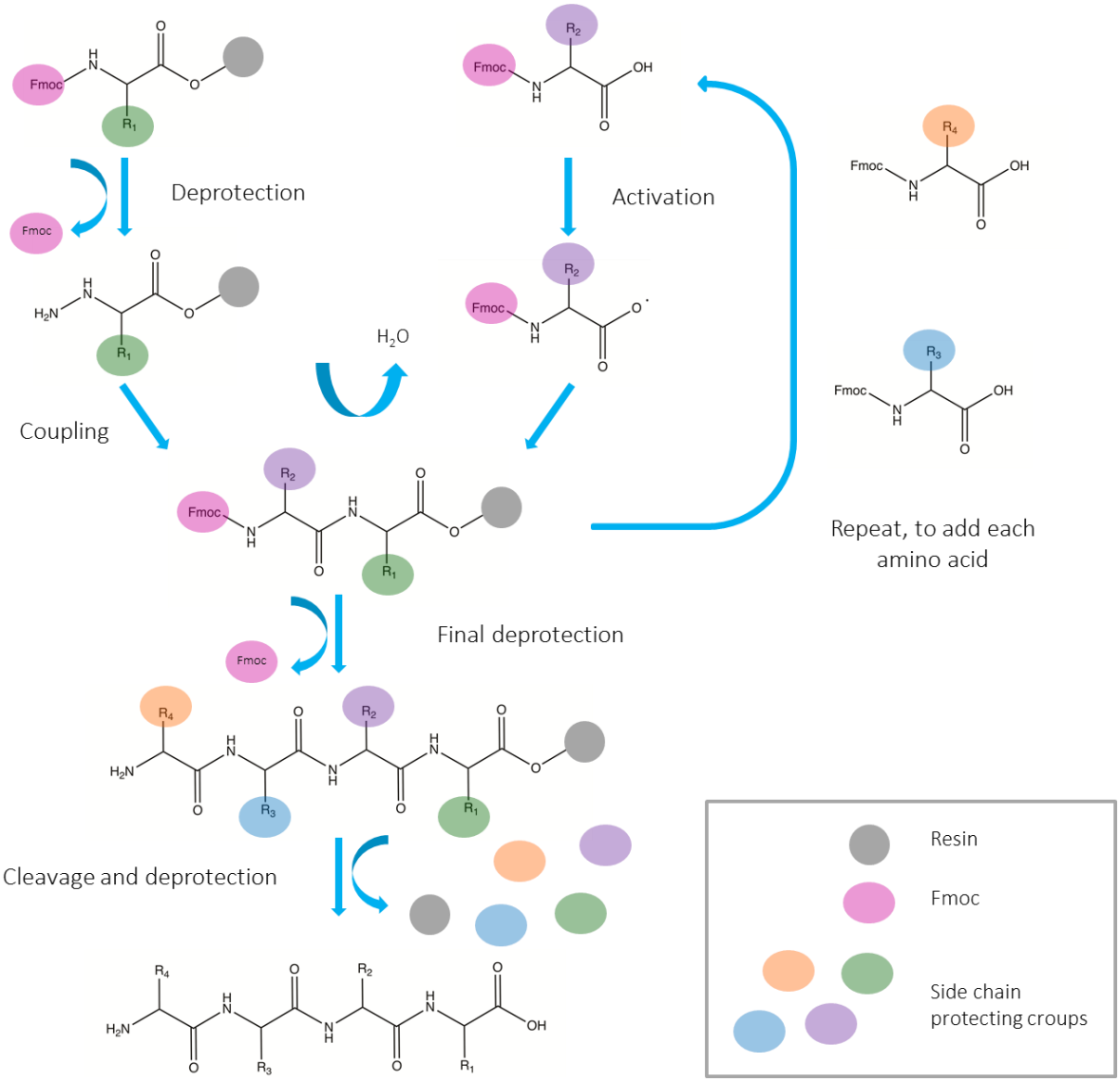

Figure 8: Schematic for solid phase peptide synthesis.

For peptide synthesis using the Liberty Blue automated microwave peptide synthesiser, Fmoc amino acids (Novabiochem, USA) were coupled to a MBHA rink amide resin (Novabiochem), amino acid couplings were performed in 4 times excess of 1-hydroxybenzotriazole hydrate (HOBt), N,N'-diisopropylcarbodiimide (DIC) (both Sigma-Aldrich). Fmoc deprotection was carried out in 20% piperidine in DMF (v/v) and the resin was washed with DMF then dichloromethane (DCM) after each round of coupling and deprotection. The peptide was removed from the synthesiser and Pep-1 was manually capped with either an acetyl group or 3-(((4-methoxyphenyl) diphenylmethyl)thio)propanoic acid. Peptides were cleaved, and side groups deprotected, using a solution of trifluoroacetic acid (TFA, Sigma-Aldrich), triisopropylsilane (Alfa Aesar, US) and water (95:2:5:2.5), or TFA, thioanisole (Sigma-Aldrich), anisole (Sigma-Aldrich) and ethylenediaminetetraacetic acid (EDTA, Sigma-Aldrich) (90:5:2.5:2.5) for 3 hours at room temperature for acetylated or thiolated peptides, respectively. The cleaved peptide solution was collected and excess TFA was removed by rotary evaporation. The peptide was precipitated by the addition of cold diethyl ether (Sigma-Aldrich) and the mixture centrifuged to pellet the peptide. The supernatant was discarded and the peptide was lyophilised.

1.2. Pep-1 capping

1.2.1. Thiol tail capping

The incorporation of a thiol group into a molecule is often used to induce the formation of self-assembled monolayers on a gold surface, as it is known that a strong sulphur-gold bond is formed.[215] To enable Pep-1 to assemble on a gold substrate, it was capped with a 3-(((4-methoxyphenyl) diphenylmethyl)thio)propanoic acid (Acros Organics, Belgium) tail (Figure 9).

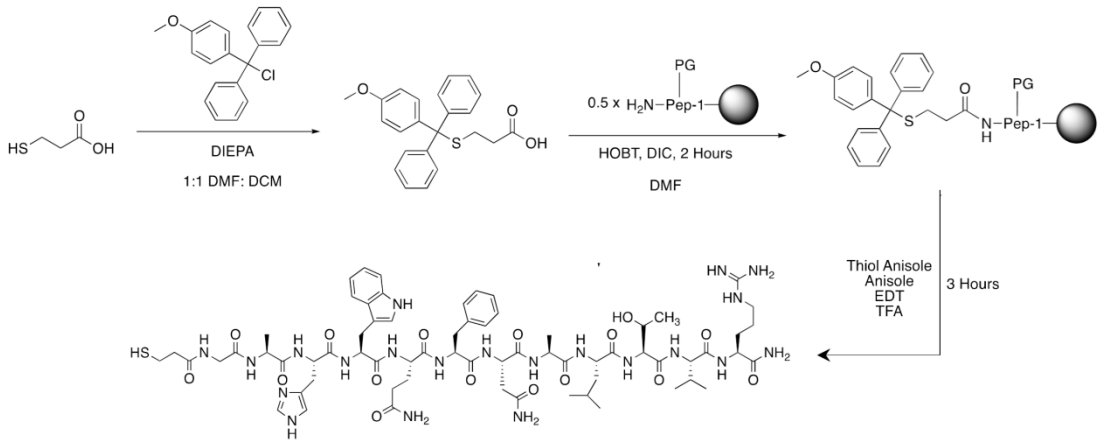

Figure 9: Reaction scheme for the coupling of Pep-1 to the thiol group.

Pep-1 was coupled manually to 3-(((4-methoxyphenyl) diphenylmethyl)thio)propanoic acid using 4 times excess of HOBt and DIC, by shaking for 2 hours at room temperature (Figure 10). The resin was washed with DMF then DCM before a Kaiser test (Sigma-Aldrich) was performed according to manufacturer's instructions, to confirm the success of the coupling. Briefly, a few resin beads were removed and 3 drops of 80% phenol in ethanol, KCN in H_2O/ pyridine and 6% ninhydrin in ethanol were each added. The sample was heated to 120 °C for 5 minutes. The beads and solution remaining yellow indicates a successful capping, whereas if the coupling is incomplete the presence of a primary amine causes a colour change to blue.

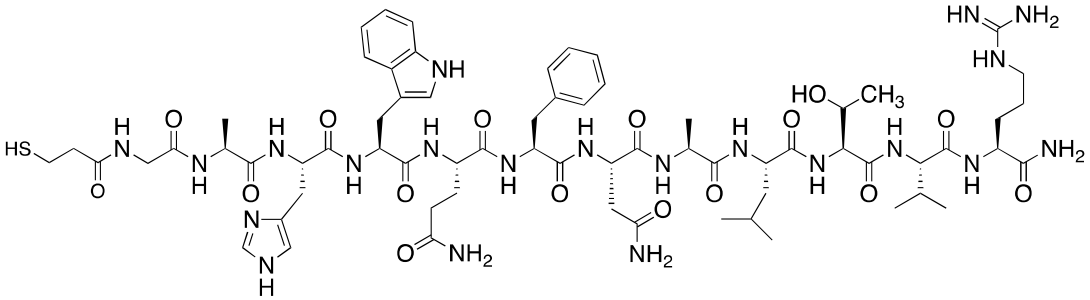

Figure 10: Structure of thiolated Pep-1, HS-Pep-1. Created with ChemDraw.

1.2.2. Acetyl capping

To confirm that the thiol group is responsible for the HS-Pep-1 forming a SAM, rather than it simply adsorbing on the gold surface through electrostatic interactions, acetylated Pep-1 (Ac-Pep-1) was used as a control (Figure 11). While still attached to the resin, Pep-

1 was capped at the N-terminal with an acetyl group, by shaking for 20 minutes at room temperature with acetic acid (Sigma Aldrich) and 10% DMF (w/v). Once the capping was done, the resin was washed with DMF then DCM. To confirm the success of the capping, a Kaiser test (Sigma-Aldrich) was performed according to manufacturer's instructions.

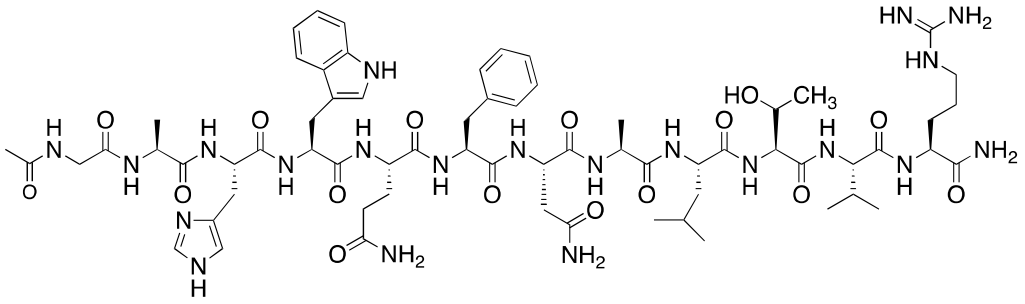

Figure 11: Structure of acetylated Pep-1, Ac-Pep-1. Created with ChemDraw.

1.3. Purification

1.3.1. Preparative high performance liquid chromatography

The purification of crude peptides was achieved by using high performance liquid chromatography (HPLC). This technique separates molecules in solution based on their interaction with a solid support, or column, where greater interaction with the column will result in a slower elution. Reverse-phase HPLC employs a non-polar solid phase and an aqueous mobile phase, where hydrophobic molecules have a greater retention time and hydrophilic molecules are eluted much more quickly. In the case of peptide purification, an aqueous solution containing the peptide is initially injected into the column and eluted over time using a gradient of aqueous/organic solvent which results in the separation and elution of the desired peptide. The more hydrophilic molecules are eluted first followed by increasingly hydrophobic ones.

As compounds are eluted from the column they pass through a detector which can monitor the absorbance at 220 nm, the wavelength at which a peptide bond has its peak absorbance, this allows analysis of the elution time.

To purify the Pep-1 peptides, preparative reverse-phase liquid chromatography using a C18 XBridge column (Waters, UK) was used with a gradient of 98% H_2O to 100% acetonitrile (Sigma-Aldrich) supplemented with 0.1 % TFA. The exchange was run over 30 minutes using a flow rate of 20 mL/min. The purified product was collected based on the

peptide mass, as detected by the SQ Mass Detector (Waters) and acetonitrile was removed by rotary evaporation followed by lyophilisation to obtain peptides as powders.

1.4. Peptide characterisation

1.4.1. Electrospray ionisation mass spectrometry

Electrospray ionisation mass spectrometry is an analytical technique for both the structural and quantitative measurement of biological molecules. Samples are aerosolised by subjecting the sample solution to an electric current, ionised samples then travel through a magnetic field and depending on their mass/charge (m/z) ration are detected by different areas of the detector. The abundance of ions at each m/z ratio can then be used to determine quantitative information about the sample.[216] In this work samples were dissolved in methanol, the mass of the peptides used in chapter III was determined by LC-MS using the 1100 LC/MSD Trap (Agilent, US), as shown in Figure 12A and B.

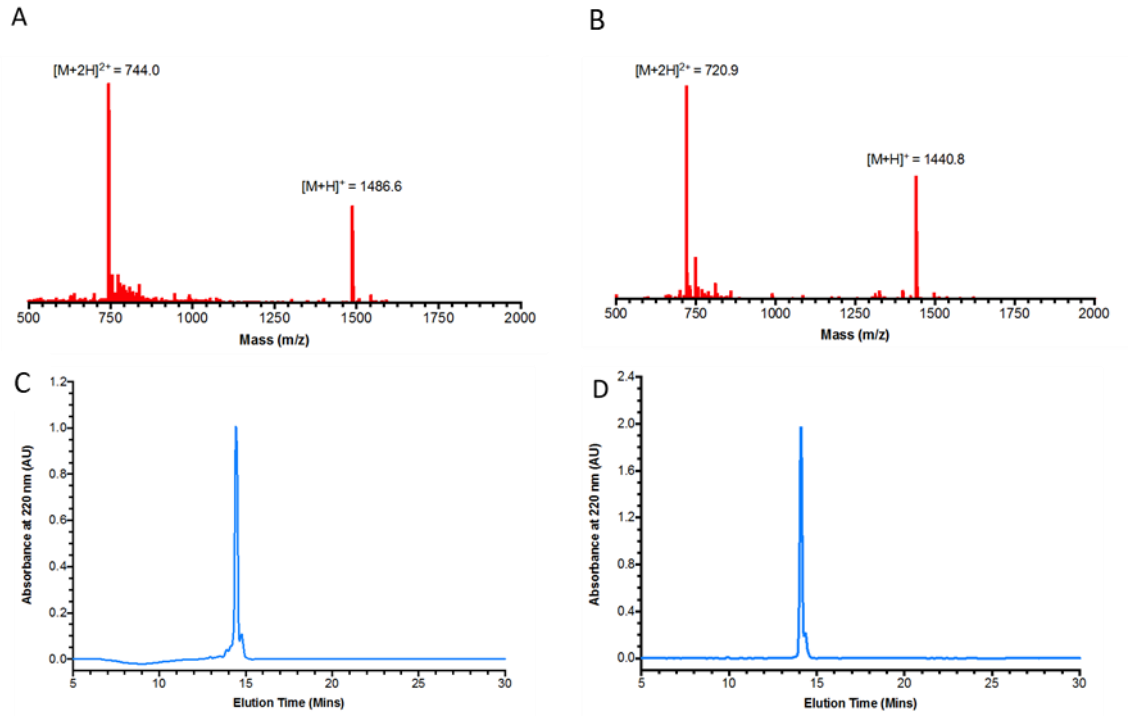

Figure 12: **Characterisation of peptides.** Electrospray Ionisation Mass Spectrometry of (A) HS-Pep-1-$CONH_2$ (Found 1486.6 $[M+H]^+$, 744.0 $[M+2H]^{2+}$. Expected 1486.7) and (B) Ac-Pep-1-$CONH_2$ (Found 1440.8 $[M+H]^+$, 720.9 $[M+2H]^{2+}$. Expected 1440.6) High Performance Liquid Chromatography trace of (C) HS-Pep-1-$CONH_2$ and (D) Ac-Pep-1-$CONH_2$ showing a single peak.

1.4.2. High performance liquid chromatography

To assess the purity of the peptides synthesised for use in this work HPLC was used (Figure 12C, D). Samples were analysed on the Alliance HPLC System (Waters, UK) with an X-bridge column (C18, 3.5 µm, 4.6 × 150 mm) with a water/acetonitrile gradient (from 98/2 to 0/100), and a flow rate of 1 mL/min. The absorbance of the peptide bond at 220 nm was monitored by 2489 UV/visible detector (Waters).

2. Hyaluronic acid

Hyaluronic acid (HA), which can also be called hyaluronate or hyaluronan, is a non-sulfated glycosaminoglycan that has numerous essential roles within the body. It comprises a large part of the extracellular matrix (ECM) as well as the tumour micro-environment. It is made up of repeating disaccharides, N-acetyl-glucosamine and D-glucuronic acid (Figure 13), and *in vivo* HA can be found with a range of molecular weights (MWs) which has been shown to influence its biological function. To investigate the role MW might play, a range of molecular weights, 20 kDa, 200 kDa or 1.5 MDa sourced from Lifecore Biomedical Inc. (Chaska, USA), was used in the experiments ofsubsequent chapters.

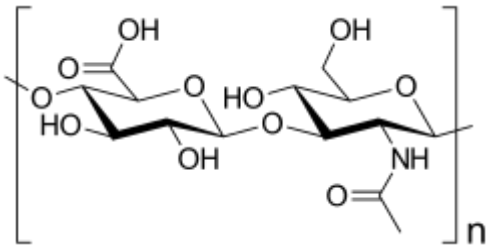

Figure 13: Structure of hyaluronic acid repeating disaccharide. Created with ChemDraw.

2.1. Sterilisation

To prevent contamination in cell-based assays, HA was filter-sterilised. HA was dissolved in distilled water and passed through a 0.22 µm filter in a cell culture hood, the filtered solution was then transferred to a 50-mL TubeSpin® Bioreactor tube (TPP, Switzerland) and lyophilised.

2.2. Texas Red tagging

To visualise the immobilisation of HA following micro-contact printing of HS-Pep-1 by fluorescence microscopy, a Texas red tagged HA (HA-TxRd) was synthesised. (Figure 14)

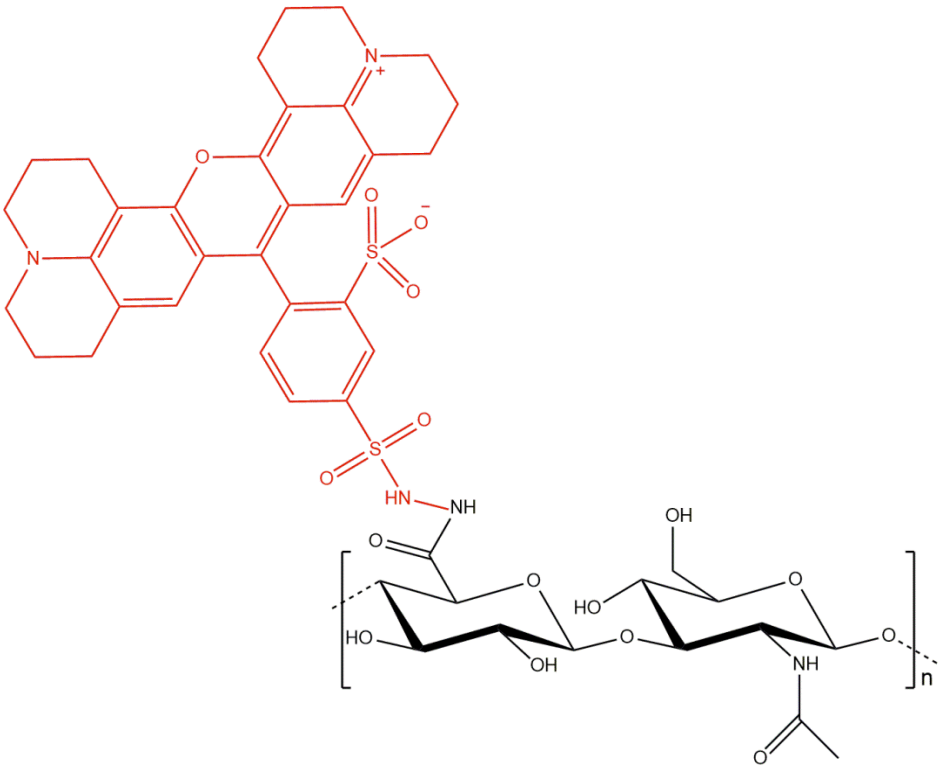

Figure 14: **Structure of Texas red- conjugated hyaluronic acid repeating unit.** Created with ChemDraw.

Texas red (Thermo Fisher Scientific) was conjugated to HA using a previously described method.[217] Briefly, 1.5 MDa HA (Lifecore Biomedical, USA) was dissolved in 20 mM MES (Sigma) pH 4.5, 30% ethanol (Sigma-Aldrich), and 3 times excess *N*-(3-Dimethylaminopropyl)-*N*′-ethylcarbodiimide hydrochloride (EDCI) (Sigma-Aldrich) compared to the number of HA disaccharide units. Texas Red hydrazide (Molecular Probes, Invitrogen, UK) was dissolved in DMF and added to the HA mixture at a molar ratio of fluorophore to disaccharide number of 1:10 and incubated at room temperature with shaking, overnight in the dark. The solution was dialysed against 75 mM NaCl (Fisher Scientific), in 40% ethanol, using regenerated cellulose membranes (10,000 molecular weight cut-off, Spectra/Por, USA), in the dark for 4 days then lyophilised and stored at -20 °C.

3. Poly-D-Lysine

Poly-lysine is a positively charged polymer which can be synthesised from the L or D forms of lysine to yield either poly-L-lysine (PLL) or poly-D-lysine (PDL). Both polymers are highly hydrophilic and at a physiological pH have a pKa~ 10.5.[218] In cell culture, poly-lysine is often used as a surface coating to enhance cell adhesion. PLL is susceptible to degradation by proteolytic enzymes expressed by cells whereas PDL is more resistant which can be beneficial to insure poly-lysine integrity throughout cell-based assays.[219] Due to their positive charge, both PLL and PDL can immobilise HA through strong ionic interactions and can be exploited for layer-by-layer assembly studies.[220] In this work HA was immobilised by poly-lysine as a comparison for Pep-1 immobilisation of HA *in vitro*. PDL was selected to minimise cell-dependent degradation. For all experiments, a solution of 0.1 mg/mL Poly-D-lysine homobromide (Sigma-Aldrich), with an average molecular weight of 70 – 150 kDa, was used.

4. HA glycopolymers

Chemically synthesised mimics of biological molecules, such as HA, can provide useful tools in cell biology. To be able to replicate the effects of biological molecules with a synthetic alternative would help to eliminate the use of animal derived products from tissue culture, which is especially advantageous for translational applications. Additionally, chemical synthesis has the potential to enhance the existing properties of the native molecule, allowing properties to be tailored towards a specific application.

Using the two HA sugars, N-acetyl-glucosamine and D-glucuronic acid, the HA glycopolymers were synthesised by Mr Dominic Collis.[221] Homo-polymers, consisting entirely of either N-acetyl-glucosamine or D-glucuronic acid, an alternating co-polymer, synthesised under conditions which ensured subunits were added alternately, and a statistical co-polymer which contains both monomers in an undefined order and ratio, were synthesised by Reversible Addition Fragmentation Chain-Transfer (RAFT) polymerisation (Table 1). The Formation of these polymers was monitored by Fourier-transformation infrared spectroscopy (FT-IR), gel permeation chromatography (GPC), and nuclear magnetic resonance (NMR).

Table 1: Structure of the HA glycopolymers as used in Chapter V, shown as individual repeating units. Created with ChemDraw.

Polymer	Structure
PVB-GlcNAc	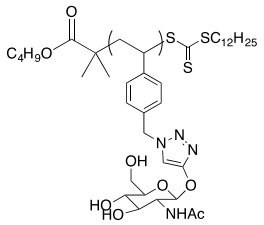
PVB-GlcA	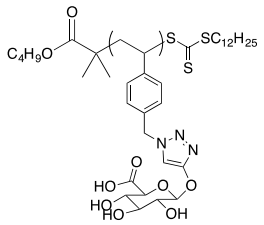
PVB-GlcNAc-alt-PMI-GlcA (Alternating)	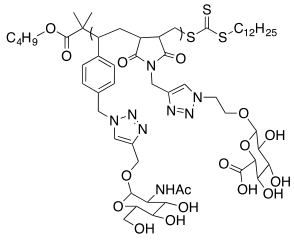
PVB-GlcA-co-VB-GlcNAc (Statistical)	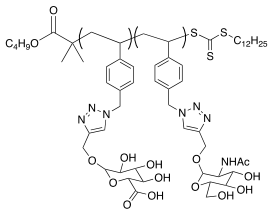

5. Formation of self-assembling monolayers and HA binding

5.1. Au substrate preparation

Gold (Au) surfaces were used for the self-assembly of Pep-1 monolayers and the adsorption of PDL for the immobilisation of HA. In addition to its ability to form gold-sulphur bonds for SAM assembly, Au is a noble metal that is widely used *in vitro* and *in vivo* without any notable side effects or toxicities.[222]

5.1.1. Coating

The gold surfaces used in this thesis for SAM formation, with the exception of the quartz crystal microbalance crystals, were produced by Mr Jotham Selvarajah from the School of Physics and Astronomy, Queen Mary University of London. Glass microscope slides were cleaned with a mixture of sulphuric acid (Sigma-Aldrich) and 30% hydrogen peroxide (Sigma-Aldrich) in a 3:1 ratio, rinsed with DI water, dried under N_2 then rinsed with acetone (Sigma-Aldrich), dried under N_2 and finally rinsed in chloroform (Sigma-Aldrich) and dried under N_2. Slides were then evaporation coated with a 3 nm chromium adhesion layer, then a 100 Å layer of gold. Thickness of the coating was measured by a quartz crystal oscillating monitor.

5.1.2. Cleaning

Prior to use, all Au surfaces, including QCM-D crystals, were cleaned using the following protocol. Gold substrates were submerged in hot (60 °C) cleaning solution (30% ammonium hydroxide (Sigma-Aldrich), 30% H_2O_2 (Sigma-Aldrich), and DI water in a 1:1:3 ratio), for between 2-5 minutes, rinsed with DI water and dried under N_2. This cleaning protocol is based on the RAC clean and removes organic residues from the surface, and is recommended by the manufacturers as the preferred cleaning procedure for the gold-coated QCM-D sensors,[223] this method is also routinely used to remove SAMs[224] and as such this method has been applied to cleaning of all the Au substrates used.

5.2. Building of SAM-HA layers/surfaces

5.2.1. HS-Pep-1 self-assembled monolayers

The formation of HS-Pep-1 SAMs was achieved by incubating pre-cleaned Au substrates with a 1 mM solution of HS-Pep-1 in 99.9% ethanol (Sigma-Aldrich) at room temperature for at least 24 hours. Samples were then rinsed with ethanol to remove any excess peptide followed by ultra-pure water and dried under N_2.

5.2.2. Poly-D-lysine coating

Coating of Au substrates was done by incubating pre-cleaned surfaces with 100 µg/mL PDL in sterile ultra-pure water at room temperature for at least 24 hours. Samples were then rinsed with ultra-pure water to remove any excess PDL and dried under N_2.

5.2.3. HA immobilisation

To investigate HA immobilisation on each of the prepared surfaces, PDL, HS-Pep-1 or on bare Au, samples were incubated with 0.05 % (w/v) HA for at least 48 hours at room temperature. They were then rinsed with ultra-pure water to remove any unbound HA and dried under N_2.

A range of molecular weights of HA were used, 20 kDa, 200 kDa and, 1.5 MDa, and for each the same percentage concentration was used.

Surfaces prepared for use in tissue culture studies were made as described under sterile conditions, using filter-sterilised HA and sterile ultra-pure water for washes.

5.3. Micro-contact printing

Micro-contact printing is a quick and simple method for creating patterns on surfaces, which is routinely used in combination with SAMs. To investigate the spatial localisation of HA by HS-Pep-1, polydimethylsiloxane (PDMS) stamps, gifted by Dr Kseniya Shuturminska, were used to transfer HS-Pep-1 onto the Au surface. A 1 mM ethanolic solution of HS-Pep-1 was applied to the PDMS stamp and dried under N_2, the stamp was brought into contact with the cleaned Au surface. Care was taken to ensure the entire surface of the stamp made equal contact, and to avoid air bubbles becoming trapped. The stamp was lifted after ~10 seconds, making sure the stamp was not moved across the surface causing the pattern to be distorted. Patterned surfaces were then washed with ethanol and dried under N_2, followed by rinsing with ultra-pure water.[225] Once the surfaces were patterned they were incubated with the fluorescent Texas Red-labelled HA, as described in 2.2.

6. Characterisation of self-assembled layers (SAMs)

To confirm the successful coating, or patterning, of Au surfaces with PDL and HS-Pep-1 and subsequent immobilisation of HA several characterisation techniques were employed.

6.1. Quartz crystal microbalance with dissipation monitoring

Quartz crystal microbalance with dissipation monitoring (QCM-D) is a technique which has been developed from the original QCM system, which typically uses an AT-cut circular

piece of quartz with a metal electrode on each side and exploits the inherent piezoelectric properties of quartz to calculate changes in mass on a quartz crystal surface. Application of an alternating electric current causes detectable oscillations in the quartz. QCM-D enables real-time monitoring of both the adsorption of material onto a surface, by observing the change in frequency (Δf) of the crystals oscillation, as well as the viscoelastic properties of the adsorbed layer, using the change in dissipation (ΔD). When mass is added to the surface of the crystal, the frequency of its oscillations is decreased, and conversely, when mass is removed from the surface the frequency increases. The Sauerbrey relationship equates the change in mass (Δm) with Δf using **Equation 1**.[226]

Equation 1: The Sauerbrey equation

$$\Delta m = -\frac{C \times \Delta f_n}{n}$$

Where Δm is the Sauerbrey areal mass density of the adsorbed layers (mass per unit area), C is the mass sensitivity constant of the quartz crystal (17.7 ng cm^{-2} s for 5 MHz quartz crystals), n is the overtone number and f is the resonant frequency.

However, the Sauerbrey equation makes several assumptions, which means that if the film deposited onto the surface is soft or has viscoelastic properties then the Δm value will be underestimated. Dampening of the crystals oscillation is characteristic of soft films, this energy dissipation (D), defined by Equation 2, can be used to model further information regarding properties of the film.

Equation 2: Energy dissipation

$$D = \frac{E_{lost}}{2\pi E_{stored}}$$

Where E_{lost} is the energy lost during one oscillation cycle and E_{stored} is the energy stored. The Δf and ΔD from multiple overtones can be used in the Voigt-based viscoelastic film model to provide information on the adsorbed mass, film thickness, viscosity and shear elastic modulus.

In this thesis, QCM-D was used to confirm and quantify the binding of HS-Pep-1 or PDL to

a gold surface using the gold-coated QSX301 sensor (Biolin Scientific, Sweden) and subsequent binding of 3 molecular weights of HA (20 kDa, 200 kDa, and 1.5 MDa). Measurements were carried out in a liquid environment using either the QS100 or Q-Sense Pro (both Biolin Scientific) at 37 °C or 25 °C, respectively. Before use, sensors were UV/Ozone treated (UVOCS T10X10 OES/E, Ultraviolet Ozone Cleaning Systems, USA or UV/Ozone ProCleaner 220, BioForce Nanosciences, Inc., USA) for 10 minutes then cleaned as described in 5.1.2. Following cleaning unmodified sensors were then UV/Ozone treated for a further 10 minutes.

The QS100 instrument uses a static system whereas the Q-Sense Pro measures adsorption under flow, at a rate of 50 µL/min. For both systems readings were collected according to the following general protocol; the baseline frequency and dissipation of the crystal was established in 0.15 mM NaCl, a solution of either HS-Pep-1, PDL, or HA in 0.15 M NaCl was then injected into the crystal chamber. Once a stable frequency was seen, the sensor was washed with NaCl to remove weakly associated molecules. A solution of 0.05 % HA (MW of 20 kDa, 200 kDa or 1.5 MDa) in 0.15 mM NaCl was then injected into the crystal chamber. Again, once a stable frequency was acquired the system was washed to remove weakly associated molecules.

For data gathered using the Q-Sense Pro, the thickness of layers was estimated using the Voigt-based viscoelastic model implemented in the Q-Sense Dfind software (version 1.1.2672.53037), assuming a fluid PDL layer density of 1000 kg/m^3, a hydrated HA sugar density of 1050 kg/m^3, and a fluid viscosity of 1 mPa s.

Assuming the adsorbed film has a uniform thickness and density, f and D can be shown as functions of overtone, thickness, density, elasticity, and viscosity.

Equation 3: Modelling the change in frequency of crystal oscillation

$$\Delta f \approx -\frac{1}{2\pi\rho_q t_q} t_l \rho_l \omega \left(1 + \frac{2t^2 X}{3\delta^2(1+X^2)}\right)$$

Equation 4: Voigt calculation of change in energy dissipation

$$\Delta D \approx \frac{2t^3\rho_l f_m}{3\pi f \rho_q t_q} \frac{1}{\delta^2(1+X^2)}$$

Where ρ_q and t_q are the density and thickness of the quartz crystal, ρ_l and t_l are the density and thickness of the adsorbed layer, f_m is the measured frequency, X the inverse of the mechanical loss tangent (tan δ) and is the ratio of the storage modulus (μ_f) and the loss modulus (η_f) as defined in *Equation 5*.

Equation 5: Mechanical loss tangent

$$\tan\delta = \frac{1}{X} = \frac{2\pi f_m \eta_f}{\mu_f}$$

δ is the viscous penetration depth of the shear wave of the bulk liquid (*Equation 6*) which describes the rate of decay of the oscillating wave.

Equation 6: Viscous penetration depth

$$\delta = \sqrt{\frac{2\eta_f}{\rho_f f_m}}$$

Using these equations, the measured f and D values at each overtone can be entered along with the assumed density and viscosity so the unknown thickness and density of the film can be extracted.

6.2. Contact angle

For assessing wettability of the surfaces at each stage, contact angle (CA) was measured using the static sessile drop method on the Drop Shape Analyser (Model DSA100, Krüss, Germany). Each surface was prepared as previously described and 1 μL of distilled water was dropped onto the sample; an image was acquired and the contact angle, between the liquid-solid and the liquid-vapour interface, was calculated using the Circle fit method in the Drop Shape Analyser inbuilt software. For all experiments, 3 independent repeats were done and contact angle was measured at 3 different locations on each sample.

6.3. Atomic force microscopy

Atomic force microscopy (AFM) enables the nanoscale imaging of a surface and for this thesis was used to investigate surface topography and to calculate the average surface roughness. AFM uses a rigid tip mounted on a cantilever which scans the sample surface, by having a laser trained to the end of the cantilever, above the tip, a detector can be used to monitor the deflection of the cantilever. Imaging can be conducted in contact, intermittent contact, or non-contact mode, for the studies carried out in chapter III intermittent contact was used in Quantitative Imaging (QI) mode using the JPK NanoWizard 4 (JPK Instruments AG, Germany). When intermittent contact modes are used, the cantilever oscillation is driven at a frequency close to that of its resonance frequency and the forces exerted on the cantilever during cycles of sample approach and retraction are measured to produce the image.

To acquire images, samples of bare Au, PDL, HS-Pep-1, PDL-HA and HS-Pep-1-HA were prepared as described above and an area of 10 μm x 10 μm was scanned at a resolution of 256x256 pixels, using silicon nitride AFM tips, MSNL-10, with a spring constant of 0.01-0.06 N/m, and a resonance frequency of 10-20 kHz were used (Bruker AFM Probes, USA). From each sample, 3 distinct regions were imaged and 3 independent experiments were performed.

An advantage of using AFM to look at the surface topography of the surfaces is the ability to conduct imaging in both hydrated and dried states. Samples to be scanned when hydrated were prepared as before and submerged in ultra-pure water prior to imaging.

Raw images were processed by subtracting the polynomial fit from each scan line independently using the JPK Data Processing software.

6.4. Fluorescence imaging

To visualise the localisation of Texas Red-labelled HA on surfaces micro-contact printed with the HS-Pep-1 SAM, fluorescence microscopy was used. Fluorescence imaging uses the ability of fluorophores to emit light of a greater wavelength than the light it was excited by. In the case of Texas Red, its peak excitation is at 596 nm and peak emission is at 613 nm.

HS-Pep1 was stamped onto Au substrates and incubated with Texas Red-HA as described

previously; images were then acquired using the Leica DMI4000B Epifluorescence microscope (Leica, Germany).

7. Tissue culture

All the cell studies were performed using either LuC4 or LuC4-GFP human oral squamous cell carcinoma-derived immortalised cell lines. Cells were cultured in Dulbecco's Modified Eagle Medium: Nutrient Mixture F-12 (DMEM/F-12) media (Gibco, Life Technologies Ltd., UK), 10% Foetal Calf Serum (FCS), 100 Units/ml penicillin (Sigma), 100 μg/ml streptomycin (Sigma), and RM+ (Table 2).

LuC4-GFP cells were generated from LuC4 cells which were transduced with a constitutively expressed green fluorescence protein (GFP) plasmid. [227]

Cells were passaged when 85-90% confluent, they were washed with phosphate buffered saline (PBS) and incubated at 37 °C with 0.25% trypsin-EDTA (Sigma Aldrich) or cell dissociation buffer, enzyme-free PBS-based (Gibco, Life Technologies) until detached. Cells were reseeded into new flasks at approximately 250 cells/cm^2.

Table 2: RM^+ components, showing final concentration prior to addition to culture medium.

	COMPONENT	FINAL CONCENTRATION	COMPANY
RM^+	Transferrin	5 μg/ml	Sigma
	Hydrocortisone	0.4 μg/ml	Sigma
	Cholera toxin	10^{-10} M	Sigma
	EGF	10 ng/ml	Serotec
	Insulin	5 μg/ml	Sigma
	Liothyronine	$2x10^{-11}$ M	Sigma

7.1. Flow cytometry

Flow cytometry is a cell analysis technique where cells in suspension are passed by a fluidics system, as a stream of single cells, through a laser beam. When a cell is illuminated by the laser, features within the cell will deflect light or fluorophores associated with the cell are excited and emit fluorescence. The direction in which deflected light is scattered is measured and used to determine characteristics of the cell. Forward scattered light

(FSC) provides information about the size of the cell, whereas side-scattered light (SSC), collected at a 90-degree angle to the laser beam, relates to the granularity or internal complexity of the cell.

When fluorophores are illuminated by the laser, they absorb light and an electron within the molecule is elevated to a higher energy state. As the electron returns to its ground state, this excess energy is emitted as fluorescence. This is collected by a photomultiplier tube (a type of photo detector), converted to an electrical signal and transmitted to the computer where it will be displayed on a data plot.

Fluorophore-conjugated antibodies are used to stain cell samples to determine the expression level of each marker protein. As the signal strength is proportional to the number of excited electrons, and therefore the number of fluorophores, a stronger signal indicates a greater level of expression of the target protein.

7.1.1. Sample preparation

For assessment of the expression of cell surface markers CD44 and EpCAM LuC4 cells were harvested, as before, with trypsin-EDTA and 5 mL of serum-containing medium was added to the cells to stop the action of the trypsin. Cells were centrifuged for at 300g for 5 minutes at 4 °C and washed with PBS. Cells were re-suspended in PBS and incubated for 15 minutes with directly conjugated antibodies, CD44-allophycocyanin (APC, Becton Dickinson, US) or EpCAM-phycoerythrin (PE, Miltenyi Biotec Ltd., Germany) diluted 1:100. Cells were washed with 5 mL PBS and resuspended in 1 mL of PBS with 200 ng/mL 4′,6-diamidino-2-phenylindole (DAPI).

7.1.2. Data acquisition and analysis

Data were acquired using the BD FACSCanto II (Becton Dickenson). Cells were initially gated based on side and forward scatter, to exclude cell debris. DAPI signal was then used to exclude dead cells, DAPI is only able to enter the cell if the cell membrane is damaged and DAPI positivity identifies cells that are not viable. The DAPI negative cells were plotted based on CD44-FITC and EpCAM-APC signal, and a quadrant marker was applied, using single-stained and unstained cells to determine the cut-off for negative signals.

Analysis was performed using FlowJo® version 10.5.

7.2. Fluorescence activated cell sorting

In addition to looking at the marker profile of cells, flow cytometry can also be used to then sort cells based on this information, isolating sub populations of interest for downstream applications. This is referred to as fluorescence activated cell sorting (FACS), once the cells have passed through the laser and the fluorescence has been detected the electronics component can identify if the cell is a target cell, based on the gating strategy used. The stream passes through a sort block where positively and negatively charged deflection plates deflect each cell into either the specified collection tube or into the waste.

7.2.1. Sample preparation

For isolation of the EMT ($CD44^{high}/EpCAM^{low}$) and Epi ($CD44^{high}/EpCAM^{high}$) populations from the LuC4 cell line, for experiments in chapter IV, cells were harvested with trypsin-EDTA, as before. Cells were centrifuged at 300*g* for 5 minutes at 4 °C and washed with PBS. Cells were resuspended in PBS and incubated with directly conjugated antibodies; CD44-FITC (Becton Dickinson, US) and EpCAM-APC (Miltenyi Biotec Ltd., Germany) for experiments not including GFP-cells, or CD44-APC and EpCAM-PE for experiments using LuC4-GFP. All antibodies were diluted 1:100 and samples incubated for 15 minutes. Cells were washed with 5 mL PBS and resuspended in 1 mL of PBS with 200 ng/mL 4′,6-diamidino-2-phenylindole (DAPI).

7.2.2. Sample sorting

Sorted populations were collected using the Aria IIIu Cell Sorter with the assistance of Dr Gary Warnes.

8. Effect of SAM-HA surfaces on human cancer cells

8.1. AlamarBlue

To investigate the viability of cells cultured on the fabricated surfaces, their reductive capacity was measured using alamarBlue cell viability reagent (Thermo Fisher Scientific, US). This is a colourimetric assay where resazurin, the active component in the alamarBlue reagent, in its unreduced state is blue and is non-fluorescent. Resazurin is a cell permeable compound which, when added to cell medium, enters the cell where it is

reduced to resorufin, a red molecule which is highly fluorescent with a peak excitation of 570 nm and emission of 585 nm (Figure 15). This colour change can be quantified using a plate reader to read the fluorescence with an excitation wavelength between 540-570 nm and monitor the emission wavelength between 580-610 nm. An increase in fluorescence should be observed where cells are viable.

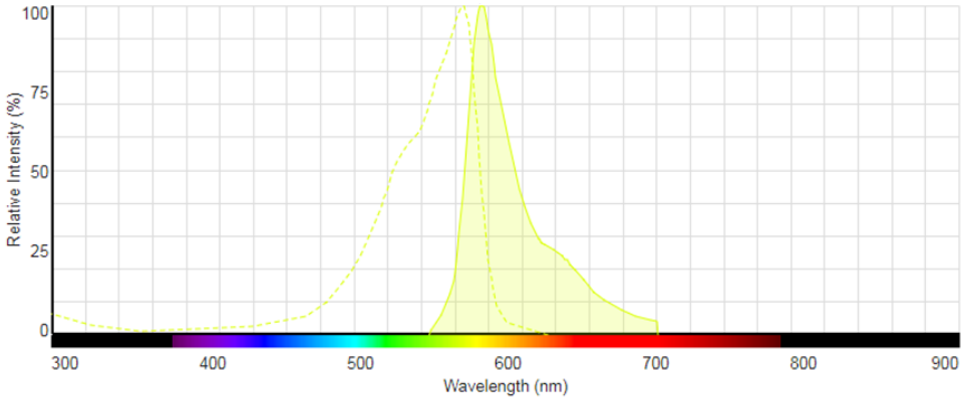

Figure 15: **Emission spectra of resorufin,** shaded curve represents the emission and hollow curve represents the excitation spectra. Spectra generated using the fluorescence SpectraViewer (Thermo Fisher Scientific).[228]

For experiments in chapter III, LuC4 cells were harvested using cell dissociation buffer, enzyme free, PBS-based and seeded onto the prepared gold surfaces described in 5.2 at a density of 5,000 cells/cm^2 in serum-free medium. AlamarBlue cell viability reagent was added after 8 hours of culture at a 1:10 dilution and samples were incubated at 37 °C, 5% CO_2 for 16 hours. To quantify the colour change 100 µL of medium was transferred to a 96-well plate (Costar, Corning, US) and the fluorescence was measured on the Synergy HT plate reader (BioTek, US) at excitation wavelength 530/25 and emission wavelength 590/35.

8.2. Scratch assay

To assess any changes in migration brought by culture on the modified surfaces, LuC4 cells were detached using cell dissociation buffer and seeded onto the prepared gold surfaces described in 3.2 at a density of 10,000 cells/cm^2 in serum-free medium. Cells were grown to confluency at 37 °C, 5% CO_2 and a scratch was made using a 200 µL pipette tip. The cell monolayer was washed with PBS to remove any cell debris and images of the scratch were captured at 0, 4, 8, 12, 24, and 48 hours using a Nikon Eclipse TE200-S

(Nikon, UK). The area of the wound was calculated using ImageJ 1.52a software (National Institutes of Health, US).

8.3. Adhesion assay

To investigate cell adhesion to the coated Au surfaces, Luc4 cells were harvested using cell dissociation buffer and seeded at 10,000 cells/cm^2 onto gold surfaces prepared as described in 3.2. Samples were incubated for either 6 or 24 hours at 37 °C, 5% CO_2. Surfaces were then washed with PBS to remove any cells not attached and images were taken using a Nikon Eclipse TE200-S and cells counted in ImageJ 1.52a.

9. Phage display

In this work, presented in chapter IV, phage display is used as a tool for screening a random 12-amino acid peptide library to identify novel sequences which bind to the EMT fraction of the LuC4 cell line. The Ph.D-12 Phage Display Peptide Library, purchased from New England BioLabs (NEB, US), uses M13 bacteriophage displaying the N-terminal fusion protein on the minor coat protein pIII. The library, with a complexity of 10^9 independent clones, is generated by using the M13KE cloning vector to insert DNA sequences into the phage genome which will then be expressed on the surface. This method provides a direct linkage between the displayed peptide and the encoding genetic information, so selection and recovery of phages based on peptide binding affinity to the target will also recover the DNA encoding it.

The M13 bacteriophage is a non-lytic phage, when it infects host bacteria turbid plaques are formed due to a reduction of bacterial cell growth.

Maintenance of M13 phages, bacterial culture, and phage titering were carried out according to the Ph.D. Phage Display Libraries Instruction Manual. Panning experiments used this manual as a starting point.

9.1. Media and solutions

9.1.1. Luria Broth medium

To make 1 L of LB 20 g of LB Broth (Lennox) powder microbial growth medium (Sigma Aldrich) was dissolved in water and autoclaved. The Lennox formulation contains 10 g/L tryptone, 5 g/L yeast extract, and 5 g/L NaCl.

9.1.2. Tetracycline stock

A 100x stock solution of Tet was made by dissolving 20 mg of tetracycline (Sigma Aldrich) in 1 mL ethanol and water at a 1:1 ratio. Stock was stored at -20 °C and vortexed before use.

9.1.3. IPTG and Xgal stock

A 100x stock of IPTG/Xgal was made by dissolving 1.25 g IPTG (Sigma Aldrich) and 1 g Xgal (Sigma Aldrich) in 25 mL DMF. Stock was stored at -20 °C and vortexed before use.

9.1.4. Luria Broth and tetracycline agar plates

LB medium was made as described in 9.1.1 and 15 g/L agar (Sigma Aldrich) was added before autoclaving. Subsequently medium was cooled to < 70 °C and Tet stock was added at a 1:100 dilution and plates were poured. Once poured plates were stored in the dark at 4 °C.

9.1.5. Luria Broth, IPTG, and Xgal plates

LB agar was made as described in 9.1.4 and cooled to < 70 °C. IPTG/Xgal stock was then added at a 1:100 dilution and plates were poured. Once poured plates were stored in the dark at 4 °C.

9.1.6. Top agar

LB medium was made as described in 9.1.1, before autoclaving 7 g/L Bacto-agar (Sigma Aldrich) was added. Aliquots of 50 mL were stored as a solid at room temperature. Top agar was melted in the microwave before use.

9.1.7. Blocking buffers

Dulbecco's Modified Eagle Medium: Nutrient Mixture F-12 (DMEM/F-12) media, 100 Units/ ml penicillin, 100 μg/ml streptomycin, RM+ (Table 2), and 1 % (w/v) bovine serum albumin (BSA).

9.1.8. Wash buffer

Wash buffer was PBS-Tween (PBST, Sigma Aldrich) 0.05 % (v/v) supplemented with 1 % (w/v) BSA.

9.1.9. Elution buffer

Non-specific low pH elution was carried out with 0.1 M glycine with 1 mg/mL BSA, pH 2.2.

9.1.10. Cell lysis buffer

Lysis buffer was 2 % (w/v) sodium deoxycholate (Sigma Aldrich), 10 mM Tris-HCl, 2 mM EDTA, pH8.

9.1.11. Tris-buffered saline

Tris-buffered saline (TBS) was made by dissolving Tris-HCl (50 mM, pH 7.5, Sigma Aldrich) and NaCl (150 mM) in water and autoclaving. Solution was stored at room temperature.

9.1.12. Polyethylene glycol sodium chloride

Polyethlene glycol-8000 (PEG-8000, 20% w/v) was dissolved in 2.5 M NaCl, autoclaved, and stored at room temperature.

9.1.13. Iodide buffer

Sodium iodide (4 M) was dissolved in 10 mM Tris-HCl (pH 8.0) and 1 mM EDTA and stored in the dark at room temperature.

9.2. Strain maintenance

9.2.1. Bacterial culture

The host bacterial strain used for the amplification of M13 bacteriophage was ER2738 (New England BioLabs). This *Escherichia coli* (*E. coli*) strain contains the following plasmid; F´ $proA^{+}$ B^{+} $lacI^{q}$ Δ(lacZ)M15 zzf::Tn10(Tet^{R}) which confers several useful features. Firstly, as the M13 phage is male-specific, presence of tetracycline resistance (Tet^{R}) in a mini-transposon within the F-factor (F') allows selection of F-factor positive cells by using media supplemented with tetracycline (Tet). Secondly, the mutation in the lacZ gene (Δ(lacZ)M15) which enable blue/white screening.

The lacZ gene encodes β-galactosidase, an enzyme which cleaves lactose, the gene product of the Δ(lacZ)M15 mutation present in the ER2738 strain is the ω-peptide. This truncated β-galactosidase is inactive; however, function can be rescued by the co-expression of the deleted residues called the α-peptide. The M13KE bacteriophage genome contains the gene encoding the α-peptide, so only when a ER2738 cell is infected

with a phage is a functional β-galactosidase produced. This α-complementation can be used for blue/white screening, where M13KE-infected *E. coli* are propagated on media containing isopropyl-β-D-thiogalactopyranoside (IPTG) and 5-bromo-4-chloro-3-indolyl-β-D-galactopyranoside (Xgal). IPTG induces the expression of the lac operon and Xgal in an analogue of lactose which when cleaved by β-galactosidase forms a blue insoluble precipitate. Therefore, blue plaques indicate colonies of E. coli which have been infected by M13KE phage and white plaques indicate infection by wild-type (WT) phage.

ER2738 glycerol (Sigma Aldrich) stocks were stored at -80 °C, for used ER2738 was plated on a LB+Tet plate and incubated overnight at 37 °C. The plate was stored wrapped in parafilm at 4 °C for up to a month and used to start liquid cultures detailed below.

9.2.2. Phage titering

To determine the concentration in plaque forming units (pfu), phages were titred by infection of ER2739 and plating on LB+Tet plates.

A mid-log phase, defined by an ocular density at 600 nm (OD_{600}) of around 0.5, culture of ER2738 was prepared by inoculation of LB medium and incubation with shaking at 37 °C for 6 hours. The phage sample to be titred was serially diluted in LB medium and 10 µL was added to 200 µL of the mid-log phase ER2738 culture. Samples were vortexed then incubated at room temperature for 5 minutes. Infected bacterial cells were then transferred to 3 mL aliquots of top agar, held at 45 °C, samples were vortexed and then poured onto pre-warmed LB/IPTG/Xgal plates. Plates were incubated overnight at 37 °C.

To calculate the titre blue plaques were counted at pfu/10 µL determined by multiplying the number of plaques by the dilution factor of each plate.

9.2.3. Bacteriophage amplification

9.2.3.1. Amplification of phage pools

To amplify M13 bacteriophage an overnight culture of ER2738 was diluted 1:100 into 20 mL of LB medium in a 250 mL Erlenmeyer flask. The culture was then inoculated with the phage sample to be amplified and incubated with vigorous shaking at 37 °C for 4 and a half hours.

9.2.3.2. Plaque amplification of individual clones

Following titering of phage eluted from the final round of panning, clones were amplified separately, so DNA could be extracted and sequenced. An overnight culture of ER2738 was diluted 1:100 in 1 mL of LB medium. Individual clones were picked, using a pipetted tip, to inoculate the culture. Cultures were incubated with vigorous shaking at 37 °C for 4 and a half hours. Cultures were transferred to a microfuge tube and centrifuged 16,000*g* for 30 seconds, 500 µL was transferred into a fresh tube for DNA extraction (see section 9.4), 400 µL was transferred to a separate fresh tube and mixed with an equal volume of sterile glycerol (VWR, US) for storage at -20°.

9.2.3.3. Purification of amplified phage pools

To isolate and purify the amplified phage, the culture was transferred into a centrifuge tube and spun at 12,000 *g*, 4 °C, for 10 minutes to pellet the bacteria. The supernatant was transferred to a fresh tube and centrifuged again at 12,000 *g*, 4 °C, for 10 minutes. The upper 80% of the supernatant was transferred to a falcon tube and 1/6 of the volume of PEG-NaCl was added. Phages were precipitated overnight at 4 °C.

The phage/PEG/NaCl mixture was centrifuged at 12,000 *g*, 4 °C, for 15 minutes, the supernatant was discarded and the sample was re-spun. The remaining supernatant was carefully removed using a pipette. The pellet was re-suspended in 1 mL TBS and transferred to a microfuge tube and the sample was spun at 16,000 *g,* 4 °C, for 5 minutes. The supernatant was transferred to a fresh tube, 1/6 of the volume of PEG-NaCl was added and incubated in ice for 1 hour. Samples were centrifuged at 16,000 *g,* 4 °C, for 10 minutes, the supernatant was discarded and the sample was re-spun, any remaining supernatant was carefully removed using a pipette. The pellet was resuspended in 200 µL TBS, microfuged for 1 minute at 16,000 *g* 4 °C and transferred to a fresh tube.

This purified, amplified eluate can then be titred as described in 7.3. For long-term storage at -20 °C, an equal volume of sterile glycerol was added.

9.3. Cell panning

To identify phage clones which specifically bind to the target EMT cells, two panning strategies were employed. In the first, positive selection was carried out on cell monolayers of unsorted LuC4 cells or EMT cells isolated by FACS with a negative selection

carried out on Epi cells also isolated by FACS. The second protocol used a mixture of EMT and GFP-Epi cells, isolated by FACS, in suspension.

9.3.1. Phage display on cell monolayers

9.3.1.1. Positive selection

Unsorted LuC4 cells used in were harvested as described in section 5 while EMT and Epi CSCs used were isolated by FACS as described in 7.2.

For all populations, affinity selection was used following the protocol: $1x10^6$ cells were seeded into a T25 flask (Corning) and incubated at 37 °C for 24 hours. Before the first round of positive selection, ~ 2 x 10^{11} pfu of the naïve library was diluted in 2 mL of blocking buffer and incubated for 1 hour at 37 °C in a fresh T25 flask. This was to deplete the phage library of plastic binders.

Following 24 hours in culture, the target cell population was blocked for 1 hour at 37 °C with blocking buffer. Phage library-containing supernatant from the empty T25 flask was then transferred to a flask containing the target cell population and incubated for 1 hour at 37 °C. Cell monolayers were washed 3 times with wash buffer and bound phages were eluted by incubation with the low-pH elution buffer for 20 minutes. The supernatant was transferred to an eppendorf and neutralised with 1 M Tris-HCl (pH 9.1). The cell monolayer was washed twice with wash buffer, medium was added and cells were scraped from the surface. Cells were pelleted by centrifugation at 200 *g* for 10 minutes at 4 °C, cell pellets were lysed with cell lysis buffer.

After each round of selection, an aliquot of eluted phage was taken for titring as described in 9.2.2. Following the first and second rounds of panning, the remaining sample was amplified and purified as described in 9.2.3, the titre was then determined (see section 9.2.2)

After the third and final round of positive selection, individual clones were picked, amplified, and DNA was isolated for sequencing (see sections 9.2.3.2 and 9.4 respectively).

9.3.1.2. Negative selection

To deplete the phage pool of clones which bind to widely expressed cell surface

molecules, panning carried out in chapter IV, a round of negative selection was employed. Before the second round of positive selection, ~ 2 x 10^{11} pfu of the amplified output phage of round one were incubated with 1x10^{6} Epi cells, which had been in culture for 24 hours and pre-blocked with blocking buffer. Following incubation at 37 °C for 1 hour, the supernatant was removed and incubated with the target, EMT, cell population and positive selection was carried out as above.

9.3.2. Suspension panning

The selection of EMT cell-binding phage clones in suspension used the dilution of target cell with non-target cells which act as a 'sink' for phage to bind to general cell surface markers. To distinguish between target EMT cells and non-target Epi cells, a stably expressing LuC4-GFP line was used in addition to the Luc4 cell line used for previous selections.

Cells were dissociated using cell dissociation buffer and cell populations were isolated by FACS as described in 7.2. The use of a GFP cell line required a different fluorophore panel was used; CD44-APC and EpCAM-PE. EMT cells ($CD44^{high}$/$EpCAM^{low}$) were isolated from the non-fluorescent LuC4 line and Epi ($CD44^{high}$/$EpCAM^{high}$) cells were isolated from the LuC4-GFP line.

For the first round of panning, 1 x 10^{6} LuC4 cells were mixed with 1 x 10^{6} Epi cells in pre-blocked polypropylene FACS tube in DMEM/F-12 media 10 % FCS, 100 Units/ ml penicillin, 100 μg/ml streptomycin, and RM^{+}. 2 x 10^{11} pfu of the naïve library was added and cells were incubated for 1 hour at 37 °C. Cells were washed 3 times with PBS and resuspended in PBS plus DAPI, FACS was used to isolate the GFP-negative target EMT cells. Sorted cells were centrifuged at 300*g* for 5 minutes at 4 °C then lysed with lysis buffer. An aliquot was taken to titre the eluted phage as described in 9.2.2. Following the first and second rounds of panning the remaining eluate was amplified as described in 9.2.3.1.

The second round of panning used a 10-fold excess of GFP-Epi cells compared to the EMT cells, and was carried out as above.

The third round of panning used 6-times the number of GFP-Epi cells compared to the EMT cells, and was carried out as above. Individual clones were picked and amplified as described in 9.2.3.2.

9.4. DNA extraction and sequencing

Once individual phage clones from the third round of panning were picked and amplified, individually extraction and sequencing of the M13 phage DNA allows identification of the peptide sequence responsible for binding.

To the 500 µL set aside, following clone amplification as in 9.2.3.2, 200 µL PEG-NaCl was added, mixed, and incubated at room temperature for 20 minutes. Samples were microfuged at 16,000*g* for 10 minutes at 4 °C and the supernatant was discarded. Tubes were re-spun briefly and residual supernatant was removed with a pipette. The pellet was resuspended in 100 µL of iodide buffer, 250 µL of ethanol was added and samples were incubated for 20 minutes at room temperature to precipitate the single stranded DNA. Samples were microfuged at 16,000*g* for 10 minutes at 4 °C and the supernatant was discarded. Pellets were washed with 500 µL ice-cold 70 % ethanol, re-pelleted and the supernatant was removed with a pipette. Pellets were dried for 5 minutes under a vacuum (Eppendorf® centrifugal vacuum concentrator, Germany). Pellets were re-suspended in TE buffer (10 mM Tris-HCl, 1 mM EDTA) and stored at -20 °C.

DNA was quantified using the Nanodrop ND-100 spectrophotometer (Labtech, UK) and aliquots were sent to Source Bioscience for Sanger sequencing using the -96 gIII sequencing primer 5´- HOCCC TCA TAG TTA GCG TAA CG –3´.

DNA sequences were processed using CLC Sequence Viewer version 8.

9.5. Assessment of phage binding

9.5.1. Enzyme-linked immunosorbent assay

To determine the ability of isolated clones to bind to the target cells, an enzyme-linked immunosorbent assay (ELISA) was used. The page binding ELISA uses a horseradish peroxidase (HRP)-conjugated mouse antibody, α-M13-HRP (GE Healthcare, US), which recognises the VIII coat protein on M13 bacteriophage.

The ELISA works based on the principle that, the α-M13-HRP will bind to M13 phages, which are bound to target molecules on the LuC4 cells. On addition of a substrate for HRP, a colour change is seen that is proportional to the amount of antibody binding and therefore the amount of M13 bound to the target.

There are several HRP substrates which can be used in ELISAs, 3,3′,5,5′-Tetramethylbenzidine (TMB, Sigma Aldrich) is oxidised by HRP (Figure 16) to produce 3,3',5,5'-tetramethylbenzidine diimine which has a blue colour. When the reaction is stopped using sulfuric acid, the colour changes to yellow which can be measured at 450 nm. TMB was selected for use in these studies as it is very sensitive to HRP so can produce a colour change more rapidly than other substrates.

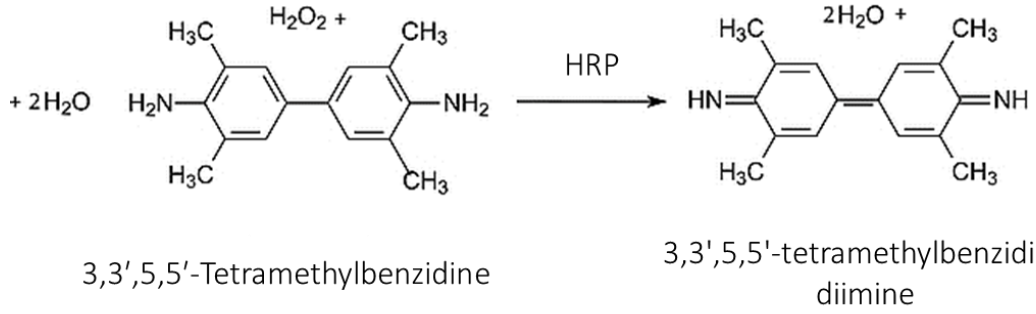

Figure 16: **Oxidation of 3,3',5,5'-tetramethylbenzidine,** by horseradish peroxidase to 3,3',5,5'-tetramethylbenzidine diamine. Image modified from product information (Sigma Aldrich).[229]

9.5.1.1. Cell monolayer

During optimisation of the method, detailed in chapter IV, and subsequent applications of the technique, all experiments used the following general protocol. Cells were harvested with trypsin-EDTA and seeded into a 96-well plate at a density of between 5,000 and 20,000 cells/well. Cells were incubated for 48 hours at 37 °C, 5% CO_2, medium was removed and blocked in PBS 3% BSA (or as described) for 1 hour at 37 °C. Approximately $1x10^9$ pfu of individual amplified phage clones was added to each well in blocking buffer and incubated for 1 hour at 37 °C. Cells were washed 3 times with PBST (0.05%) and HRP-conjugated anti-M13 antibody was added in block buffer diluted 1:5000 and plates were incubated for 1 hour at 37 °C. Cells were washed 3 times with PBST (0.05%) and TMB, the HRP substrate solution, was added. Plates were incubated at room temperature for 45 minutes and the reaction was stopped by addition of 1 M H_2SO_4. Absorbance values were measured on the Synergy HT plate reader at 450 nm and 540 nm.

9.5.2. Cell suspension

To assess the binding of the clone selected by FACS-assisted panning, the ELISA detailed

in 6.6.1.1 was modified so phage binding could be carried out on cells in suspension. EMT and Epi cell populations were isolated by FACS, described in 4.2, seeded into tissue culture flask and incubated for 48 hours at 37 °C, 5% CO_2. Cells were dissociated using cell dissociation buffer and washed with PBS. ~ 1 x 10^5 cells were transferred into polypropylene FACS tubes. Approximately 5x10^9 pfu were added to the cells, in block buffer (9.1.7), and incubated for 1 hour on ice. Cells were washed with PBS anti-M13-HRP was added (1:5000) in block buffer and incubated for 1 hour on ice. Cells were washed and were transferred to a fresh tube. TMB the HRP substrate was added and tubes were incubated for 20 minutes at room temperature. Reaction was stopped by addition of 1 M H_2SO_4 and 100 µL of supernatant was transferred to a 96-well plate. Absorbance values were measured on the Synergy HT plate reader at 450 nm and 540 nm.

9.5.3. Flow cytometry

To assess phage binding by flow cytometry, cells were harvested with either trypsin-EDTA or cell-dissociation reagent, for clones identified by methods in 9.3.1 or 9.3.2, respectively.

Cells were washed, and resuspended in PBS. Samples were incubated with ~1x10^8 pfu of a single clone in block buffer for 1 hour on ice. Cells were washed and anti-M13 was added (1:5000) in block buffer and incubated for 1 hour on ice. Cells were washed and Alexa fluor 488 goat anti-mouse secondary antibody (Thermo Fisher Scientific) was added in block buffer and incubated for 1 hour on ice. Samples were washed twice and transferred to a fresh tube, CD44-APC and EpCAM-PE were added (1:100) in block buffer and incubated for 15 minutes. Samples were washed for the final time and resuspended in PBS-DAPI (200 ng/mL).

Double stained (CD44-APC and EpCAM-PE) samples were used to assess the presence of the EMT sub-population and control samples were used to determine thresholds for positive and negative signals (Table 3). The same antibodies were used in both the Alexa fluor 488 positive and negative samples, however, the order in which they were incubated with the cells was different. The CD44 and EpCAM antibodies are murine antibodies, and as such the Alexa fluor 488 goat anti-mouse will bind to them, which would produce a positive signal even in the absence of the anti-M13 which is its target in this assay. For the Alexa fluor 488 positive sample, the CD44 and EpCAM antibodies were

added first and the Alexa fluor 488 was added subsequently. For the Alexa fluor 488 negative sample, the 488 was incubated with the cells, which were then washed before the other antibodies were added. Antibodies which were added first are denoted by * in Table 3.

Table 3: Antibody staining of control samples for detection of phage binding by flow cytometry. Where an X indicates the used of antibody in the staining mix.

	PHAGE	ANTI-M13	ALEXA FLUOR 488	CD44-APC	EPCAM-PE	EPCAM-APC
UNSTAINED	-	-	-	-	-	-
SECONDARY ONLY	-	-	X	-	-	-
CD44-APC ONLY	-	-	-	X	-	-
EPCAM-PE ONLY	-	-	-	-	X	-
EPCAM-APC ONLY	-	-	-	-	-	X
ALEXA FLUOR 488 POSITIVE	-	-	X*	X	X	-
ALEXA FLUOR 488 NEGATIVE	-	-	X	X*	X*	-
STANDARD CSC STAIN	-	-	-	X	X	-

10. Effect of HA glycopolymerson cancer cells

To investigate the biological properties of the HA glycopolymers described in section 4 two assays were performed to ensure that the polymers were non-toxic and to see if they altered the sphere-forming ability of HNSCC cells.

10.1. Live dead assay

Before cell behaviour assays could be carried out, the LIVE/DEAD™ Viability/Cytotoxicity Kit for mammalian cells (Invitrogen), was used to assess cell viability following treatment with the synthetic polymers. The two-colour fluorescence assay used Calcein acetoxymethyl (AM) to label live cells and Ethidium homodimer-1 (EthD-1) to label dead cells. Calcein AM is a non-fluorescent molecule which is cell-permeable, once inside the cell hydrolase enzymes are able to convert it to the fluorescent calcein, which has a peak excitation of 495 nm and peak emission is at 517 nm. As dead cells are not enzymatically active they are not stained green by calcein. Conversely, EthD-1 is not able to cross the intact cell membrane, so is excluded from live cells and once it has entered dead cells it will bind to DNA which increases fluorescence intensity. EthD-1 has a peak excitation of 528 nm and peak emission is at 617 nm.

The kit was used as per manufacturer's instructions, briefly LuC4 cells were seeded at 5,000 cells per well into a 96 well plate and cultured in a humidified atmosphere at 37°C, 5% CO_2 for 48 hours. Cells were treated with glycopolymers at a range of concentrations, 100, 10, 1, 0.1 µg/mL, and incubated for 24 hours. Medium was removed and Live/dead stains were added, diluted in PBS and incubated for 1 hour at 37°C. Fluorescence was read at ex: 485/20, em: 528/20 and ex: 530/25, em: 590/35 using Synergy HT. The number of live and dead cells was calculated as a percentage compared to controls (see Table 4) and analysis was carried out using Prism 7 (GraphPad, US).

Table 4: Live/dead viability/cytotoxicity assay controls. Where an X indicates the cell viability, dye, and presence of glycopolymer in each control group.

	CELL TYPE		CELL STAIN		
	Live	Dead	Calcein AM	EthD-1	Glycopolymer
LIVE CELL POSITIVE	X	-	X	-	-
DEAD CELL NEGATIVE	X	-	-	X	-
LIVE CELL NEGATIVE	-	X	X	-	-
DEAD CELL POSITIVE	-	X	-	X	-
GLYCOPOLYMER CONTROL	-	-	X	X	X

10.2. Sphere assay

The ability of cells to form spheres in culture has historically been used as an indicator of stem-cell potential.[230] When cells are seeded at a low density in non-adherent plates, a fraction of cells is able to proliferate and form spheres which can grow in suspension, thus satisfying the self-renewal component of stem cell requirements.

10.2.1. Non-adherent plate formation

Non-adherent plates were prepared by coating with Poly(2-hydroxyethyl methacrylate) (polyhema, Sigma Aldrich). A 12 mg/mL solution of polyhema was made up in 95% ethanol and 200 µL was transferred to each well of a 24-well plate (Corning). Plates were left to dry inside a closed tissue culture hood, with the lid off, overnight. Plates were stored at 4 °C until needed.

10.2.2. Plating cells for spheres

Cells were isolated as described in section 4, passed through a 100 µm filter to ensure a single cell suspension, and counted. Cells were resuspended in medium, as defined in section 7, containing 1% methylcellulose (Sigma Aldrich). They were then plated at a density of 1000 cells/ well in the polyhema-coated plates and treated with either HA or glycopolymers as stated. Plates were incubated at 37 °C, 5% CO_2 for two weeks, formation of spheres was monitored throughout and images were acquired with the IN Cell Analyzer 2200 (GE Healthcare, US). Analyses were performed using GE Developer Toolbox 1.9.2, ImageJ 1.52a software, and Prism (GraphPad).

11. Statistical Methods

Statistical analyses were carried out using GraphPad Prism software version 7.0. Standard deviation (SD) is a measure of the variation with in a data set and was used to assess the spread of the data about the mean. It was calculated using Equation 7.

Equation 7: Standard Deviation

$$s = \sqrt{\frac{\sum_{i=1}^{N}(x_i - \overline{x})^2}{N-1}}$$

To determine any statistically significant differences present between experimental groups Analysis of variance (ANOVA) was used. A one-way ANOVA was used to compare

the means of data from experiments investigating one factor, where grouped data were collected and the effects of two factors were investigated a two-way ANOVA was used.

Multiple comparisons testing was carried out following both one- and two-way ANOVA, the Tukey-Kramer test was selected to calculate multiplicity adjusted P values as the mean of each group was compared to the mean of each of the other groups.

SECTION 3: RESULTS AND DISCUSSION

Chapter III: Supramolecular Presentation of Hyaluronan onto Model Surfaces for Studying the Behaviour of Cancer Stem Cells

1. Introduction

The ability to fabricate well-defined substrates to control and investigate cell behaviour provides a useful tool for *in vitro* cell culture. For instance, it is increasingly important for the regulated production of *in vitro*-expanded or differentiated cells for cell-based therapies. In this regard, self-assembled monolayers (SAMs) can provide a rapid and simple method for fabricating well-ordered surfaces with a wide range of useful functionalities.

SAMs provide a useful platform for high-throughput screening of peptide-cell interactions to identify surfaces able to elicit the desired effect on cells in culture.[101,201,231] They have been successfully employed to influence cell adhesion, support proliferation, and direct differentiation or even maintain pluripotency of stem cells.[194–196,198,199] One potential benefit from using SAMs in cell expansion is the elimination of the need for animal-derived products to support cell proliferation, which is crucial for the expansion of cells which are to be used in cellular therapies.

The interaction between SAMs and cell culture components, in the form of either cells or serum proteins, can be exploited to examine in more detail the role of such proteins in cell behaviour. For example, how the conformation of adsorbed fibronectin impacts the way in which it interacts with cells, influencing adhesion, focal adhesion formation, cell spreading, and differentiation.[198,232,233] In addition, the density and spacing of functional groups can be controlled[234] and the use of micro-contact printing (μCP) enables SAMs to be formed in discrete patterns, which can be used to further regulate cell adhesion and even migration.[200,206]

However, the use of SAMs for the non-covalent immobilisation of individual extracellular matrix (ECM) components is less frequently used. Hyaluronic acid (HA) is the only non-sulfated glycosaminoglycan (GAG) which comprises a large part of the ECM of many tissues. It is made up of alternating D-glucuronic acid and *N*-acetyl-D-glucosamine monomers, containing hydrophilic and hydrophobic patch domains.[61,66] While the

hydrophilic carboxyl, hydroxyl and acetamido groups confer high water solubility to HA, the hydrophobic regions, created by axial hydrogen atoms, can reversibly interact with each other to form a meshwork. In addition, hydrogen bonding between the hydrophilic side groups contributes to the porous mesh-like structure which is formed in solution, and retains water. Internal swelling pressure is generated on compression of HA networks and, when this pressure is released, mutual repulsion between carboxyl groups allows a return to its original shape.[63] *In vivo*, this is a key characteristic which significantly contributes to the viscoelastic properties of several tissues, including cartilage[235] and the vitreous humour.[64]

These features make HA a very promising biomaterial for biotechnological and biomedical applications. Through chemical crosslinking, robust hydrogels can be created whose mechanical characteristics can be precisely tuned by the type and degree of crosslinking.[236] Additionally, HA can be modified to incorporate signalling molecules [237] or cell binding peptides[238] to stimulate cell adhesion and proliferation, or be used to functionalise scaffolds to the same effect[239] and to direct cell differentiation.[237,240]

In addition to its desirable biophysical characteristics for use in bioengineering, HA itself interacts with cells via cell-surface receptors such as CD44 and receptor for hyaluronan-mediated motility (RHAMM), eliciting a range of cellular responses. HA is also seen to accumulate in the tumour microenvironment, and signalling via these receptors, can support metastasis, cancer cell proliferation, and multidrug resistance.[59,74,217,241,242] Within head and neck squamous cell carcinoma (HNSCC) there is a sub-population of stem-like cells (herein referred to as cancer stem cells or CSCs) with tumour-initiating potential and the ability to restore tumour heterogeneity.[6] These cells are thought to play an important role in tumour progression and are identified predominantly by their higher CD44 expression levels.[6,15] It has been demonstrated that signalling downstream of HA-CD44 interactions can regulate stem cell markers and highlights the role of HA in HNSCC progression.[243,244]

Due to the pivotal role of HA in many cellular processes, numerous strategies have been developed to immobilise HA on surfaces, aiming to study its effects in a 2D *in vitro* environment. These approaches often require the chemical modification of native HA by

biotinylation,[84] conjugation to dopamine,[86,87] thiolation,[88] azidation,[89] or functionalisation of surfaces to allow covalent attachment of HA.[90–93]

However, such modifications can interfere with the native properties of HA. For example, thiolation has been shown to inhibit HA degradation by hyaluronidases,[96] and influence its conformation once immobilised. Altered presentation of macromolecules has been shown to affect cell adhesion and highlights the sensitivity of mammalian cells to their culture environment and the importance of creating well-defined surfaces for *in vitro* studies of cell behaviour.[97,98]

Herein, we demonstrate a straightforward platform for the immobilisation of HA in its native form on a gold surface using a SAM consisting of a thiolated HA-binding peptide.[131] To the best of our knowledge, the supramolecular assembly of HA using HA-binding peptides has not yet been exploited to study the effects of HA *in vitro*. We believe that this approach provides important advantages over the previously mentioned methodologies. Firstly, it does not require any chemical modification of HA, thus allowing a more biomimetic presentation similar to the natural ECM. Secondly, our method is simple and rapid, while offering precise control over HA presentation, which is advantageous when attempting to control cell behaviour.

2. Results and Discussion

2.1. Thiolated HA-binding peptide for and the supramolecular presentation of HA

In this work, we have taken a 12-amino acid HA-binding peptide identified through phage display, named Pep-1, to produce SAMS on gold via peptide thiolation at the N-terminal (Figure 17A). Alanine scanning revealed that there are six residues which are required for Pep-1-HA binding, these residues are organised in two groups of three at positions 4,5,6 and 9,10,11.[131] Of these amino acids four are non-polar, as such it is hypothesised that hydrophobic-hydrophobic interactions between these residues and the hydrophobic patches present on HA are responsible for binding.[132]

It has been suggested that the free N-terminal in phage-displayed peptides may be important for sequence binding function. So it is possible that as our system tethers the N-terminal to the Au surface, and the C-terminal of the peptide is free, that binding may

be affected. However, we anticipate that the repeating disaccharide structure of HA, means that there are not discreet binding sites and Pep-1 is able to interact along the length of the molecule. Additionally, immobilisation of Pep-1 via the N-terminal has previously been demonstrated to have no obvious effect on HA-binding ability.[133]

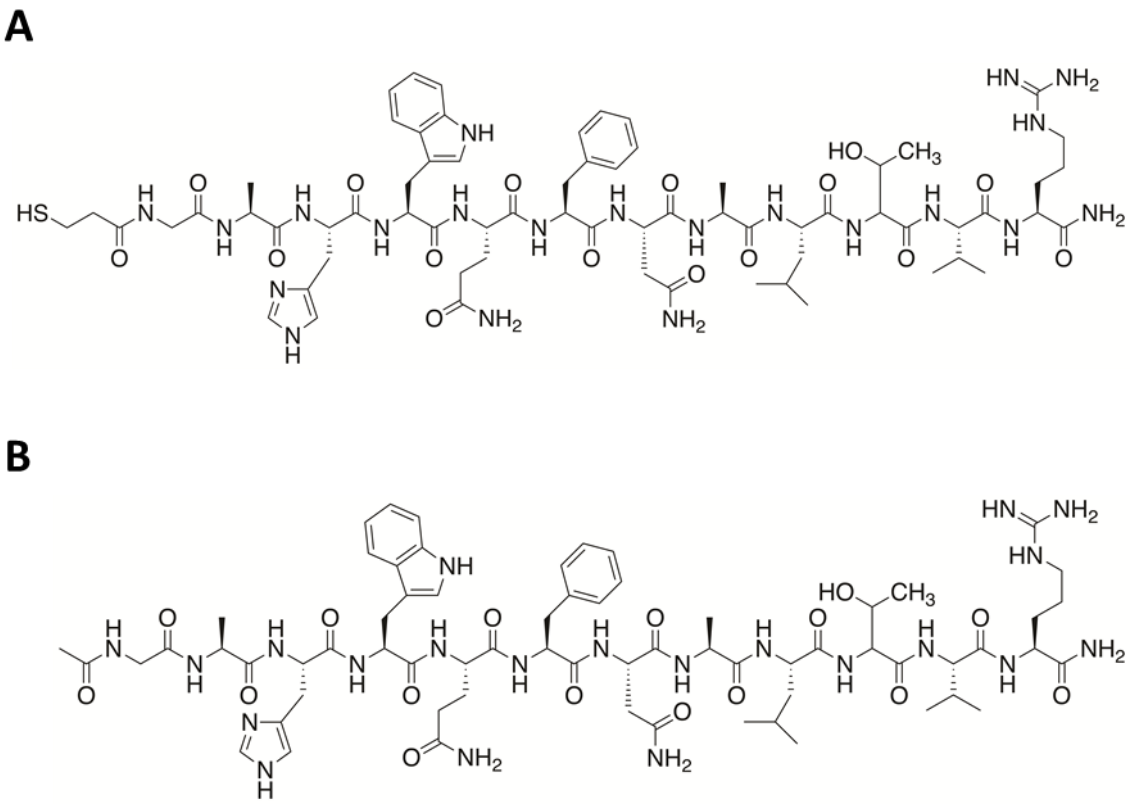

Figure 17: Chemical structure of peptides used: thiolated Pep-1 (A) and acetylated Pep-1 (B) drawn in Chemdraw Prime 17.1

This peptide has a distinct sequence which does not contain the consensus domain observed in several HA-binding proteins, including CD44 and RHAMM.[131] The assessment of this peptide's binding ability to HA-coated beads has revealed a dissociation constant (K_d) value of ~ 1.65 µM.[131] Studies into the function and effects of Pep-1 have been conducted,[245] demonstrating its ability to bind HA in solution, immobilised on a surface or in complex with cells both *in vitro* and in tissue sections.[132,213] On binding, Pep-1 influences HA-mediated signalling and has been used as an inhibitor of HA function.[134,246] It has previously been modified and subsequently used to form a peptide layer on human

cartilage samples and contact lenses, which sequestered HA, improved water retention and resulted in an enhanced surface lubrication.[133,247] The covalent bond between thiol groups and gold (Au) is well-known and is often used in the formation of SAMs on Au substrates. As such, we expect that the thiolated Pep-1 (herein referred to as HS-Pep-1) will form a monolayer on Au, which can further immobilise HA in its native form. Figure 18 illustrates the proposed model for HS-Pep-1 SAM formation (Figure 18B) on an Au surface (Figure 18A) and the subsequent immobilisation of HA (Figure 18C) and interaction will mammalian cells (Figure 18D). To confirm that the HS-Pep-1 binds to the Au substrate, we used both quartz crystal microbalance with dissipation (QCM-D) monitoring and water contact angle to monitor changes in the film's hydrated thickness and areal mass density, as well as in the surface hydrophobicity, respectively.

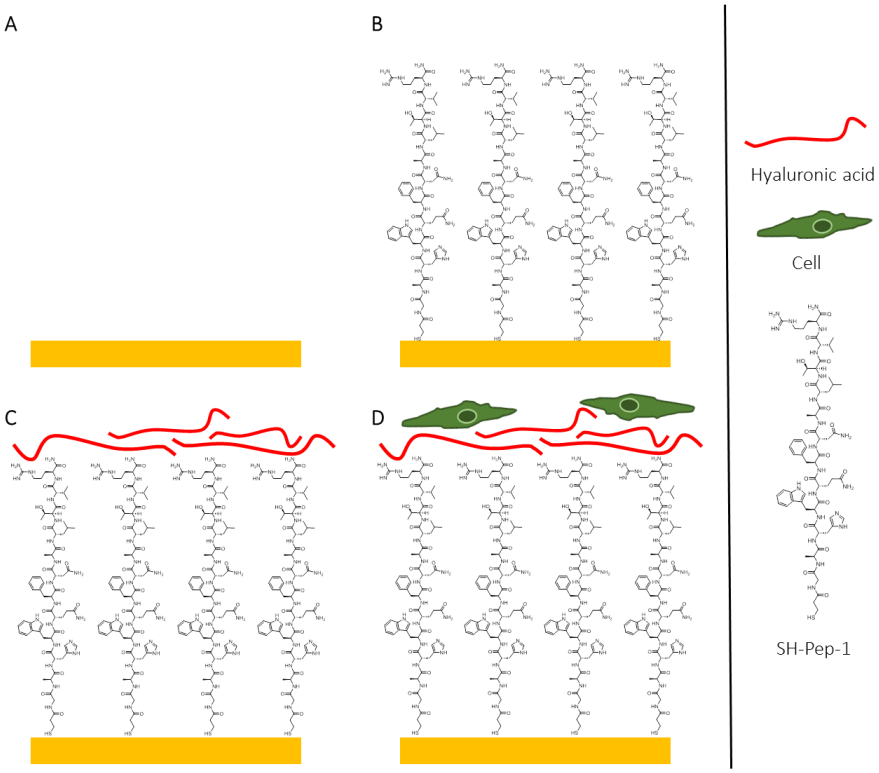

Figure 18: **Illustration of the proposed supramolecular immobilisation of HA on surfaces to study cell behaviour**. Bare gold surface (A), incubated with a solution of HS-Pep-1 to form a SAM (B) which can bind HA (C) and in turn can be used to probe HA interactions with cells in culture (D).

Using QCM-D apparatus, a decrease in the resonance frequency, normalised to the 7th overtone (n = 7; 35 MHz; $\Delta f_7/7$), was observed as a function of time following the addition

of a 0.01 mM aqueous solution of HS-Pep-1 (-18.7±1.2 Hz). This decrease in the $\Delta f_7/7$ was maintained following washing steps (Figure 19), which reveals the strong interaction of the HS-Pep-1 layer with the Au surface. At the same time, a negligible shift in the energy dissipation factor was obtained at the 7th overtone ($\Delta D_7 < 0.3\times10^{-6}$). The very low dispersion in the $\Delta f_n/n$ confirms that HS-Pep-1 adsorbs rigidly onto the Au surface (Figure 19).

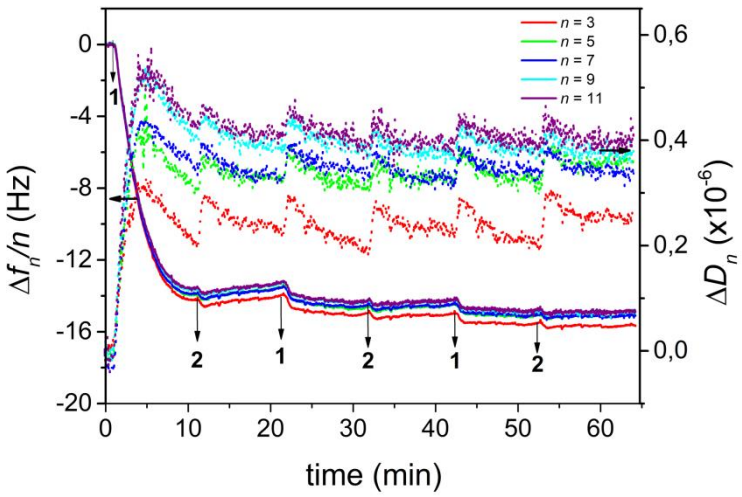

Figure 19: Representative QCM-D data for the normalised frequency ($\Delta f_n/n$) and dissipation (ΔD_n) shifts obtained as a function of time for the deposition of HS-Pep-1 (1) onto Au-coated quartz crystal sensors and intermediate rinsing steps (2).

Therefore, the adsorbed HS-Pep-1 layer can be considered as a rigid film and, thus, the Sauerbrey equation can be used to estimate the areal mass density of the adsorbed HS-Pep-1 layer ($\Delta m_{Sauerbrey}$ = 329.6±65.5 ng/cm^2). Based on this assumption, the QCM-D data and the Sauerbrey relationship were also used to estimate the thickness of the adsorbed HS-Pep-1 layer ($h_{Sauerbrey}$ = 3.3±0.6 nm). However, as the film is hydrated, one should bear in mind that the obtained areal mass density of the film may include the mass of the adsorbed layer plus coupled solvent. Therefore, for comparison, the areal mass density and hydrodynamic thickness of the adsorbed HS-Pep-1 layer were also estimated using the Voigt-based viscoelastic model ***Table 5***. In addition to the observed changes in the normalised frequency and energy dissipation shifts, the water contact angle decreased from 76.9±6.2° on bare Au, to 66.7±2.7° after incubation with a 1 mM ethanolic solution of HS-Pep-1 (Figure 20D, E). This indicates an increase in the hydrophilicity and a change

in the surface chemistry of the Au, through HS-Pep-1 deposition. A further decrease in the water contact angle to 57.9±4.2° was observed when the surfaces coated with the HS-Pep-1 SAM were exposed to an aqueous solution of 1.5 MDa HA (Figure 20D, E), indicating that the overall surface became more hydrophilic. This decrease in hydrophobicity upon HA binding was expected due to the high number of hydroxyl and carboxyl groups present in HA which confer its high water solubility. This value is higher than those reported in the literature, where values of 24.8±0.1° and 12.8±0.6° were obtained for similar HA-coated surfaces. However, in those cases HA was immobilised by co-deposition with poly-dopamine or by covalent attachment to the Au surface, respectively.[35, 38] Such differences in the immobilisation methods can be proposed as the main reason for the discrepancy between these values and the ones obtained in the current study reaching values of 354.1±96.6 ng/cm^2 (Δm_{Voigt}) and 3.7±1.0 nm (h_{Voigt}), respectively. These values are in the range of those obtained using the Sauerbrey model, thus meaning that the obtained areal mass density and thickness are mainly assigned to the adsorption of the HS-Pep-1 layer, and the effect of the coupled solvent can be considered negligible.

A further decrease in the $\Delta f_7/7$, and thus increase in the areal mass density, as well as an increase in the ΔD_7, was seen after the adsorption of the HA biopolymer (1.5 MDa) onto the HS-Pep-1-coated Au surface, reaching values of -9.1±2.7 Hz and (1.8±0.2) ×10^6, respectively (Figure 20A). The overtones become separated after the addition of the HA layer, which is a typical behaviour of a soft and hydrated film (Figure 21). This reveals the viscoelastic behaviour of the adsorbed HA layer, which is a common characteristic of most polymeric systems.[248,249] Therefore, the Voigt-based viscoelastic model was used to estimate the areal mass change (1154.0±492.1 ng/cm^2) and the hydrodynamic thickness (10.8±4.8 nm) of the adsorbed 1.5 MDa HA layer. This is within the thicknesses reported in the literature, Choi *et al.* see a HA layer thickness of between 8.9 and 2.1 nm depending on the pH. Their work also suggests that depending on the pH of the HA solution the amount of HA deposition can be controlled.

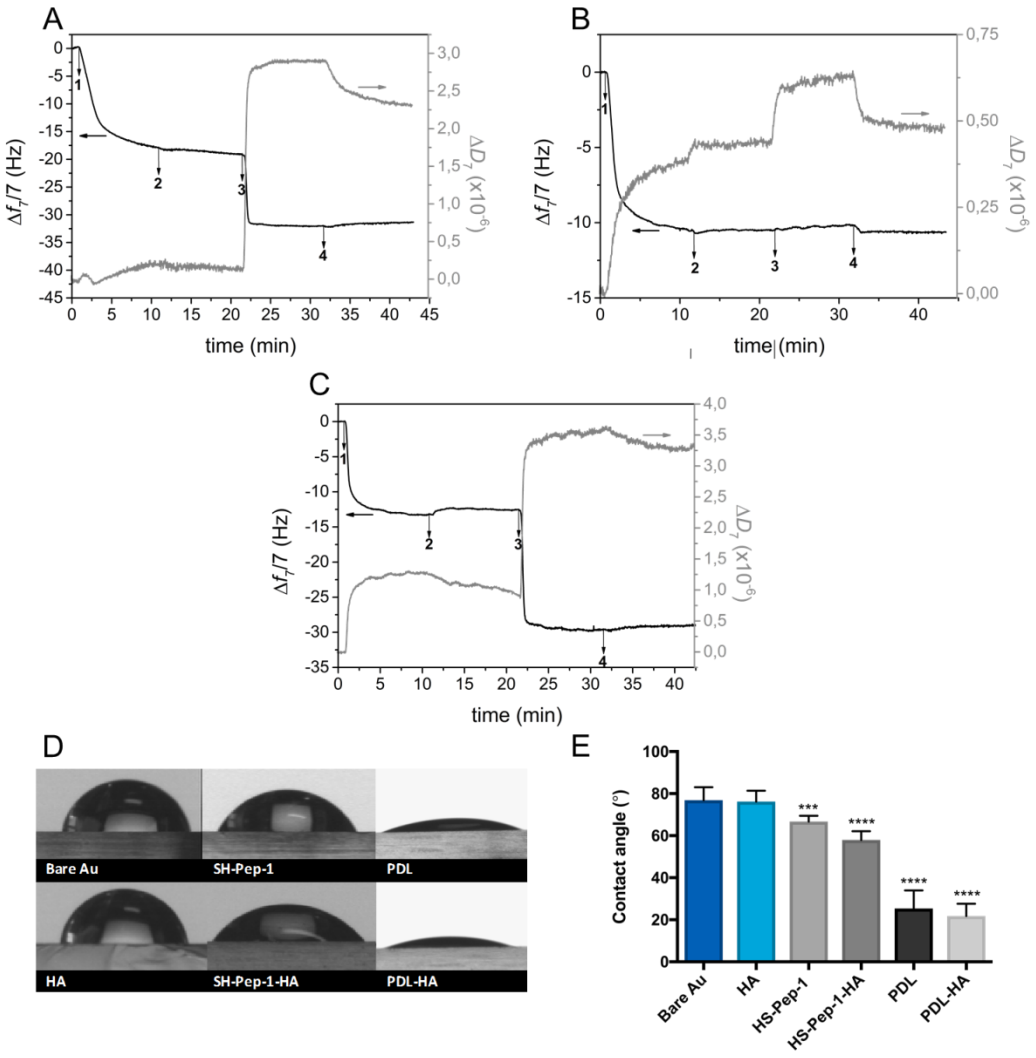

Figure 20: HS-Pep-1 attaches to an Au substrate which can then bind HA. Representative QCM-D data showing the normalised frequency ($\Delta f_n/n$) and dissipation (ΔD_n) shifts obtained at the 7th overtone (n = 7; 35 MHz) as a function of time for the deposition of HA onto HS-Pep-1 (A), Ac-Pep-1 (B), or PDL (C) modified Au-coated quartz crystal sensors with intermediate rinsing steps. Numbers refer to the adsorption of HS-Pep-1, Ac-Pep-1, or PDL (1), 1.5 MDa HA (3), and rinsing steps (2 and 4). The addition of a 0.01 mM HS-Pep-1, 0.01 mM Ac-Pep-1, or 0.1 mg/mL PDL in 150 mM NaCl (1) leads to a decrease in the frequency shift which is maintained upon washing (2). The addition of 1.5 MDa HA in 150 mM NaCl (3) to HS-Pep-1 or PDL-coated crystals causes a further decrease in frequency shift (A and C). The addition of 1.5 MDa HA in 150 mM NaCl (3) to Ac-Pep-1 coated crystals did not alter the frequency. Water contact angle images of the prepared surfaces (D) and a graph showing the average contact angles for all surfaces (E). n=3, error = SD, ****= p<0.0001, ***=p<0.001 compared to bare Au control (one-way ANOVA with Tukey's multiple comparison).

For comparison, when acetylated Pep-1, without the thiol group (herein referred to as Ac-Pep-1) was used, a smaller decrease in the $\Delta f_7/7$ (-10.5 Hz) was seen, which was maintained upon washing (Figure 20B). To explain these results, we hypothesise that the Ac-Pep-1 was able to interact with the bare Au surface through the positively charged arginine residues (i.e. amino groups) at the C-terminal of the peptide. This would also explain the lack of adsorption of the negatively charged HA onto the Ac-Pep-1-modified Au surface as the amino groups would be inaccessible and the acetyl groups would not interact with the HA (Figure 20B).

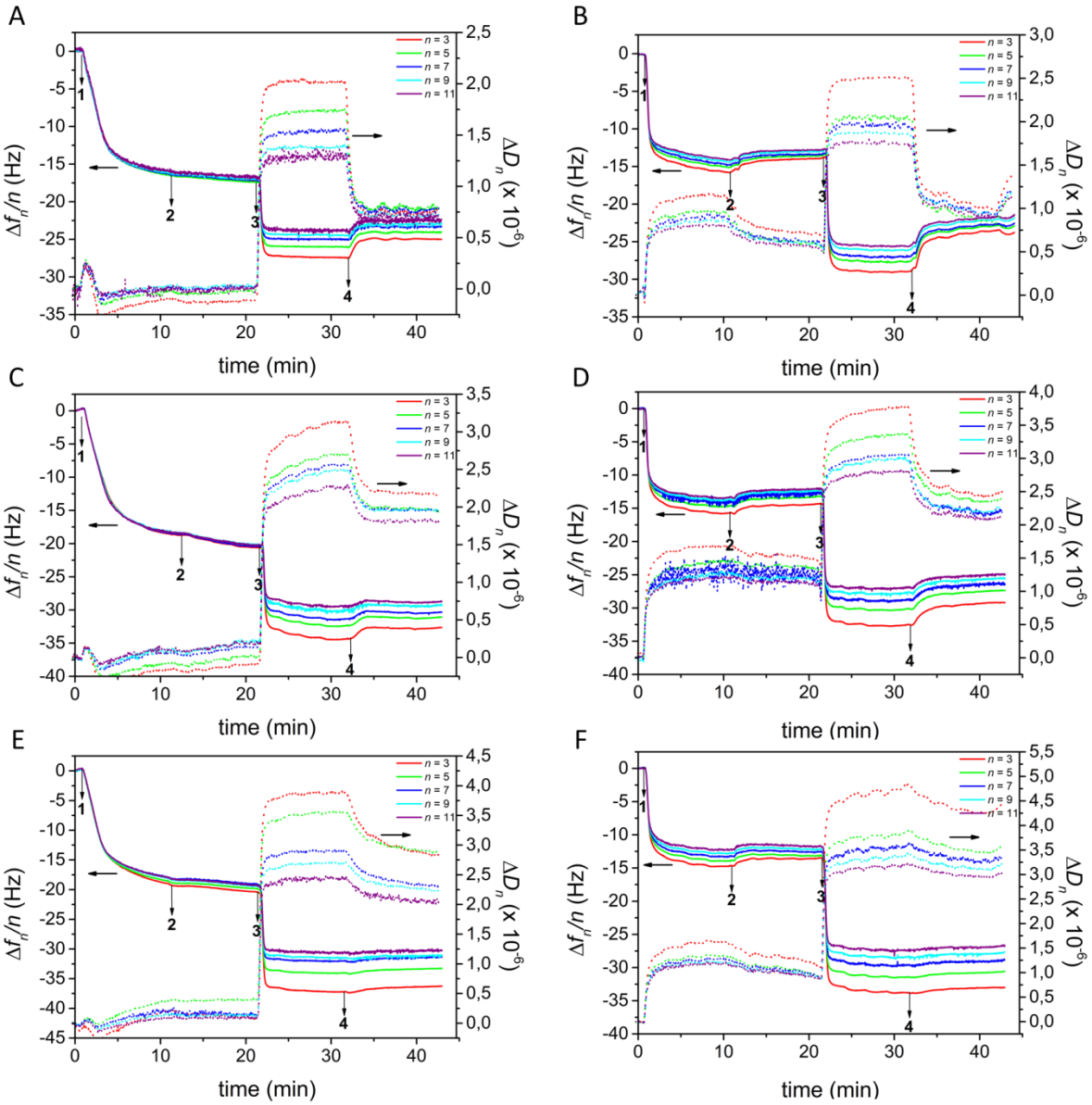

Figure 21: **QCM-D measurement of the normalised frequency ($\Delta f_n/n$) and dissipation (ΔD_n) shifts with a range of HA molecular weights.** Representative QCM-D data for $\Delta f_n/n$ and ΔD_n as a function of time for the deposition of HA onto HS-Pep-1- and PDL-modified Au-coated quartz crystal sensors and rinsing steps. Numbers refer to the adsorption of (1) HS-Pep-1 (A, C, E) or PDL (B, D, F), (2) rinsing step, the adsorption of (3) 20 kDa HA (A, B), 200 kDa (C, D) or 1.5 MDa HA (E, F) and a further (4) rinsing step. For both HS-Pep-1 and PDL their addition in an aqueous solution of 150 mM NaCl leads to a decrease in frequency shift which is maintained on washing. A further decrease in frequency shift was seen on addition of each HA molecular weight, which was also maintained on washing.

Table 5: Average changes in $\Delta f_7/7$ (Hz) and ΔD_7 at the equilibrium, as measured by QCM-D, and modelled thickness (h, nm) and areal mass density (Δm, ng/cm^2), derived using the Sauerbrey equation and the Voigt-based viscoelastic model. Values show a decrease in frequency and an increase in dissipation when HA solution is incubated with different surfaces. All values are the average of at least 3 independent experiments ± SD.* denotes experiment with only 2 independent repeats.

	$\Delta f_7/7$ (Hz)	ΔD_7 (x10^{-6})	Voigt Thickness, h_{Voigt} (nm)	Voigt Mass Density, Δm_{Voigt} (ng/cm^2)	Sauerbrey Thickness, $h_{Sauerbrey}$ (nm)	Sauerbrey Mass Density, $\Delta m_{Sauerbrey}$ (ng/cm^2)
Adsorption onto Au						
HS-Pep-1	-18.7±1.2	0.3±0.3	3.7±1.0	354.1±96.6	3.3±0.6	329.6±65.5
PDL	-12.4±1.5	0.7±0.3	12.9±3.6	1276.0±366.4	-	-
Adsorption onto HS-Pep-1						
1.5 MDa HA	-9.1±2.7	1.8±0.2	10.8±4.8	1154.0±492.1	-	-
200 kDA HA	-9.7±2.5	1.4±0.4	10.4±1.4	919.5±329.5	-	-
20 kDa HA	-5.5±1.1	0.6±0.2	5.4±1.8	640.0±147.3	-	-
Adsorption onto PDL						
1.5 MDa HA	-16.1±0.3	2.4±0.3	12.1±6.6	1342.0±653.7	-	-
200 kDA HA	-11.5±1.6	1.5±0.4	3.8±1.5	396.7±166.2	-	-
20 kDa HA*	-9.7±0.4	0.5±0.1	1.6±0.4	270.0±99.0	-	-

The direct exposure of the Au surface to an aqueous solution of HA, in the absence of a HS-Pep-1 SAM, did not result in a change in the contact angle (Figure 20D, E) or deposition onto the bare Au surface (Figure 22).

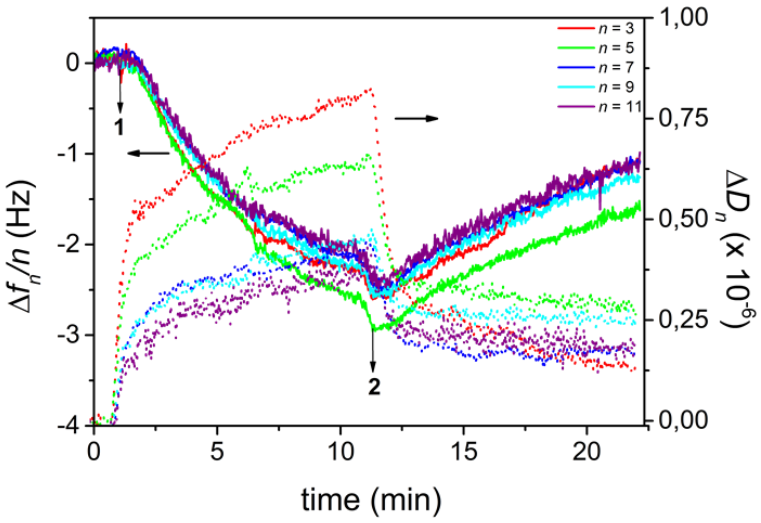

Figure 22: **Representative QCM-D data for the normalised frequency ($\Delta f_n/n$) and dissipation (ΔD_n) shifts** as a function of time for the deposition of 200 kDa HA on Au-coated quartz crystal sensors and rinsing steps. Numbers refer to the adsorption of (1) HA and (2) rinsing step. The addition of HA aqueous solution in 150 mM NaCl leads to a decrease in frequency shift which is reversed on washing. This result shows negligible HA adsorption onto the Au-coated quartz crystal.

Taken together, these results demonstrate that the immobilisation of HS-Pep-1 onto the Au surface leads to a rigid film and does not inhibit its ability to bind HA through the arginine residues at the C-terminal. Hence, it can be used for the supramolecular presentation of HA. This system could be advantageous over other platforms for *in vitro* studies, due to the ease of HS-Pep-1 monolayer formation without loss of HA-binding ability. Moreover, it does not require multi-step chemical modification of the surface or the chemical modification of HA. The supramolecular immobilisation involves weaker attractive forces (electrostatic interactions between negatively charged HA and the positively charged HS-Pep-1-modified Au surface), therefore producing a more physiologically relevant platform for the investigation of cell behaviours.

2.2. HA immobilisation using HS-Pep-1 and poly-D-lysine model surfaces

To probe any differences in HA deposition between our system and existing methods, poly-lysine was used as a model surface for comparison. Poly-lysine is a positively charged hydrophilic polyelectrolyte at a physiological pH (p*K*a ~10.5[218]) and is frequently used in layer-by-layer assembly studies in combination with oppositely charged HA.[250] Poly-lysine

readily adsorbs onto prepared surfaces and due to its positive charge can immobilise HA through ionic interactions. As reported in the literature, poly-D-lysine (PDL) has been used to minimise any degradation of adsorbed layers by inherent cellular enzyme activity.[219]

The QCM-D data showed a decrease in the $\Delta f_7/7$ signal and an increase in ΔD_7 when the aqueous solution of PDL was introduced into the system, which demonstrates the adsorption of PDL onto the bare Au surface (Figure 20C). Again, the rinsing step led to negligible changes in both the $\Delta f_7/7$ and ΔD_7 values, thus suggesting the strong association of the PDL, as well as the irreversible nature of the adsorption process. A further decrease in the $\Delta f_7/7$ was observed after the addition of an aqueous solution of 1.5 MDa HA onto the PDL-modified Au surface, indicating HA immobilisation (Figure 20C). The comparison of the deposition of HA onto the HS-Pep-1 (Figure 20A) and PDL (C) modified Au surfaces reveals a greater decrease in the $\Delta f_7/7$ signal for the adsorption of HA onto the PDL-modified Au surface, -9.1±2.7 Hz compared with -16.1±0.3 Hz, respectively. The Voigt-based viscoelastic model was used to determine the areal mass density and hydrodynamic thickness of the HA layer adsorbed onto PDL, reaching values of 1342.0±653.7 ng/cm^2 and 12.1±6.6 nm, respectively (Table 5).

It should be noted that the SD of the thickness and mass density calculations is not insignificant. As such it is important to consider this when drawing conclusions from the results, and it indicates that there is variability in the thickness and mass each time the films are formed. To provide greater confidence in the reliability of the data, and to get a more accurate gauge of the mass and thickness of the deposited HA further repeats should be carried out.

These results indicate that HS-Pep-1 is capable of immobilising HA in a similar manner to that of PDL; we believe that using the HS-Pep-1 based system offers a number of advantages above those of PDL. Primarily due to the specificity of Pep-1-HA binding, this has been demonstrated extensively throughout the literature. Using Pep-1 as a probe for detecting HA in tissue samples showed that staining was eradicated if samples were pre-treated with hyaluronidases.[132] Pep-1 was also shown to have significantly higher binding to HA-coated beads when compared to chondroitin sulphate-coated beads, in fact the

levels of Pep-1 binding to CS beads was equivalent to binding following enzymatic digestion of HA. [131] This level of specificity could contribute to the formation of HA surfaces containing fewer contaminants, which in turn could lead to greater consistency between experiments. The use of a self-assembling system, driven by the Au-S interaction, means that the localisation of peptide, and therefore HA, can easily be controlled and surfaces can be patterned using simple contact printing protocols. This ability is demonstrated in subsequent experiments detailed in section 2.4.

The average water contact angle of the PDL-coated Au was 25.4±8.6° which did not change significantly on incubation with HA, 21.8±5.8°, indicating a highly hydrophilic surface (Figure 20D, E). These results demonstrate that the immobilisation of HA by HS-Pep-1 SAM creates a surface with lower hydrophilicity when compared with its immobilisation by PDL. The sequence of HS-Pep-1 (Figure 17B) contains several hydrophobic domains, indicating it is less hydrophilic compared to PDL. As such, the lower hydrophilicity of the HS-Pep-1-HA surface may be due to incomplete HA coverage of the surface, resulting in patches of the surface where the peptide is exposed; we observe greater deposition of HA on PDL, which would corroborate this explanation. Conversely, regions where the PDL is exposed can contribute to the higher hydrophilicity demonstrated by the PDL-HA surface.

2.2.1. Effect of HA molecular weight on immobilisation

HA of different molecular weights (MWs) is known to be present throughout biological fluids and tissues,[251] while exogenous HA has been shown to elicit different effects on cell behaviours both *in vitro* and *in vivo*. Lower, but not high MWs, can induce maturation of dendritic cells and are seen to be immunogenic.[252,253] Additionally, oral administration of high WM HA can modulate inflammation in mouse models of autoimmune disease.[254] Using QCM-D, we have further analysed the effect of HA molecular weight (20 kDa, 200 kDa and 1.5 MDa) on its immobilisation by the HS-Pep-1 SAM or PDL (Figure 21). The average final mass deposition of HA following washing was not statistically different between the three sizes of HA used when immobilised by the HS-Pep-1 SAM. However, significantly more 1.5 MDa HA was immobilised by PDL than 20 and 200 kDa HA (Figure 23A). Using the Voigt-based viscoelastic model to determine the thickness of the HA layer formed on the HS-Pep-1 SAM or PDL, no significant difference was observed on HS-Pep-

1, with the thicknesses ranging from 5.4±1.8 to 10.8±4.8 nm. The 1.5 MDa HA layer on PDL was 12.1±6.6 nm, which was significantly thicker than the layers formed by the 20 and 200 kDa HA (*Table 5*).

Furthermore, there was a trend towards a greater mass and, to a lesser extent, thickness (Figure 23A and B respectively) with increasing MW of HA. This could be explained by HA adsorbing onto the substrates through a similar number of contact points, however increased chain length of the higher MW HA would mean a larger amount of HA was attached to the surface per binding site. The tethering of high MW HA is likely to result in a less condensed conformation of HA would allow for a greater amount of water to be held within the HA lattice structure. As a result the mass of the hydrated HA layer on the HS-Pep-1 surface would be greater than when a lower MW was used. This model would also account for a slightly thicker layer observed with the 1.5 MDa HA. If chains are more loosely bound then they may extend out into the surrounding solution and, as mentioned previously, retain more water, resulting in both an increased mass and thicker layer.

In addition to the information on the areal mass density, the QCM-D also allows information on the viscoelastic properties of HS-Pep-1-HA and PDL-HA films.[255] Figure 23C shows the mean change in dissipation following the incubation of HS-Pep-1- and PDL-modified Au surfaces with HA of different molecular weights. The increase in dissipation values indicates that the HA-based films are softer than the HS-Pep-1 or PDL layers alone.[256,257] No statistically significant differences between the ΔD values observed for PDL compared to HS-Pep-1 as a means of immobilisation were seen (Figure 23C). However, the MW of HA was shown to influence the viscoelastic properties, resulting in a more viscoelastic film being formed when a higher MW was used. This is likely due to the hydration of the film, where larger HA molecules will be able to incorporate more water into the layer.

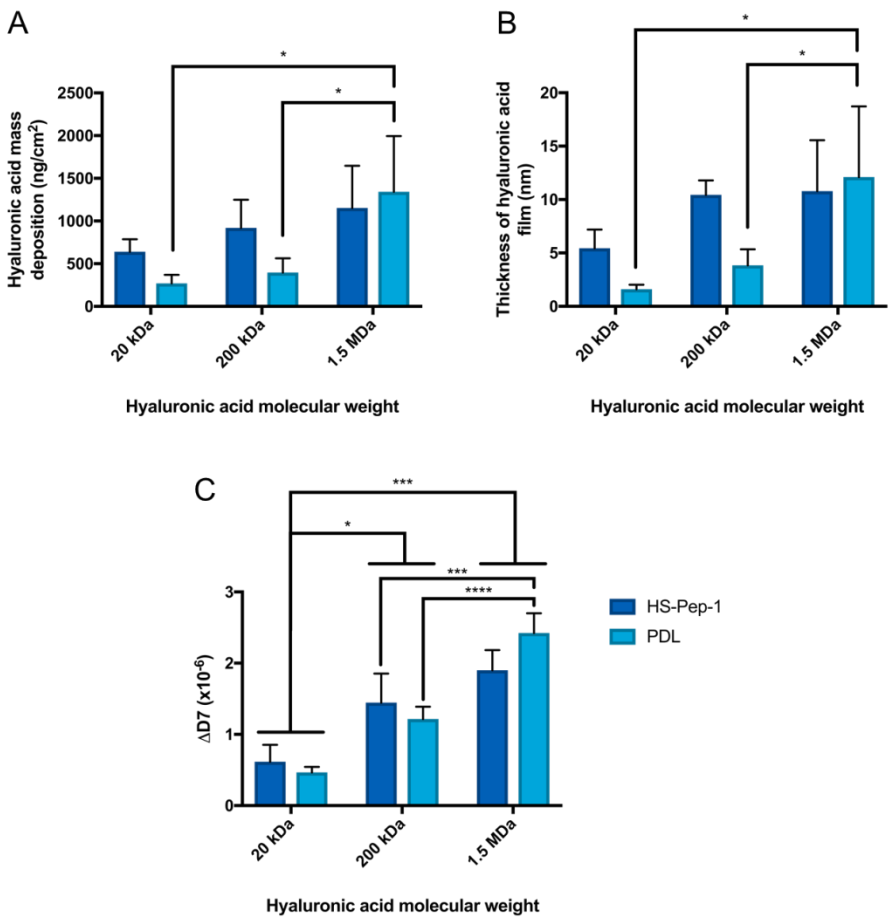

Figure 23: Molecular weight of hyaluronic acid has minimal impact on its deposition on HS-Pep-1 and PDL coated surfaces. Bar graph showing the average areal mass density (A) and hydrodynamic thickness (B) of HA deposited onto either a HS-Pep-1 or PDL surface calculated using the Voigt-based viscoelastic model. Bar graph showing the change in the dissipation factor at the 7th overtone upon HA binding to HS-Pep-1 or PDL surfaces following washing as measured by QCM-D (C). n=3, error = SD, ****=p<0.0001 ***= p<0.0002, *= p<0.0332 (Two-Way ANOVA, with Tukey's multiple comparisons).

2.2.2. Topography of HA surfaces

As a difference in hydrophobicity was observed between the HS-Pep-1-HA and PDL-HA surfaces, atomic force microscopy (AFM) was used to assess the topographical features of the films. It was seen that the average roughness of the single HS-Pep-1 or PDL layer was 4.85±2.16 and 3.77±1.78 nm, respectively (Figure 24B-D).

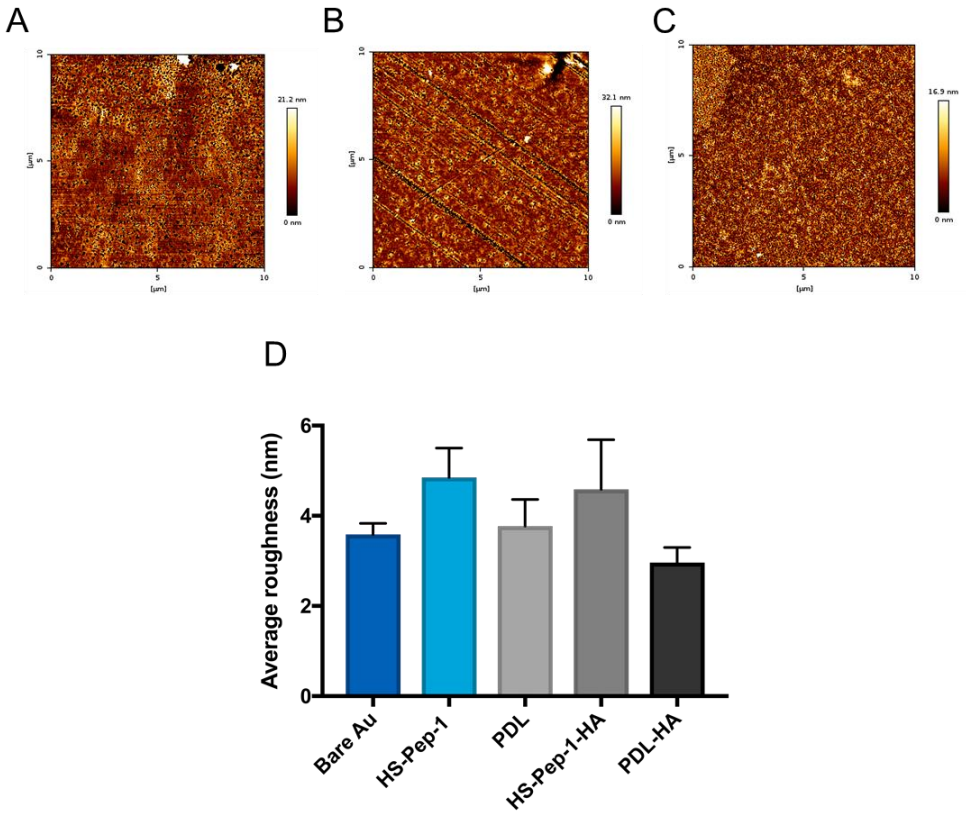

Figure 24: AFM analysis of surfaces. Representative AFM images of bare Au (A), HS-Pep-1 only (B) and PDL only (C) in a dried state. Bar graph showing the mean average roughness of bare AU, HS-Pep-1, PL, HS-Pep-1-HA and PDL-HA surfaces in a dried state (D). n=3, error = SD.

On incubation with 1.5 MDa HA, the average roughness was measured as 4.59±3.12 nm for the HS-Pep-1-HA surface and 2.96±1.00 nm for the PDL-HA (Figure 25A-B, E). In both cases, the average roughness decreased on addition of HA (Figure 24D).

Since the intended application of the developed surfaces are cell culture studies and these are performed in an aqueous environment, the roughness of HS-Pep-1-HA and PDL-HA surfaces was also assessed in a hydrated state. No significant change in roughness was seen between the dry and hydrated surface when HA was immobilised by PDL (Figure 25E). A significant increase in average roughness was observed when the HS-Pep-1-HA sample was hydrated, from 4.59±3.12 nm to 31.08±36.12 nm. When dry, the polymers making up the coating will sit close to the Au surface, however, when hydrated untethered sections of HA chains can extend out into the solution from the surface resulting in increased roughness.[65]

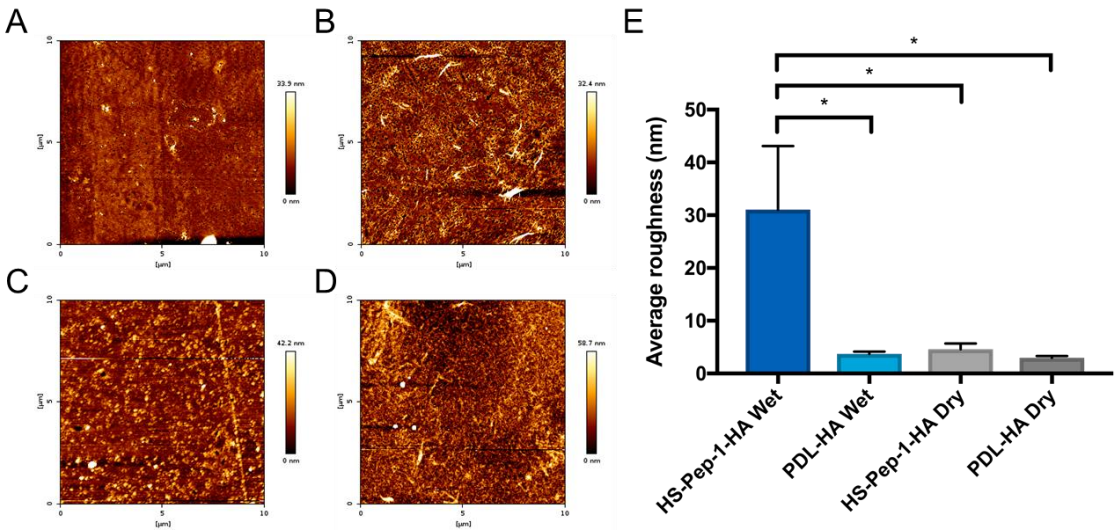

Figure 25: **Immobilisation of HA by PDL and HS-Pep-1 produces substrates with different topographies.** Representative AFM images of PDL-HA (A, C) and HS-Pep-1-HA (B, D) layers in dried (A, B) and hydrated (C, D) states, respectively. Bar graph showing the mean average roughness of HS-Pep-1-HA and PDL-HA samples under dry or hydrated conditions (E). n=3, error = SD, * = $p < 0.0332$, (one-way ANOVA with Tukey's multiple comparisons).

The hydrated HS-Pep-1-HA samples were also significantly rougher than the hydrated PDL-HA surface (Figure 25C, D and E). The difference in roughness between HA immobilisation by PDL and HS-Pep-1 suggests that the mechanism and strength of binding is influencing the presentation of HA.

The strong attractive electrostatic attraction between the positively charged PDL and the negatively charged HA chains is distributed evenly along both molecules, creating a coating which can uniformly resist the increased forces following swelling resulting in a smoother surface. Whereas HS-Pep-1 binding to HA occurs at discrete sites on the HA polymer, these individual points of contact may not be strong enough on their own to withstand increased forces generated by the HA layer hydration, resulting in more free ends or segments of HA which could account for the increased surface roughness observed.

Compared to both PDL and HS-Pep-1-HA in a dried state the standard deviation of the average roughness of the hydrated HS-Pep-1-HA surface is large. Having a larger error reduces the confidence with which we can draw conclusions from the data; however the

statistical analysis conducted corrected for multiple comparisons and takes into account the variability of the data. As this large error was only seen with one condition, rather than across all experiments, it is possible this variability in data is reflective of the variability in the roughness of the hydrated HS-Pep-1-HA surface.

Combining the QCM mass and thickness data with this apparent increased roughness of the 1.5 MDa HA bound by HS-Pep-1 it could be suggested that the HS-Pep-1-HA layers form a more dynamic surface. The unbound sections of HA would be free to move in the surrounding solution, this movement would not only contribute to the surfaces roughness, but could result in a constantly changing topography. If this is the case then this state of flux could be expected to have an effect on the reproducibility and consistency of the data acquired. Further repeats of these experiments would help increase the confidence with which we are able to present these data.

2.3. Culture of LuC4 cells on HS-Pep-1-HA and PDL-HA surfaces

Current research suggests that while HA surfaces are anti-fouling[90] and able to promote anchorage-independent cell growth,[259] they can also mediate CD44-dependent cell adhesion.[246] We also wanted to assess if the different surface properties observed by contact angle and AFM would have any effect on the cell behaviour. Initially, to assess the number of cells adhering to the surface following 6 and 24 hours of incubation, LuC4 cells were cultured in serum free medium on either tissue culture treated plastic, bare Au, HS-Pep-1, PDL, HS-Pep-1-HA, or PDL-HA surfaces. After both 6 and 24 hours of culture, no statistically significant differences in cell attachment were seen between any of the culture conditions (Figure 26).

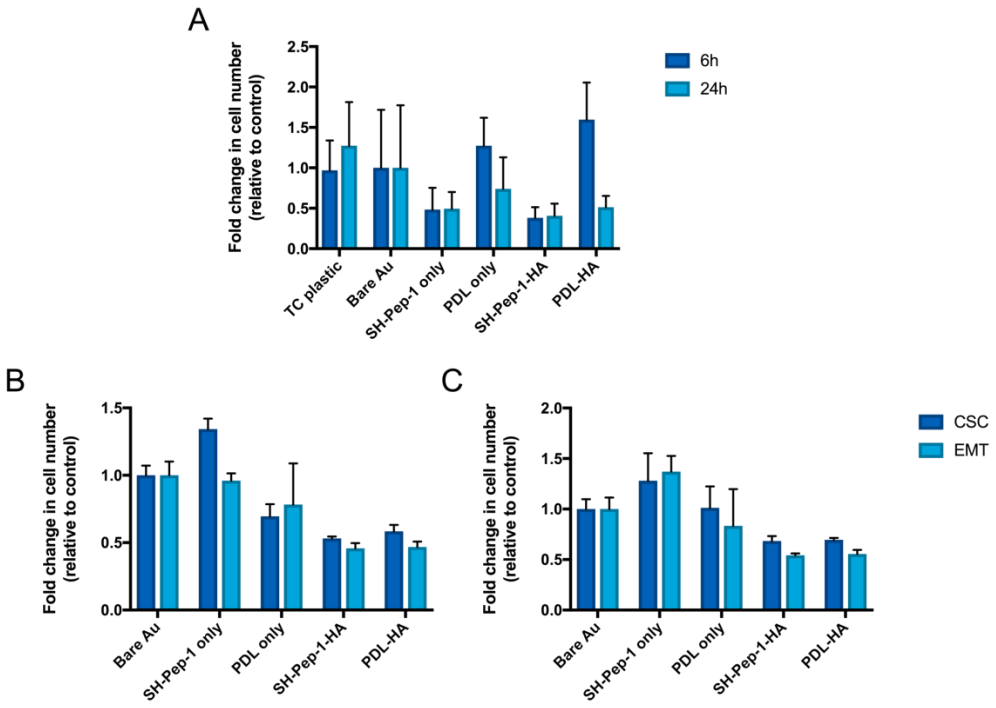

Figure 26: Supramolecular presentation of HA on surface does not alter the adhesion of LuC4 cells. Bar graphs showing the average fold chance in cell number attached to each surface after 6 and 24 hours. Unsorted parent population of LuC4 (A), two sorted stem cell fractions EMT and CSC after 6 (B) and 24 (C) hours. n=3, error = SD.

The assessment of the cells metabolic activity using AlamarBlue indicated that there was also no significant effect on metabolism (Figure 27), which suggests that the experimental conditions are not having a detrimental effect on normal cell function, measured by their redox capacity.

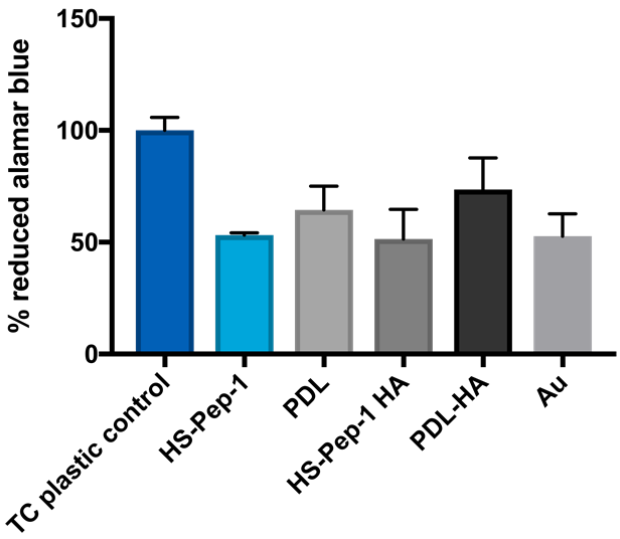

Figure 27: Change in metabolic activity following incubation on the different surfaces. Bar graph showing the % reduced alamar blue by LuC4 cells following 24 hours of culture on each surface. n= 3, error = SD.

Within the LuC4 cell line, a further subset of the CSCs has been characterised, which appear to have undergone epithelial to mesenchymal transition (EMT). These so-called EMT cells display a more elongated morphology and express mesenchymal markers.[26] Taking this work into consideration, we hypothesised that the EMT subset of CSCs within the LuC4 cell line, which is characterised by high CD44 and low to negative ESA expression levels, would preferentially bind to the HS-Pep-1-HA surfaces. Cells were isolated by FACS, seeded onto the surfaces and incubated as previously described. Again, after 6 and 24 hours, no difference was observed between the fold-change in number of cells attached compared to the range of surface treatments Figure 26B, C).

One consideration is that these experiments were performed in the absence of serum; cells were serum-starved for these experiments as the undefined, variable nature of FBS can result in cells being exposed to different levels of an array of growth factors, increasing the potential for variation in results.[260] While removal of serum can increase experimental reproducibility, the absence of growth factors and proteins present in serum can influence cell survival and proliferation. Proteins that promote cell attachment, such as fibronectin and collagen are found in serum; as such it would not be surprising to see different levels of adhesion in serum-free cultures.[261] When these components are present they adsorb onto the culture surface and can facilitate cell

adhesion and subsequent cell spreading.[262] It has been shown that in the absence of serum proteins cells do not form classical focal adhesions, and non-canonical signalling pathways are activated.[263]

The experiments carried out in this work compared cell adhesion on fabricated surfaces to adhesion on tissue culture-treated plastic under the same, serum-free, conditions. By doing this, any serum-dependent effect on cell adhesion should occur in all conditions. It might be of interest to see the effect of a range of serum concentrations on cell adhesion when cultured on HA surfaces.

Initial experiments looking at the effect of serum concentration on LuC4 adhesion to glass slides and tissue culture-treated plastic show significantly higher adhesion on glass when 5% serum is used, while greatest adherence to tissue culture-treated plastic is also seen at 5% serum, 0% provides similar results (Figure 28A). However, after 24 hours the influence of serum percentage on adhesion seems to be lost (Figure 28B), demonstrating that incubation time is also an influencing factor when it comes to cell adhesion.

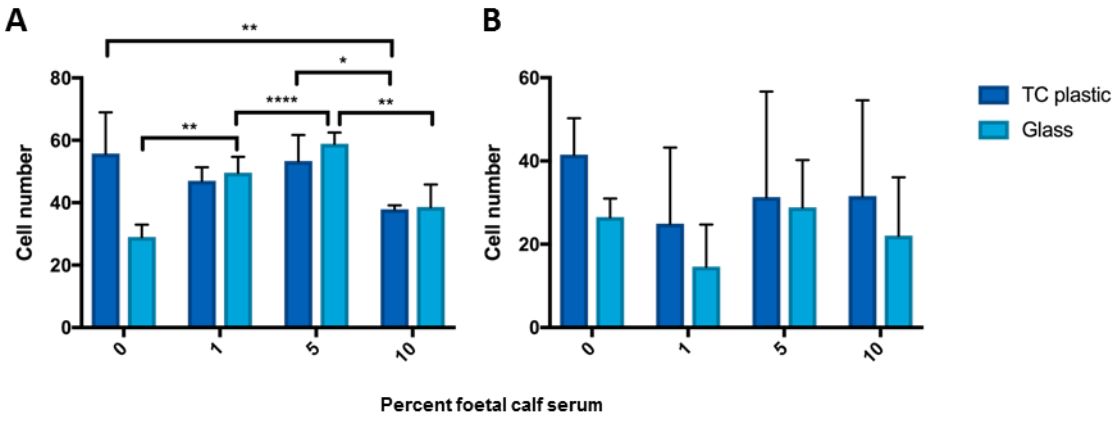

Figure 28: Effect of serum concentration on cell adhesion. Cells were seeded onto either tissue culture-treated plastic or glass slides with media contacting 0, 1, 5, or 10% FCS. After 6 (A) or 24 (B) hours in culture the number of adhered cells was counted. (n=3), error = SD, **** = $p < 0.0001$, ** = $p < 0.0021$, * = $p < 0.0332$, (two-way ANOVA with Tukey's multiple comparisons).

Differences in cell adhesion to the various surfaces may be diminished following 24 hours of culture as a result of the different CD44 expression profile of the LuC4 cell sub populations. Within the literature it was reported that glioblastoma multiforme (GBM) tumour cells are able to adhere to HA-crosslinked hydrogels following as little as 30 minutes incubation in serum-free medium, this interaction was shown to be mediated by

CD44 as its knockdown eliminated cell binding.[264] So if cells are given a longer period of time to adhere the distinction between cells which rapidly form attachments and those that take much longer to interact with the surface is lost.

It may seem surprising that enhancement of adhesion was not observed on immobilised-HA. However, Kim and colleagues did not compare CD44-mediated adhesion on HA to other substrates. Additionally, the CD44 isoform expressed may play a role in cellular adhesion, HNSCC EMT cells show lower levels of variant isoforms and higher standard isoform expression than the bulk population.[44] Variant isoform CD44v6 has been shown to increase adhesion of prostate cancer cells,[265] as this isoform is lower in EMT cells this could in part explain why low levels of binding were seen. Further to this, a similar subpopulation of HNSCC cells, defined by CD44v3^{high}ALDH1^{high} expression, shows CD44/HA-dependent enhanced sphere formation.[266] Spheres are formed in suspension and do not require adhesion to a surface which suggests that HA may promote contact-independent growth, rather than adhesion in this cell type, which may also apply to binding of LuC4 EMT cells to immobilised HA.

The mechanical properties of a HA surface are also able to modulate cell binding, where more binding is seen on stiffer HA hydrogels compared to softer structures.[264] This could indicate that the HA immobilised by HS-Pep-1 and PDL are similarly stiff as the amount of binding on each surface was comparable.

It has previously been demonstrated that treatment of head and neck cancer cells with soluble HA show increased migration.[43] Although no effect on cell adhesion was observed on the different surfaces, we assessed the HS-Pep-1-HA surfaces ability to alter cancer cell migration using a scratch assay. LuC4 cells were seeded onto the surfaces and cultured until confluent. Following this, a scratch was made and over the course of 48 hours the area of the wound was monitored.

During experimental set up, and creation of the scratch, it is known that cells at the wound edge can be damaged and result in the release of signalling molecules from these cell which can influence the results.[267,268] As such, it is also possible that the underlying SAM, and adsorbed HA, are also disturbed on scratch formation. If this is the case, and there is no HA in the wound, then the experimental question being asked is different from

if the HA coating remains intact. However, provided this is a uniform event across all conditions, then a valid comparison can still be made.

To determine if this is the case further experimental work would be required, fluorescently tagged HA could be used to form the coating such that loss of HA could be visualised, by the absence of a fluorescent signal. A fluorescent amino acid[269] could also be incorporated into the HS-Pep-1, provided it does not disrupt the interaction with HA, to see the effect of the scratching process on the SAM. Alternatively, or in parallel, AFM could be used to identify any changes in topography as a result of the scratch process.

For all conditions the wound area decreased as it began to close (Figure 29), except for the HS-Pep-1 modified Au substrate, which did not support cell growth to confluence. Comparing the area of the scratch, as a percentage of its area at time 0, it was seen that both HS-Pep-1-HA and PDL-HA conditions showed significantly reduced cell migration. This apparent inhibition of migration was also significantly greater when HS-Pep-1 was used to immobilise the HA (Figure 29B).

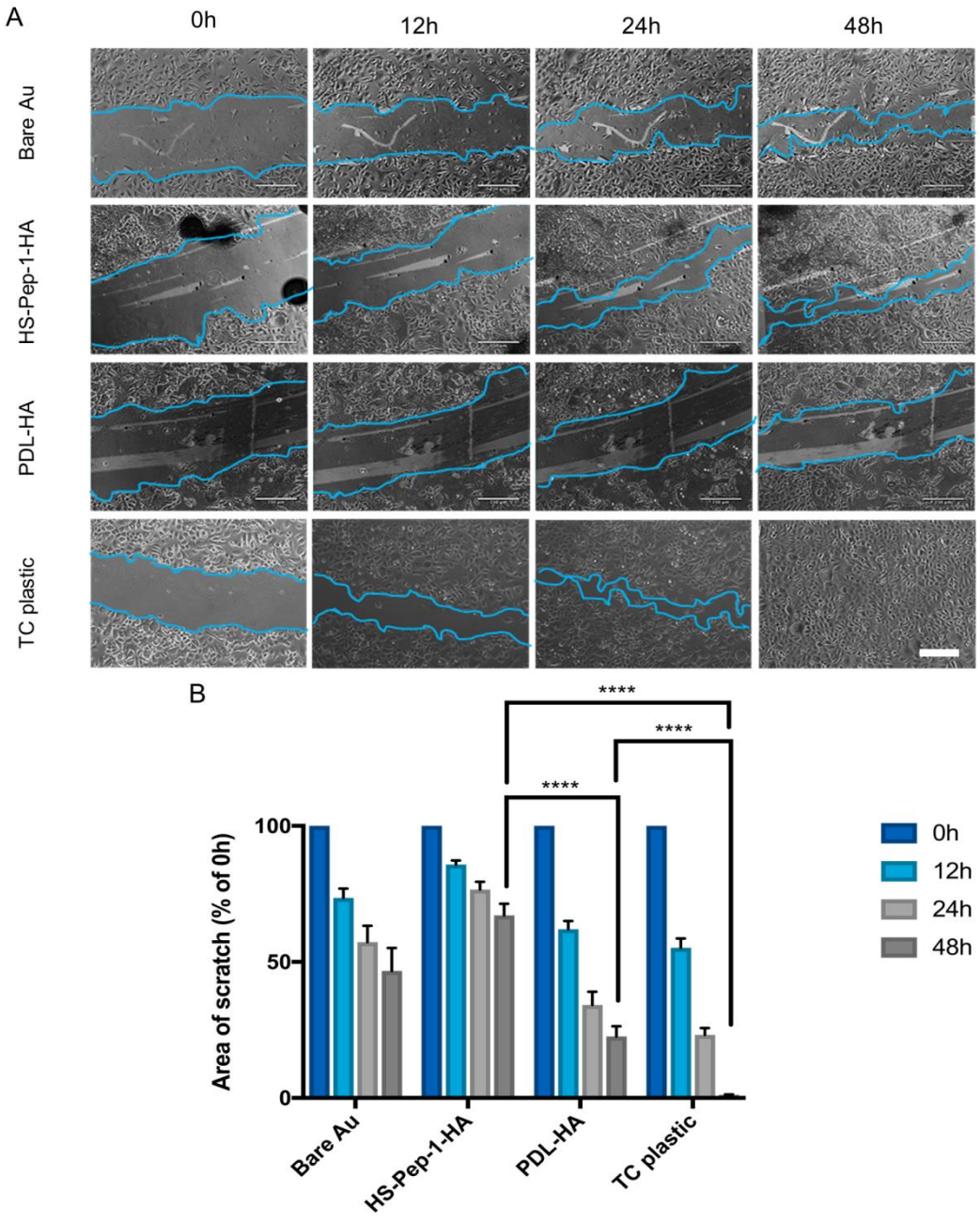

Figure 29: Immobilisation of HA by PDL and HS-Pep-1 reduces LuC4 cell migration. Representative phase contrast images of the scratch area at 0, 12, 24 and 48 h (A). Bar graph showing the mean area of scratch as a % of time 0 (B). (*n*=3), error = SEM, **** = $p < 0.0001$, scale bar = 500 µm, (two-way ANOVA with Tukey's multiple comparisons).

This indicates that immobilised HA can exert a different effect on head and neck cancers cells compared to soluble HA and that the method of immobilisation may also influence cell behaviour. Several reports suggest that surfaces coated with HA are also able to promote the migration of cells. However, this is dependent on cell surface receptors,

where the expression of the standard CD44 isoform resulted in increased migration.[270] It is known that the EMT fraction of HNSCCs downregulate variant isoforms in favour of the standard form.[44] The lack of increase in migration observed in our system could be explained by the low EMT percentage in the LuC4 cell line.[26] It has previously been shown that when PDL-HA 'bilayers' are formed, the PDL is able to diffuse into the HA layer.[271,272] If this is happening in our system, this may contribute to the higher rate of scratch closure on the PDL-HA surface over the HS-Pep-1-HA surface.

2.4. Micro-contact printing of HS-Pep1 and HA patterning

Patterned surfaces are a useful tool in cell culture and can be used to influence cell survival, adhesion, proliferation, migration, and differentiation.[205,273] With this in mind, PDMS stamps were used to micro-contact print (μCP) the HS-Pep-1 onto the bare Au substrate. Incubation with Texas Red labelled HA resulted in deposition in distinct foci (Figure 30C) or to form a background of HA with patches of bare Au creating a pattern (Figure 30D). This demonstrates a simple and rapid method for creating HA patterned surfaces with thiolated HA-binding peptide (HS-Pep-1, Figure 30A). Future work to investigate the interaction of LuC4 cells with a variety of patterns could provide further insights into the role of HA in cancer progression.

3. Conclusion

Here we demonstrate the supramolecular immobilisation of unmodified hyaluronan on gold surfaces using a thiolated HA-binding peptide. This method produces surfaces which are capable of supporting cell growth and, when compared to the immobilisation of HA by poly-lysine, have a higher average surface roughness. It is also seen that these surfaces reduce migration of head and neck cancer cells, although the mechanism of this was not investigated. Finally, this method of immobilisation in combination with μCP provides a simple and rapid way of creating HA-patterned surfaces, which could be used to further probe the effect of HA on cells *in vitro*.

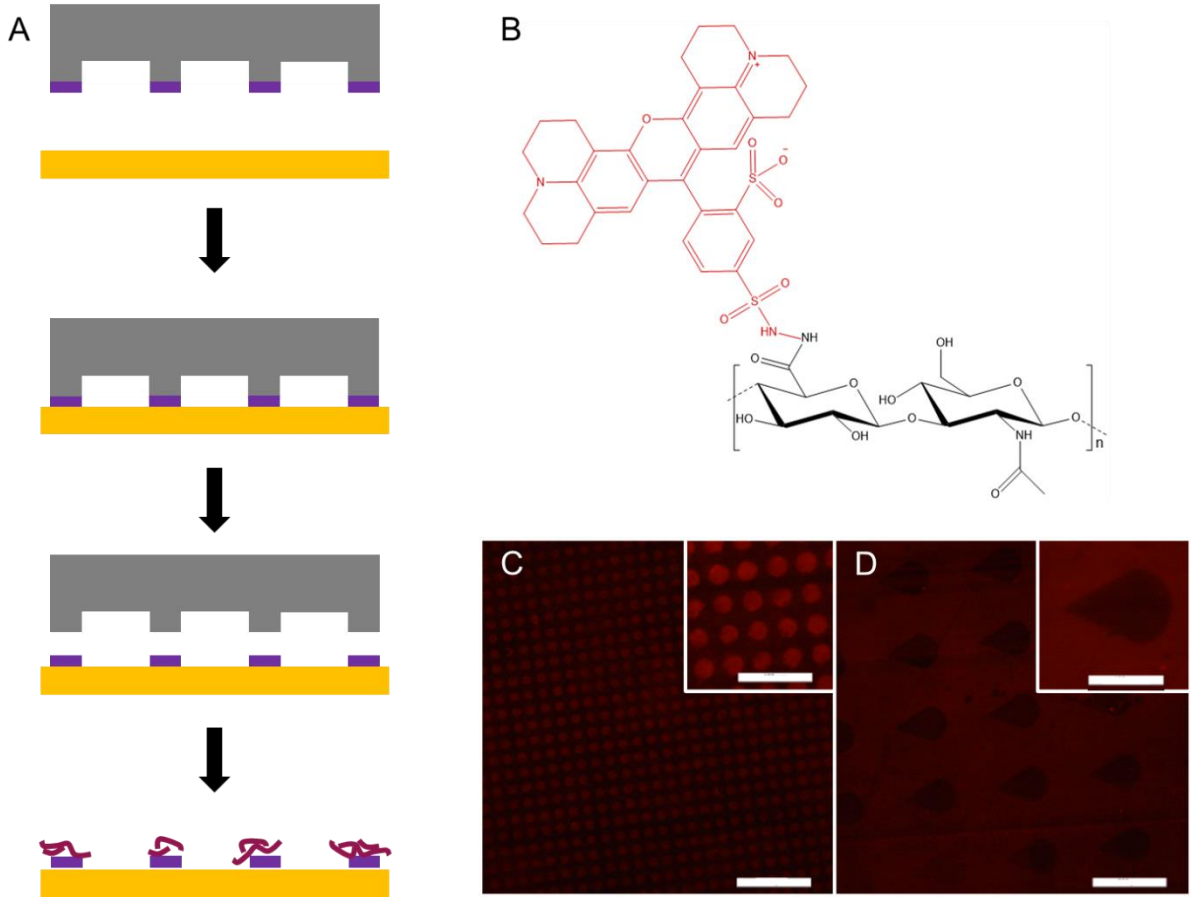

Figure 30: HS-Pep-1-HA patterning of surfaces using μ-contact printing. Schematic of PDMS stamp (grey) loaded with peptide (purple), which is transferred to the gold surface on contact. The islands are then able to immobilise HA (red) (A). Chemical structure of the Texas Red-labelled HA (B). Fluorescence images of surfaces patterned with a HS-Pep-1-coated PDMS stamp then incubated with Texas Red-labelled 1.5 MDa HA, creating a spot pattern (C) or a 'negative' drop pattern (D) Scale bar = 200 μm on large image, 100 μm on insert.

4. Outlook and future work

The ability to use μCP of HS-Pep-1 to control the immobilisation of HA to create patterned surfaces has the potential to be used to manipulate cell adhesion and *in vitro* culture. Micro-contact printing to create patterns of immobilised proteins such as fibronectin,[205] myoglobin,[274] antibodies, and BSA[275] can be used to precisely control culture conditions. Within the literature, μCP is used to restrict cell adhesion to specific zones and create patterns with cultured cells.[276] Depending on the size and shape of these regions, μCP can also be used to encourage cell alignment[277] and combining μCP of fibronectin with temperature-responsive surfaces, to release patterned cell-monolayers which can be

stacked or manipulated to form organised 3D structures provides a useful platform for the future of tissue engineering.

Patterned culture of cells has been used to study cell traction forces, which are known to influence cell behaviours such as migration and signalling.[278] Migration can also be studied using μCP.[279] Altering the spacing of the ECM protein laminin by μCP has been used to observe the migration capacity of different progeny of adult neuronal stem cells.[280] Migration of epithelial cells between channels of cell-permissive fibronectin over a non-adhesive background resulted in the formation of cell 'bridges' suspended above the surface, providing an insight into how cell migration may progress during wound healing.[281]

Depending on how HA-patterned surfaces interact with HNSCC cells, HS-Pep-1 μCP and HA immobilisation could be applied in similar ways to further study cell migration. Combining HS-Pep-1-HA patterns with additional surface modifications could lead to the development of more complex systems to immobilise more than one cell type in well-defined locations.[282] The interactions between these cell types and effect of co-culture can then be studied. Alternatively, mixtures of SAMs with different functionalities, such as cell-binding peptides could be used to determine how co-exposure to extracellular cues may stimulate behaviours associated with cancer progression.

To fully exploit the system developed here, the intended future work would focus on the applications of μCP. Where the first research question to be investigated would be can μ-contact printed islands of HS-Pep-1-HA surface coatings sequester LuC4 cells *in vitro*. Establishing the stability of these patterns under normal tissue culture conditions would also be an important set of experiments, again Texas Red-tagged HA could be used to visualise the immobilised HA. It would be of use, for performing co-culture experiments, to develop this system to support the culture of two cell types which are grown in distinctly separate areas without the need for a physical divide.

Current work in the Mackenzie lab utilises conditioned medium, which is spent media collected from culture flaks which contains the metabolites, extracellular matrix proteins, and growth factors excreted by the cultured cells. This is mixed with fresh media and used for subsequent cell culture.[283] Harvesting the conditioned medium requires

centrifugation and filtration steps, which is time consuming, co-culture would remove the need for isolating conditioned medium as components secreted by one cell type would be able to diffuse and directly act on a second, co-cultured, cell type.

Chapter IV - Development and application of a phage display protocol for the selection of head and neck cancer cell-binding peptides

1. Introduction

Advances in peptide synthesis technology, such as automated peptide synthesis and the use of microwaves, have drastically reduced the cost, time and man hours required to generate peptides in the lab. This has made the use of synthetic peptides a more attractive and accessible option for numerous applications, including therapeutics,[284] regenerative medicine,[285] and for biomaterials.[286]

1.1. Cell-targeting peptides

The use of cell-binding peptides in these applications shows promise for improving disease treatment, as seen with Glucagon-like peptide-1 receptor agonists (GLP-1RAs), 5 of which have been approved for the treatment of type two diabetes[287] Where the sequences of GLP-1RAs are based on the sequence on the native GLP-1 or extendin-1, another signalling molecule which binds to the glucagon-like peptide-1 receptor, and is able to effect weight-loss in clinical trials.[288] Further to this, cell-targeting, or homing peptides can be useful tools for targeted therapeutics. Conjugation of cytotoxic drugs to such peptides has been shown to allow selective delivery of cargo to target cells and improve treatment effectiveness both *in vitro* and *in vivo*.[181]

Peptides have also been identified which are capable of crossing the cell membrane and incorporation of these cell-penetrating peptides (CPPs) can enhance cellular up-take of molecules coupled to CPPs.[289] Combining cell-penetrating and cell-targeting peptide sequences can exploit both their properties to synergistically overcome treatment limitations linked to tissue penetration and tissue specificity.[163,188]

Within regenerative medicine, incorporation of peptides into 3D-gels and scaffolds can provide functionality and improve cell survival, proliferation, and differentiation. Culture of endothelial cells on a scaffold containing three peptides derived from ECM components, YIGSR, RYVVLPR from laminin 1 and TAGSCLRKFSTM from collagen IV, was seen to mimic *in vivo* conditions more closely than standard culture techniques and enhanced endothelial cell function.[290]

1.2. Methods for identification of peptide sequences

1.2.1. Protein-derived

Selection of a peptide sequence can be approached in several, ways which will be dependent on the intended application. Useful peptides can be identified by digestion of natural proteins followed by screening for their desired function, antioxidative peptides have been derived from milk proteins in this way.[291]

For cell-based applications, such as creating hydrogels or surfaces for cell growth, peptide sequences extracted from known functional domains of proteins can be used to promote cell adhesion, survival, differentiation, or maintenance of stemness. Knowledge of the critical role integrins play in a cells interaction with the ECM and initiation of signal transduction makes their ligands, such as laminin,[292] collagen,[293] and fibronectin,[294] prime candidates for isolating bioactive sequences. Of the several peptides which are routinely used for supporting cell adhesion the three primary motifs, RGD, IKVAV, YIGSR, were identified within laminin chains.[295] Their incorporation into cell culture substrates has been used to support adhesion and proliferation of human neural stem cells and was able to direct their differentiation towards a neuronal cell fate observed through increased neurite outgrowth.[296,297]

Being able to recapitulate the ECM in such a controlled way, without the need for animal derived macromolecules, allows the function of individual molecules, or even small domains within a molecule, to be probed. In addition, developing *in vitro* culture systems which mimic the *in vivo* environment more accurately can only lead to a better understanding of cell behaviours through minimising artefacts resulting from culture conditions.

1.2.2. Rationally designed

Identification of biologically relevant peptides can also be achieved through rational design. For example, Joshi *et al*.[298] designed a peptide inhibitor of Aminopeptidase N (APN), a metalloprotease which is overexpressed in several cancers whose activity has been shown to facilitate angiogenesis and cancer metastasis. This was achieved by analysis of known substrates and identification of key residues in combination with analysis of the APN crystal structure. This strategy for obtaining novel peptides requires

a large amount of knowledge of the target molecules structure, function and its natural ligands. A similar option which may require less starting information would be rational redesign. This approach has been used to generate a peptide with improved binding affinity for the target, cysteine-rich intestinal protein 1 (CRIP1), a biomarker for breast cancer. Initial peptide binders of CRIP1 were selected by phage display and the sequence which had the highest affinity was redesigned using computer modelling.[299] This redesigned peptide has subsequently been successfully used in an assay, as a capture probe, to detect levels of CRIP1 in cancer patient samples, indication the potential to be developed as a diagnostic tool.[300]

An advantage of using rational design and redesign is the ability to engineer a peptide which contains fewer hydrophobic patches, which may lead to aggregation, as well as ensuring reasonable water solubility, which is often a limitation of cell-binding peptides. Incorporation of non-natural amino acids can help achieve an increased *in vivo* half-life by reducing the action of peptidases.

1.2.3. Phage-derived

While using rational design and known target-binding motifs from native proteins to identify peptides to generate optimised *in vitro* culture conditions, tissue scaffolds, and targeting molecules has been successful, in most cases prior understanding of the target molecule or its natural ligands is required. This can present a problem for cases where the exact target molecule is unknown, for example isolation of a peptide which is able to home to a specific cell type such as tumour cells.

Without a candidate receptor, to use as a basis for rational design, phage display offers a high-throughput screening platform which does not require any detailed knowledge of the target or potential ligand. Random peptide phage display libraries consist of genetically modified bacteriophage displaying a random peptide sequence on its surface, which is encoded by a fragment of DNA inserted into the phage genome. Large commercially available libraries, with a diversity in the order of 10^9 clones, allows the rapid screening of peptides which bind to a target, and, due to the physical linkage between genotype and phage phenotype, simultaneous partitioning of encoding DNA.

Existing literature demonstrates how phage display can be applied to isolate peptides which home specifically to complex targets such as tissues or cells. Peptide phage display was used to identify a peptide, HAP-1, that could target synovial cells and, when conjugated to an antimicrobial peptide, induce their apoptosis.[301] A cell-homing peptide for targeting chondrocytes was identified by incubation of a random peptide library with *ex vivo* pieces or cartilage, in order to improve cell specificity, Pi and colleagues[302] employed a round of negative selection against synovial tissue and fluid, to remove clones which recognised molecules present in these tissues. Again, the identified peptide (chondrocyte-affinity peptide, CAP) was conjugated to polyethylenimine, a nucleotide delivery reagent, and CAP was able to increase cartilage-specific delivery of DNA.

In addition to the use of phage display-discovered peptides for cell-targeting, they are also useful reagents for building *in vitro* cultures systems, to influence and investigate cell behaviours. An excellent example of this is screening of peptide libraries to identify peptides which can support embryonic stem cell (ESC) proliferation.[202] This work by Derda *et al.* elegantly combined the peptides identified through panning on embryonal carcinoma cells with an alkane thiol SAM system. Candidate peptides were synthesised and coupled, via their C-terminal, to alkane thiols. When incubated with a gold surface, the thiol group binds to the gold causing the self-assembly of the alkane thiol-peptides to generate a monolayer functionalised with peptide sequences. As mentioned, this surface supported ESC proliferation through interactions independent of integrins or proteoglycans, again illustrating the power of phage display for selection of peptides which can probe the molecular mechanism of cell-environment interactions.

1.3. Cell-binding peptides in head and neck cancer

The success of targeting the human epidermal growth factor receptor 2 (HER2), which is over-expressed in some breast cancers, highlights the possibility of achieving similar targeted therapies against other malignancies.[303,304] The complexity of the cell surface means that while identification of a target cell population based on phenotypic and behavioural characteristics is not always coupled with a single, targetable cell surface marker which can be used as a starting point for creating peptide-based targeting molecules.

The presence of a subpopulation of cancer stem cells (CSCs) within head and neck cancer provides an example of this. These cells exhibit elevated tumourgenicity in mouse models, therapeutic resistance, the ability to self-renew when compared to the bulk of the tumour.[6,14] However, their isolation is based on expression of CD44, a single pass transmembrane protein, which is found on the surface of almost all cell types.[305] Splice variants of CD44 show tissue-specific patterns of expression. Thus, targeting isoforms which show high expression in tumour cells and have a more restricted expression in normal tissues was investigated. The CD44 variant isoform, CD44v6, was identified as a target and monoclonal antibodies were raised to target CD44v6-expressing cells and to study their distribution.[22] While these studies showed a favourable expression pattern of CD44v6 significant off-target side effects were seen in phase I trials targeting CD44v6-expressing cells in HNSCC.[306] These off-target effects were observed in the skin, where CD44v6 is also expressed, this demonstrated that there is still work to be done defining specific markers of HNSCC.

Added complexity is introduced into mapping markers of HNSCC and their stem cells by the presence of a further subset of CSCs. Of these, there is one population which is more heavily associated with an aggressive tumour phenotype, with a greater propensity for metastasis, therapeutic resistance, and recurrence.[31,32] HNSCC cells with $CD44^{high}/EpCAM^{low}$ expression profile are believed to have undergone EMT, induced by signals in the tumour microenvironment.[26] These cells show altered gene expression, markers of epithelial cells, including Calgranulin B and involucrin, are downregulated and mesenchymal genes such as Twist, Snail, and Vimentin are upregulated.[26] Functional assays demonstrate corresponding shift if cell behaviour, where EMT cells have a slower growth rate, enhanced migration, and a more elongated morphology.

It is not uncommon for combinations of markers to be used when defining cell populations, as is the case with EMT cells. In addition to a $CD44^{high}/EpCAM^{low}$ profile aldehyde dehydrogenase (ALDH) activity and low epidermal growth factor receptor (EGFR) expression are also used as part of a marker panel to isolate HNSCC CSC subpopulations.[307–309]

Identification of a molecule which could specifically target one of these subpopulations would have important implications for improved isolation of these cells *in vitro* and potential for development of *in vivo* cell targeting.

With this in mind, the purpose of the experiments discussed in the following chapter was to use phage display to isolate peptide sequences which would selectively bind to a sub population of HNSCC cells which are associated with tumour progression, metastasis, therapeutic resistance, and recurrence following treatment. Once isolated, the aim would be to modify the peptide to include a sulphur moiety so that it can be immobilised on an Au surface as a SAM, following the protocol developed in Chapter III. This platform could then be used for *in vitro* cell studies as a tool to further probe cellular characteristics.

2. Results

There are several commercially available random peptide phage display libraries. For this work, the Ph.D. - 12 ™ Phage display library was purchased from New England BioLabs Inc. The library provides pentavalent display of peptides on the surface of the M13 filamentous bacteriophage. A Gly-Gly-Gly-Ser linker precedes the 12-amino acid peptide which is fused to the N-terminal of the pIII coat protein, thus the N-terminal of the peptide is free.

2.1. Biopanning on LuC4 cells enriches for cell-binding clones

To establish a suitable protocol for panning, the parent population of LuC4 cells was used.

Three rounds of positive selection were carried out on LuC4 monolayers. To determine the recovery and enrichment for cell-binding clones, the number of input and output plaque forming units (pfu) was used as shown in Table 6. An enrichment of cell-binding phages was observed with each round or panning. This demonstrates the ability of this protocol to select for target-binding clones, which, in this case is a cell monolayer.

Table 6: Bacteriophage input and output, values for each round of biopanning on a monolayer of unsorted LuC4 cells.

	INPUT (PFU)	OUTPUT (PFU)	RECOVERY (OUTPUT/INPUT)	ENRICHMENT (PER ROUND)
ROUND 1	2×10^{11}	1×10^{7}	5×10^{-5}	-
ROUND 2	4×10^{10}	1.2×10^{6}	3×10^{-5}	1.67
ROUND 3	2.2×10^{11}	2.7×10^{7}	1.2×10^{-4}	2.45

To further confirm the selection of cell-binding phages, a whole cell ELISA was performed to compare the binding capacity of the amplified eluate from each round of panning against the wild-type (WT), insert-less phage, and the naïve library. The insertless (WT) phages and the naive library had similar levels of binding. The phage pools from the first and second rounds of panning showed equivalent binding to both WT and un-panned library, while the third round amplified eluate showed a two-fold increase in signal, indicating increased binding (Figure 31). Although, as the standard deviation for each sample was relatively large, there was no statistically significant increase in binding following one or two rounds of biopanning on a LuC4 cell monolayer.

Taking the increase in recovery ratio and minimal increase in binding, as measured by ELISA, together, the results would suggest the phage clones being enriched may not be target-specific and may simply be binding the tissue culture plastic.

To address this issue, modifications were made to the panning procedure. One key change was the removal of Tween 20 from the wash buffer during the ELISA. It has been demonstrated that inclusion of such non-ionic detergents can increase the non-specific binding of M13 phage in a dose-dependent manner that can result in a high background signal. The use of Tween in conjunction with a PEG-based purification of amplified phage can also contribute to non-specific interactions, PEG molecules associated with the virus coat proteins interact with Tween promoting aggregation.[310] Additionally cell viability was seen to be reduced when Tween was used in panning (Figure 32).

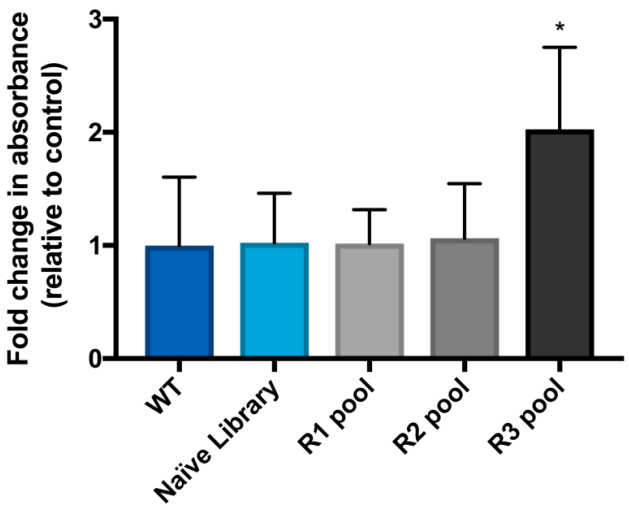

Figure 31: **Enrichment of phage binding following three rounds of selection.** Whole-cell phage binding ELISA results of eluted phage after each round of panning on a cell monolayer of unsorted LuC4 cells. (*n* = 3), error = SD, * p= 0.0332, one-way ANOVA with Tukey's multiple comparisons.

The two cell populations isolated by FACS, EMT and Epi, were cultured for 24 hours before selection for EMT-specific clones was carried out. This was done to give the cells time to adhere and to recover from the shear forces exerted during FACS. Additionally, it would provide some time for receptors and cell surface proteins, degraded by trypsin during cell harvesting, to be synthesised and returned to the cell surface.

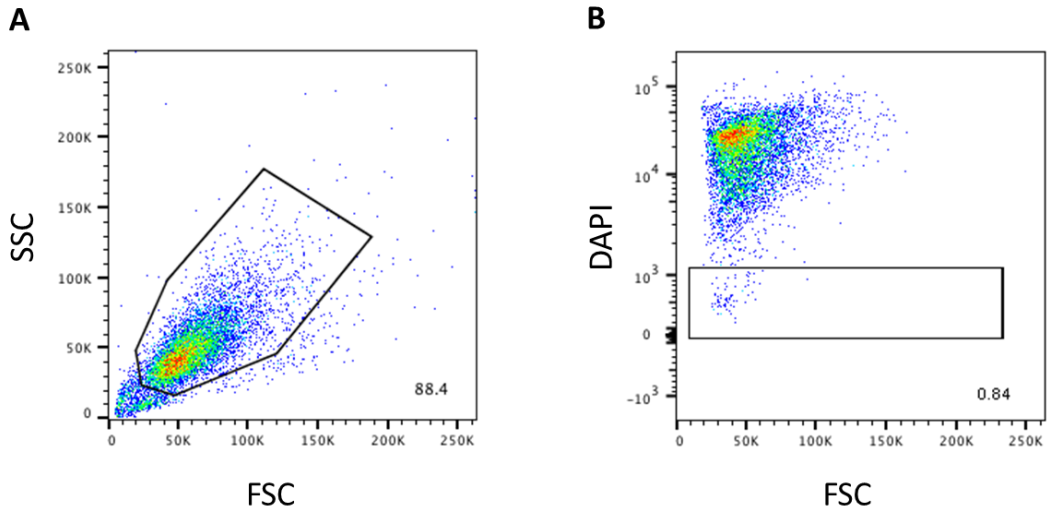

Figure 32: FACS plots of LuC4 cells, showing cell shape and complexity, determined by forward scatter (FSC) and side scatter (SSC) respectively (A) and viability, where a positive DAPI signal

indicated a disrupted cell membrane and poor cell health (B) following washing with wash buffer containing 0.01% Tween 20.

2.2. Biopanning on CD44^{high}/EpCAM^{low} cell monolayers.

Sorted cell populations used in subsequent experiments used the gating strategy outlined in Figure 33.

EMT cells tend to make up between 1 and 10% of the LuC4 cell line, for the cell panning experiments large numbers of EMT cells are required, where 1x10^6 cells are used in each round of panning. To ensure there were enough cells for each round, cells were sorted in advance, frozen down then pooled and cultures for 24 hours as mentioned above. As such, the effect of freezing down sorted cells on their marker profile was investigated, to assess if this was a viable option for supplying cells for each round of panning. It was seen that cells which were sorted, frozen at -80 °C for one month, thawed, and cultured for 48 hours showed only a slight change in marker profile; 93.8% ± 0.7 of EMT cells and 99.4% ± 0.3 of CSC cells retained their CD44^{high}/EpCAM^{low} and CD44^{high}/EpCAM^{high} marker profile, respectively (Figure 34). These results demonstrate that sorting cells in advance, for subsequent use in panning experiments, and storage at -80 °C for a short period of time, does not affect the population phenotype in a way that would impact biopanning.

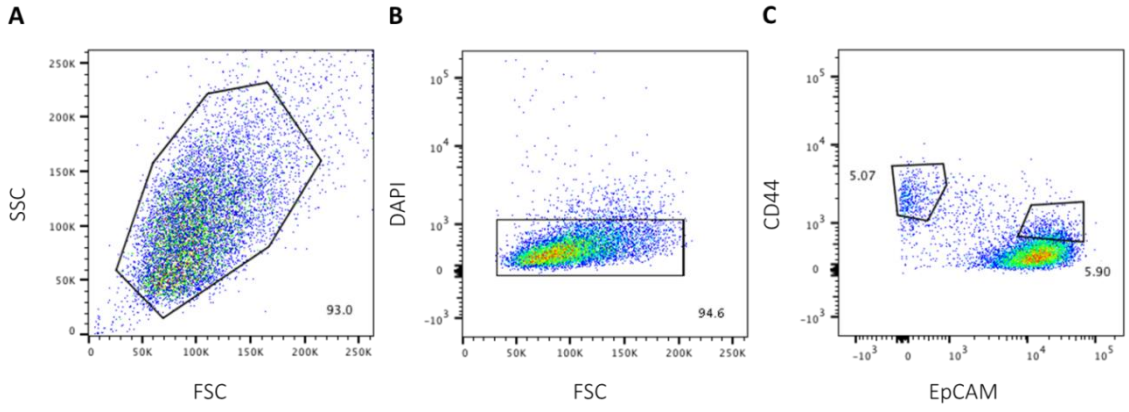

Figure 33: Representative gating strategy for sorted cell populations. Cells were first selected based on side and forward scatter (A), then DAPI was used to identify viable cells, those which are DAPI negative, (B). Finally CD44 and EpCAM expression was used to select the CD44^{high}/EpCAM^{low} and CD44^{high}/EpCAM^{high} populations (C).

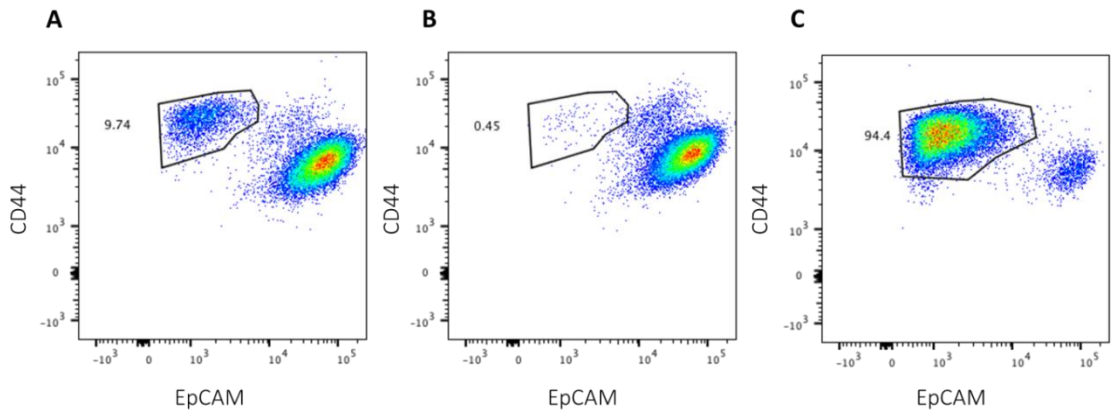

Figure 34: Analysis of LuC4 marker expression by flow cytometry. Percentage of EMT cells in LuC4 following 48 hours in culture after storage at -80 °C for 30 days. Unsorted parent population shows two distinct sub populations, with approximately 10% of cells falling under the EMT profile (A). Cells sorted for $CD44^{high}/EpCAM^{high}$ expression prior to culture show less than 1% of the population switch to the EMT phenotype (B). Finally, of cells sorted for $CD44^{high}/EpCAM^{low}$ expression prior to culture, 94% retain their EMT phenotype (C).

The modified protocol was then used, in combination with FACS, to select for phages which bind to the EMT sub-fraction of the LuC4 cell line. Following a pre-clearing step to deplete the phage library of sequences which had an affinity to the tissue culture plastic, one round of positive selection on a monolayer of $CD44^{high}/EpCAM^{high}$ was carried out. To minimise the number of clones carried through to the next round of panning which are binding to general cell surface markers, or molecules expressed by other HNSCC cells, a round of negative selection was conducted. The amplified phage pool from the first round was incubated with LuC4 Epi ($CD44^{high}/EpCAM^{high}$) cell monolayer prior to a second round of positive selection with EMT cells, without an amplification step in-between.

A final third round of positive selection was conducted and the unamplified eluate was titred. Blue plaques were picked and individually amplified, sequencing of phage DNA revealed 4 different insert sequences, Table 7, of these three appeared only once while the fourth sequence, QVNGLGERSQQM-GGGS was present in 10 of the clones. Analysis of these sequences using SAROTUP: Target-Unrelated Peptides Scanners[311] revealed that there were no known target-unrelated peptide (TUP) motifs within any of the isolated peptides. To assess the probability of these sequences being selected due to their binding to polystyrene the TUPredict polystyrene surface-binding (PSB) tool, PSBinder, was used.

Three of the four sequences were predicted to bind to polystyrene (Table 7), with VCSPCGPVPPAK-GGGS being the sequence least likely to bind polystyrene.

It was interesting to see that both the VCSPCGPVPPAK-GGGS and GNNPLHVHHDKR-GGGS peptides had been selected as binders to aggregated monoclonal antibodies.[312] Analysis of phage binding by Cheung *et al*. using an ELISA showed VCSPCGPVPPAK-GGGS did not show enhanced binging to the target, but GNNPLHVHHDKR-GGGS showed a 7-fold increase. The GNNPLHVHHDKR-GGGS was also selected as a Jurkact cell-binder; it showed preferential binding for Jurkat cells over MCF-7 and PC3 cells as measured by ELISA. [313]

Table 7: Sequences identified from biopanning on $CD44^{high}/EpCAM^{high}$ cells. Including the number of times they appeared, the probability and the overall prediction as to whether they will bind to polystyrene.

SEQUENCE	APPEARANCES	PSBinder PREDICTION	
QVNGLGERSQQM-GGGS	x10	0.58	Yes
GANDGVSLWRNV-GGGS	x1	0.86	Yes
GNNPLHVHHDKR-GGGS	x1	0.67	Yes
VCSPCGPVPPAK-GGGS	x1	0.38	No

A whole cell phage ELISA was performed to assess the binding capacity of each clone following protocol optimisation. Optimisation experiments used unsorted, parent, LuC4 cells and compared the effect of cell fixing and blocking buffer components on the ELISA signal with WT phage and amplified third sound eluate (Figure 35). Results showed the background signal tended to be reduced when wells were blocked with PBS and 3% BSA, rather than PBS with 5% milk powder (Marvel, UK). No difference was seen between signals produced when using fixed or live cells. As such, samples were blocked with PBS 3% BSA and live cells were used to keep the conditions as close to those used during selection.

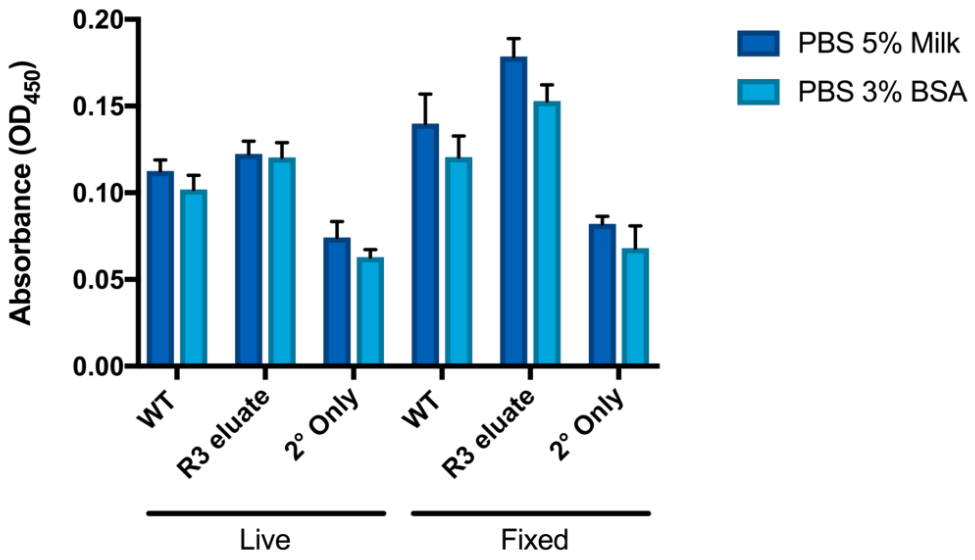

Figure 35: Comparison of ELISA signal, PFA fixed or live cells were blocked with PBS 5% milk or PBS 3% BSA prior to incubation with bacteriophage, antibodies, and HRP substrate. No statistically significant differences were observed. (*n* = 3), error = SD, two-way ANOVA with Tukey's multiple comparisons.

During the ELISA, considerable cell detachment and loss was observed, particularly of the EMT cells. This can be explained by the mesenchymal phenotype of these cells, loss of EpCAM expression is used to define this cell population so it makes sense that these cells are less adherent. EpCAM is a cell-cell adhesion molecule, where EpCAM on once cell will bind to EpCAM on adjacent cells,[314] in a cell monolayer this interaction is likely to make cell attachment more robust and individual cells more resistant to detaching. Whereas EMT cells with low or no EpCAM expression do not have this additional adhesion, thus a greater proportion of them were lost during the multiple wash steps in the ELISA.

To reduce the amount of cell-loss seen, plates were coated with poly-D-lysine, a polymer which readily adsorbs to tissue culture-treated plastic and has been shown to enhance cell adhesion.[315] In addition to using PDL-coated plates the cell density was increased from 10,000 cells/well to 20,000 cells/well. Results of the optimised ELISA did not demonstrate that any of the tested clones were able to preferentially bind to EMT cells; however, clones did tend to show increased binding to both cell populations over the no cell control.

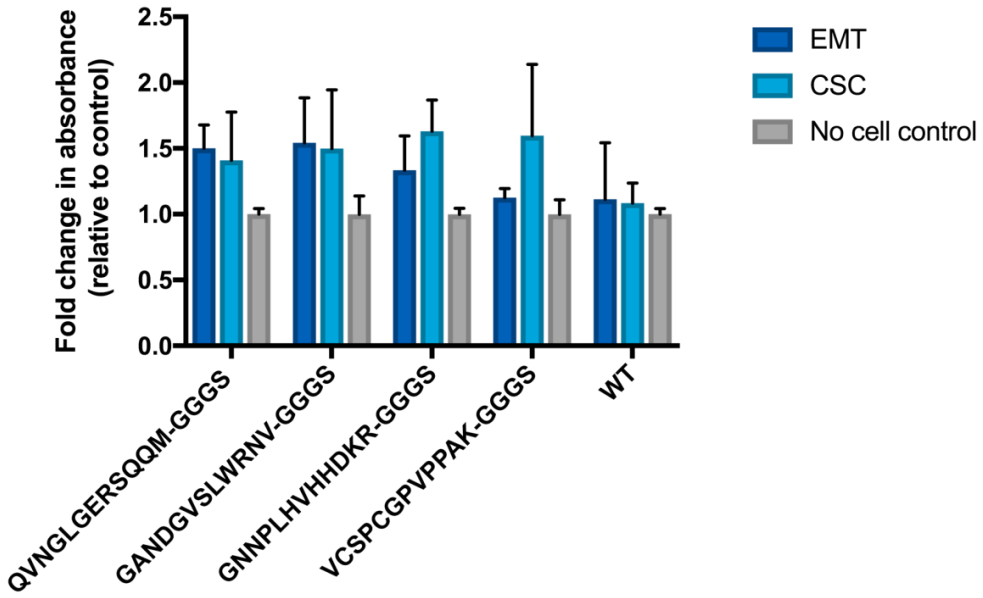

Figure 36: **Whole cell phage binding ELISA.** Assessment of the binding of peptides isolated following three rounds of biopanning on EMT cell monolayers. Clones were incubated with FACS populations of EMT and Epi LuC4 CSCs to identify differences in binding. Again, no statistically significant differences were seen in ELISA signal between either the peptide sequences or the cell types. (*n* = 3), error = SD, two-way ANOVA with Tukey's multiple comparisons.

In order to further assess phage binding, a secondary method, flow cytometry, was used. In theory, it is possible for the specific and preferential binding of phages to target cells within a mixed population to be detected by flow cytometry. Cells were also stained for CD44 and EpCAM alongside phage binding to allow visualisation of the EMT population within the sample. Analysis of clones isolated previously was unable to detect any phage binding (Figure 37). While the use of flow cytometry has the potential to remove the need for cell sorting prior to assessment of binding, it is likely that it would only be possible to detect clones with a high binding affinity for the target, due to the physical forces exerted on the cells.

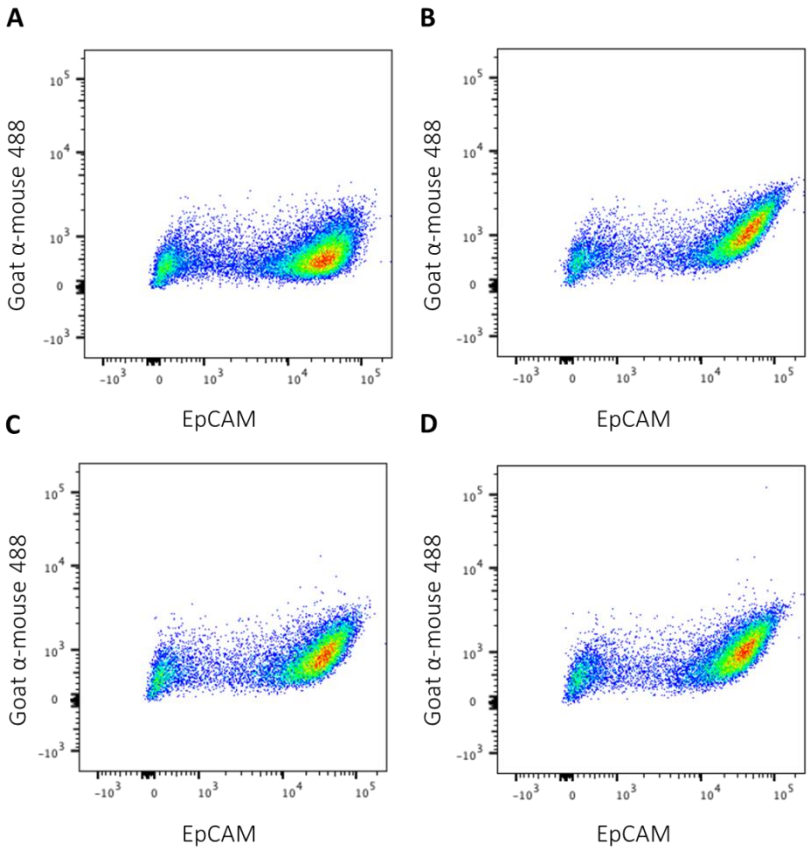

Figure 37: Phage binding assessment by flow cytometry. Unsorted LuC4 cells were incubated with individual phage clones displaying either GNNPLHVHHDKR-GGGS (A), QVNGLGERSQQM-GGGS (B), GANDGVSLWRNV-GGGS (C), or VCSPCGPVPPAK-GGGS (D) sequences. Phages were then detected by the anti-M13 antibody which is turn was detected by Alexa Fluor 488 goat anti-mouse. Cells were also stained with APC-conjugated anti-EpCAM antibody.

2.3. FACS-assisted biopanning with competitive selection

As panning on a cell monolayer failed to select for cell type-specific binders, a further iteration of phage display was used incorporating competitive selection. Taking inspiration from Siegel and colleagues, [102] phage display was combined with FACS. Before incubation with the naïve library LuC4 cells were sorted based on CD44 and EpCAM expression and the Epi ($CD44^{high}/EpCAM^{high}$) cells were collected, to make up the non-target cell population. The target EMT ($CD44^{high}/EpCAM^{low}$) cell population was isolated from a stably expressing GFP LuC4 cell line. Once isolated these two cell populations were mixed and incubated with the phage library in suspension. Target cells and associated phage could then be isolated by FACS based on GFP levels alone without further staining,

where GFP-positive cells were discarded and only GFP-negative cells were collected. The isolated target cells were lysed and a phage titre was carried out as usual.

The first time this protocol was employed the number of GFP-negative target cells was very low, so it was decided that the most appropriate action would be to repeat the panning procedure from the beginning, with a higher cell input. Following these subsequent three rounds of selection, no enrichment was seen (Table 8). However, Sanger sequencing of extracted DNA and analysis of the sequence using CL Sequence Viewer 8 (Qiagen, Germany) revealed the following peptide; TLGGLYQFEYAL-GGG, as a potential target-specific peptide (Figure 38A)

Table 8: **Bacteriophage input and output,** values for each round of FACS-assisted panning on LuC4 cells in suspension input/output.

	INPUT (PFU)	OUTPUT (PFU)	RECOVERY (OUTPUT/INPUT)	ENRICHMENT (PER ROUND)
ROUND 1	2×10^{11}	2.7×10^{6}	1.3×10^{-5}	-
ROUND 2	4.7×10^{12}	7.2×10^{5}	1.5×10^{-7}	0.01
ROUND 3	1.5×10^{12}	5×10^{4}	3.3×10^{-8}	0.22

The binding capacity of this phage clone was then assessed using a whole-cell ELISA and flow cytometry. The ELISA was carried out on cells in suspension and results show that the TLGGLYQFEYAL-GGGS displaying clone has enhanced binding for EMT cells (Figure 38B). It does, however, show significant binding to epi CSCs compared to the WT phage binding which suggests that its binding partner may be expressed, albeit at different levels, on both cell populations. Using flow cytometry, 1.99% of the population was positive for Alexa Fluor 488; it is not clear if this correlates to target cell binding, as it is not a distinct population (Figure 38D). When the CD44/EpCAM profile of the 488^{+} population (Figure 38D) is compared to unsorted LuC4 cells (Figure 38C) the 488^{+} cells have high EpCAM and CD44 expression which suggests that they do not represent the EMT population.

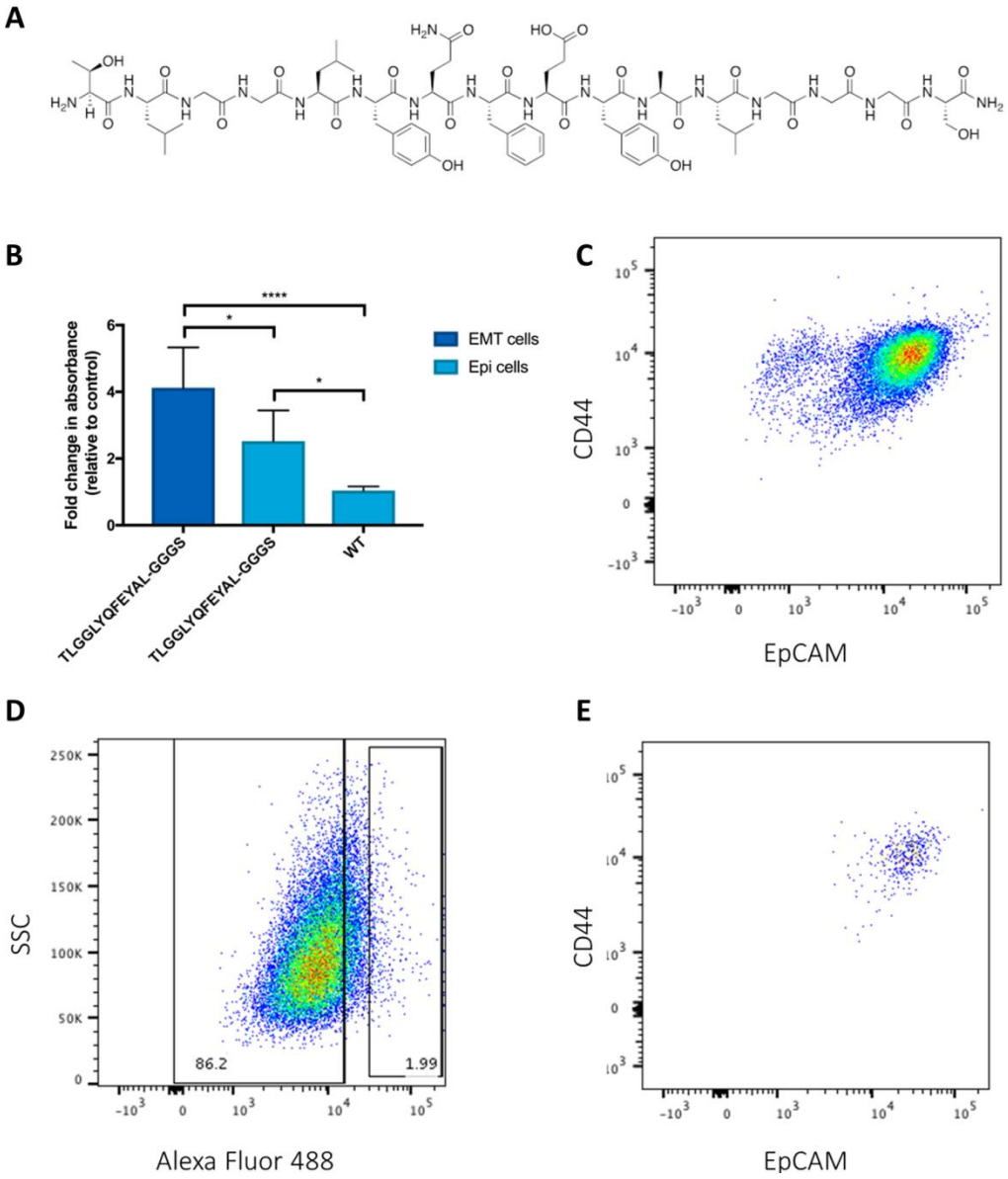

Figure 38: Assessment of TLGGLYQFEYAL-GGGS binding. Structure of TLGGLYQFEYAL-GGGS peptide sequence, identified by FACS-assisted biopanning on LuC4 cells in suspension (A) Sorted EMT and Epi LuC4 cells were incubated with the TLGGLYQFEYAL-GGGS displaying phage in suspension and the binding was determined by ELISA (B). Unsorted LuC4 cells stained with anti-CD44 and anti-EpCAM show the typical FACS plot (C). Unsorted LuC4 cells incubated with the TLGGLYQFEYAL-GGGS clone followed by anti-M13 and Alexa Fluor 488 goat anti-mouse to detect phage binding, the gate on the left captures cell which have a negative to low level of 488 staining, 86% of the population, the gate on the right captures the cells with the highest 488 signal (D). CD44 and EpCAM expression profile of the 1.99% Alexa Fluor positive LuC4 cells from the right had gate in the previous plot (E). (n = 3), error = SD, one-way ANOVA with Tukey's multiple comparisons.

3. Discussion

While panning on EMT cell monolayers failed to select clones showing significantly enhanced binding to the target cell type, the use of FACS assisted panning to isolate target cell-associated phage clones from a cell mixture in suspension did identify a candidate which warrants further investigation.

On embarking on this research there was no existing phage display facility or established protocol in place in our laboratory. As such, it is not surprising that initially experimental progress was slow as a large amount of time was dedicated to optimisation of bacterial culture, phage panning, and titring. By the end of the work the protocols employed were successfully yielding peptide sequences which demonstrated binding, of varying degrees, to cell targets. It would not be unreasonable to expect that subsequent experiments would build on the existing results to produce more robust results, as is typical as a method becomes more routine and standardised.

Lack of clear binding by flow cytometry may be due to the detection method, rather than an absence of binding or lack of specificity, which was seen by ELISA. The anti-M13-HRP conjugated antibody has not been validated for use in flow cytometry so may not be suitable. As a result, detection of binding by flow cytometry is reliant on 3 interactions, between the phage and the cell, the anti-M13 and the phage, and between the secondary antibody and the anti-M13, whereas the staining of CD44 and EpCAM only requires binding between the fluorophore-conjugated antibody and the receptor. Use of a directly conjugated anti-M13 antibody in future work may make detection of phage-cell complexes possible.

Phage display is a theoretically simple, high-throughput method for screening protein-protein interactions and while there are thousands of papers which have succeeded in selecting target-binging peptides or antibodies there are a number of limitations which it is important to consider.

Firstly, the commercially available peptide library from New England BioLabs, which was used in this work, provides a complexity of ~ 10^9 clones. However, in the case of the 12-mer library, this does not come close to covering all 4 x 10^{15} possible combinations of amino acids. This means that it is possible that the binding sequence or motif for any

given target will not be represented in the library. However, commercial libraries do provide an excellent screening tool that does not require researchers to construct their own random libraries, which can be a laborious and time consuming process,[108] thus making phage display a much more accessible platform.

A second important consideration is target specificity. As seen with the sequences identified by panning on EMT cell monolayers, it is possible for peptides to be selected as binders for more than one target in entirely independent experiments. This can have implications for downstream applications, such as cell-targeting, if the peptide turns out not to be as specific as initially thought. In the case of the GNNPLHVHHDKR-GGGS peptide, two of the experiments it was isolated in were conducted on live cells. It is conceivable that the target molecule it is binding to is present on both cell types. In the subsequent assessment of phage binding, we were unable to confirm preferential binding to the target, but an increase in binding to LuC4 cells was seen. This would support the notion that GNNPLHVHHDKR-GGGS binds to a ubiquitous cell surface molecule. While the identified general cell-binding peptide may have a number of useful experimental applications, we sought to identify a peptide which would allow specific targeting of a subset of LuC4 cells. As such, further work needs to be done, in similar experiments, Cheung *et al.*[312] were able to show an enrichment of binding to their target Jurkat cells when compared to two unrelated cell lines. Additionally, when incorporated into a fusion protein with interferon-α (IFNα), it could enhance the effects of IFNα treatment *in vitro*.

It has been demonstrated that in the absence of positive selection some phage clones have a growth advantage, leading to their over representation within the pool of phage.[148] Selection of the GNNPLHVHHDKR-GGGS peptide in our study, but lack of positive ELISA signal, could be a result of an increased replicative advantage, thus enhancing its frequency within the pool, and a panning strategy employed to isolate EMT specific binders was not stringent enough. As such, only a weak interaction between the peptide and cells would be sufficient to carry the GNNPLHVHHDKR-GGGS peptide through to the final round of panning. Additionally, this sequence, along with QVNGLGERSQQM-GGGS and GANDGVSLWRNV-GGGS, was predicted to bind to polystyrene which suggest that it may have been selected through non-specific interactions. The final sequence, VCSPCGPVPPAK-GGGS, was also identified by another

group, but failed to show target specificity in an ELISA.[312] Because we also selected this sequence, but were unable to see a positive signal by ELISA, suggests that this clone may also have a replicative advantage, especially as it was not predicted to bind to polystyrene.

The method of panning can have a large impact on the phage clones eluted and therefore carried into the next round. By conducting panning on cells in suspension, binding sites which may be occluded when cells are adhered to a surface will be revealed and can increase the number of potential binding sites. The used of FACS to isolate cell-associated phages also provided a more stringent method, seen by a reduced rate of phage recovery compared to panning on a monolayer of EMT cells (Table 7 and Table 8), which in theory would facilitate selection of clones with the highest affinity. However, a lack of enrichment suggests that there is still work needed to optimise the outcomes. The decrease in phage recovery after each subsequent round of panning could be a result of an overly stringent method, or the phage input being too high, where selective clones only make up a very small percentage of the pool and due to a replicative disadvantage are not proportionally represented following amplification. In this case, further rounds of panning may be required to see phage enrichment.

4. Future work

Cell-binding peptides identified by phage display have been applied to a range of applications, including enhanced drug-delivery,[16] optimisation of cell culture,[101] and imaging.[178] Once the protocol for panning HNSCC cells in suspension has been optimised, to isolate target-cell/phage complexes using FACS, and a peptide which specifically binds to the EMT subpopulation has been identified, there are three main avenues of further research; *in vitro* studies, development of translational applications, and identification of the cell-surface binding partner.

As reported in chapter III, modification of peptides with a thiol group can be used to display these peptides as a self-assembled monolayer. Using a similar strategy, EMT cell-binding peptides could be used to create surfaces which would interact selectively with this subpopulation. Aside from investigation how culture on a peptide SAM would influence cell behaviour, these surfaces could also be used for a very crude purification of the EMT population from an unsorted cell suspension. There are several commercially

available kits for the separation of cells from a heterogeneous population; the majority of these kits use magnetically labelled antibodies which bind to a marker of the cell type of interest on the cell surface. Cell populations are incubated with these antibodies and then the mixture is passed through a column loaded, into a magnetic block, and cells which have been labelled are immobilised by the magnetic field.[316,317] There are three main commercially available options, Dynabeads™,[318] MACS™ technologies,[316] and EasySep™[319]. Identified peptides could be used as a direct alternative to antibodies in these technologies by conjugation to magnetic beads. An example of a similar strategy from the literature demonstrates it is possible to use phage display to identify a protein-binding peptide, which when conjugated to magnetic beads can be used to extract its protein target from a solution containing multiple proteins.[320] NHS-activated magnetic beads can be purchased which would make the conjugation step a straightforward process, by incubating the peptide and beads at room temperature for 4-6 hours in an appropriate buffer.

Crude enrichment of target cells would be a useful tool before further isolation by FACS to maximise the yield of target cells. FACS is an accurate tool for isolating highly defined cell populations. However, it requires expensive reagents, fluorophore conjugated antibodies, and can be time consuming. In the case of EMT cells within HNSCC cell lines, they represent only a small percentage of the total population, which requires a large number of cells to be sorted to isolate enough EMT cells for downstream applications. Enrichment of EMT cells prior to sorting would reduce the amount of time and cells needing to be sorted.

It would also be of interest to develop the peptide for use as a reagent for flow cytometry, by conjugation to a fluorophore. This has the potential to provide a single marker for the identification of the EMT population, which could be used in conjunction with the 2-marker expression profile currently used. The fluorophore conjugated peptide could also be used for immunohistochemistry to identify EMT cells in patient samples.

More translational applications, subject to successes in the use of an EMT cell-binding peptide to enrich target cells *in vitro*, would be to utilise the peptide to detect circulating tumour cells (CTCs), or as a cell-homing peptide for targeted cancer treatment.

Currently, EpCAM is routinely used as a marker to detect CTCs out of HNSCC patient blood samples.[321] However, CTCs which have downregulated EpCAM, such as cells that have undergone EMT, will not be detected. A peptide able to bind such a population of cells would fill a current gap in CTC detection. The ability to bind peptides to a gold surface through the inclusion of a thiol could also be exploited to functionalise a gold-coated medical wire for the *in vivo* capture of CTCs.[322,323]

The development of targeted therapeutics offers the potential for improved treatment of malignancies, while reducing the impact on normal healthy cells. As off target effects seen with intra-venous administration of anticancer can be limiting factors in cancer treatments and can impact patient quality of life, reduction of these by using targeted treatments is an attractive option.[324] Conjugation of peptides which home to specific cancer cells have shown successes in reducing tumour growth[325] and increasing cell death.[326] Development of peptides, found by phage display, to specifically target the EMT subpopulation has the potential to improve treatment and reduce recurrence of the disease. Nanoparticle functionalisation has been shown to improve drug delivery to target cells with limited accumulation in healthy tissues.[327] Peptides discovered by phage display have also been used to target both nanoparticles and drug compounds to the tumour site,[163] highlighting the potential for a similar result to be achieved in HNC through selective delivery.

For all these applications, generation of a secondary phage sub-library could be used to enhance the affinity with which selected peptides bind to the EMT cells. The DNA encoding the selected peptide can be mutated to construct a library based around the original sequence, which can then be panned against EMT cells to select for the best binder.[108,328]

Finally, another interesting future project would be to determine the cell-surface binding partner of selected peptides. This could be achieved through co-immunoprecipitation experiments, where synthesised peptides can be conjugated to biotin, magnetic beads, or a thiol-containing molecule that then enables immobilisation of the peptide by streptavidin, a magnet, or a gold surface, respectively. Peptides can then be incubated with cell lysates, to allow them to bind to their binding partner, and immobilised resulting in the co precipitation of any molecules that have been bound. A Western blot can then

be done by running precipitated complexes on an electrophoresis gel, to separate proteins present based on size. Once the protein is transferred to a membrane, this can be probed with the peptide displayed as a fusion on the M13 phage, which in turn can be detected using the ant-M13 HRP-conjugated antibody. Once the approximate molecular weight, and location of the band on the gel, which belongs to the potential binding partner has been determined, the experiment can be repeated. This time the gel is stained with Coomassie brilliant blue to visualise the bands, and the one containing the potential binding partner can be cut out and analysed by mass spectroscopy. Any returned sequences from this analysis can be BLAST searched to see if they correspond to known cell proteins.[329,330]

To summarise the discussion of future works, I believe that from the current data the key areas moving forward are as follows:

I. To repeat the FACS-assisted panning procedure, taking on board all the tweaks to methodology identified during the previous rounds, such as ensuring the number of cells used is sufficiently high to allow isolation of target cells at the final sorting step. Replication of the panning process will aim to identify additional sequences which can be tested for binding, and hopefully the re-identification of the TLGGLYQFEYAL-GGGS peptide.

II. Continuation of TLGGLYQFEYAL-GGGS binding assessment. Establishing the peptides binding capacity will inform subsequent uses as either a detection probe, or in the SAM platform developed in Chapter III.

III. Modification of TLGGLYQFEYAL-GGGS, or newly identified EMT cell-binding peptides, to use to form SAM surfaces which can be tested for their suitability for *in vitro* cell culture.

5. Conclusion

Overall, this work has established a protocol for panning on live HNSCC cells in suspension which dilutes the target cell time with an equal number, or excess, of non-target cells to select for clones that selectively bind to target cells. Using a cell line which has a stably-expressing GFP line has enabled the separation of target from non-target cells by FACS without the need for additional staining. This method is capable of selecting for peptides

which preferentially bind to the target cell type. However, results could be improved by additional optimisation and peptides with enhanced binding could be generated by constructing a focused library based on the TLGGLYQFEYAL-GGGS sequence.

Chapter V - Hyaluronic acid-inspired glycomonomers and their application to cell culture as potential mimics of hyaluronic acid

1. Introduction

The use of hyaluronic acid (HA) in the medical field is far reaching. It is employed in, but not limited, plastic surgeries as a dermal filler,[331] the clinic for the treatment of arthritis,[332] biomaterials applications as a hydrogel scaffold,[236] *in vitro* studies to influence cell function,[74] and drug delivery.[333]

In mammals, HA is synthesised by three enzymes belonging to the HA synthase family, HAS1, HAS2, and HAS3.[334] HAS enzymes are membrane bound, and each contain 7 membrane domains, and polymerise alternating molecules of uridine-diphosphate-D-glucuronic acid (UDP-GlcA) and uridine diphosphate-N-Acetyl-D-glucosamine (UDP-GlcNAc) at the intracellular surface to form HA chains, which can then be translocated to the extracellular space through the HAS complex.[334] Each of these enzymes are capable of synthesising HA, but they have been shown to have different properties. HAS2 is embryonic lethal in mouse models, $HAS2^{-/-}$ knock out mice were seen to exhibit significant cardiac defects at embryonic day 9.5,[335] whereas knockdown of HAS1 and HAS3 does not result in any gross abnormalities.[336,337] In addition to differing roles in embryogenesis, the HAS isoforms show differential levels of enzymatic activity. HAS1 exhibits the highest K_m for UDP-GlcA and UDP-GlcNAc which correlates with the smaller HA coat generated when COS-1 cells were transfected with HAS1 cDNA when compared to HAS2 and HAS3, with HAS3 having the highest rate of activity.[338] The average molecular weight of the HA synthesised by each of the enzymes is also different, with HAS2 producing higher molecular weight HA, in the region of 2×10^6 Da.[338]

Current methods for production of the large quantities of HA needed for use in disease treatment, translational and basic science, involves either isolation from animal sources, bacterial synthesis, or cell-free systems, each of which comes with its own benefits and drawbacks.

Extraction from animal tissues, predominantly from bovine vitreous and rooster comb, was the primary method used to obtain HA on an industrial scale.[339] This protocol

produces polydisperse high molecular weight HA, which presents several limitations. During the extraction process, tissues are homogenised which causes release of hyaluronidases from within cells. This, coupled with the harsh extraction conditions, can result in the degradation of HA, thus contributing to the wide range of molecular weights generated. While rooster comb and bovine vitreous have high HA expression levels when compared with other animal tissues, the yield produced is still very low.[340]

Through bacterial fermentation, HA can be produced with a higher yield of approximately 6-7 g/L. Increased viscosity of the bacterial culture broth, caused by the secretion of HA, results in poor mixing and oxygenation which, in turn, limits the amount of HA that can be synthesised and isolated from each batch.[341] Using bacteria to synthesise HA allows a level of control over the molecular weight range of the HA produced and greater oxygenation of cultures leads to the production of HA with a greater molecular weight. The availability of the precursor sugars UDP-GlcA and UDP-GlcNAc also influences HA MW. By keeping the ratio of hyaluronan synthase to monomers below 2, the size of HA polymers can be maximised.[342]

Both bacterial synthesis and extraction from animal tissues carry the risk of the HA product being contaminated by amino acids, DNA, or viruses with purification techniques providing a costly solution. Contamination with bacterial or animal products is of particular importance when HA is to be used as a therapeutic agent. As a result, production of HA using cell-free systems has been developed by Jing and DeAngelis.,[343] They were able to engineer a soluble HAS protein which retained its glycosyltransferase activity. Using this method, it is possible to synthesise HA molecules with a much narrower distribution of MWs and, by controlling the availability of the UDP-sugars to each enzyme, the MW of HA generated can be regulated. For example, having a large number of enzyme molecules, but restricted sugar availability, will result in smaller chains being synthesised as the limited sugars will be distributed across all of the HAS units,[344] demonstrating how important the molar ratio of enzyme to substrate is. Using this method affords greater control over the HA produced, without the risk of animal product contamination, but the yield still remains low.[345]

One alternative to overcome the challenges of HA synthesis is to develop synthetic mimics, using a polymer backbone functionalised with the HA (GlcA and GlcNAc) sugars.

Similar strategies to synthesise glycopolymers inspired by natural carbohydrates have been used and shown to have a degree of biological activity.[346,347] The ability to synthesise bioinspired mimics has helped advance the study and understanding of signal transduction downstream of glycan-receptor interaction at the cell surface. [348]

Chemical synthesis of HA glycopolymers has been attempted using HA-derived dimers of GlcA and GlcNAc. The disacchride was coupled to a polymerisable chemical group via a linker to form a glycomonomer. Once polymerised, the polynorbornene acts as a backbone to display the HA fragments, and it is suggested to act to inhibit native saccharide-protein interactions.[349] Additionally, by using this method of synthesis the glycopolymers formed showed a low level of polydispersity, demonstrating the ability of chemical synthesis to produce glycopolymers of a uniform size. A similar study used heparan sulfate saccharides on a bottleneck polymer backbone to inhibit the activity of the heparan sulfate-cleaving enzyme heparanase.[350]

The literature demonstrates that there is still a requirement for animal product-free synthesis of uniformly high molecular weight HA on an industrial scale to meet the commercial demand in a market. It is anticipated that the HA market will reach a value of $7.25 billion by 2023,[351] While the replacement of HA by biomimetic glycopolymers in cosmetics and therapeutics may not happen in the near future, their use as probes to perform in vitro studies may be a closer eventuality.

In addition to the removal of the risk of animal product contamination, other potential benefits of synthetic HA analogues include enhanced control over MW and increased uniformity, and the possibility for pre- and post–synthesis functionalization. Greater control over HA MW is of particular interest due to the size-dependent effects of HA in cells signalling which is also implicated in disease.[79,80] The different effects of HA based on its MW highlights the importance of having control over the size of HA chains used in in vitro studies aimed at elucidating the function of HA.

The work developed by a colleague in the lab, Mr. Dominic Collis elegantly demonstrates the chemical synthesis of a number of glycopolymers comprising of the two HA monosaccharides. [221] Four of these glycopolymers were selected for investigating their potential effects on cells in vitro. The chosen glycopolymers included two homopolymers, consisting of either GlcA or GlcNAc glycomonomers, a statistical copolymer, and an

alternating copolymer (Figure 39). All four glycopolymers were formed by polymersisation of the poly(4-vinylbenzyl chloride) backbone and subsequent addition of the two sugars using 'click' chemistry.[352]

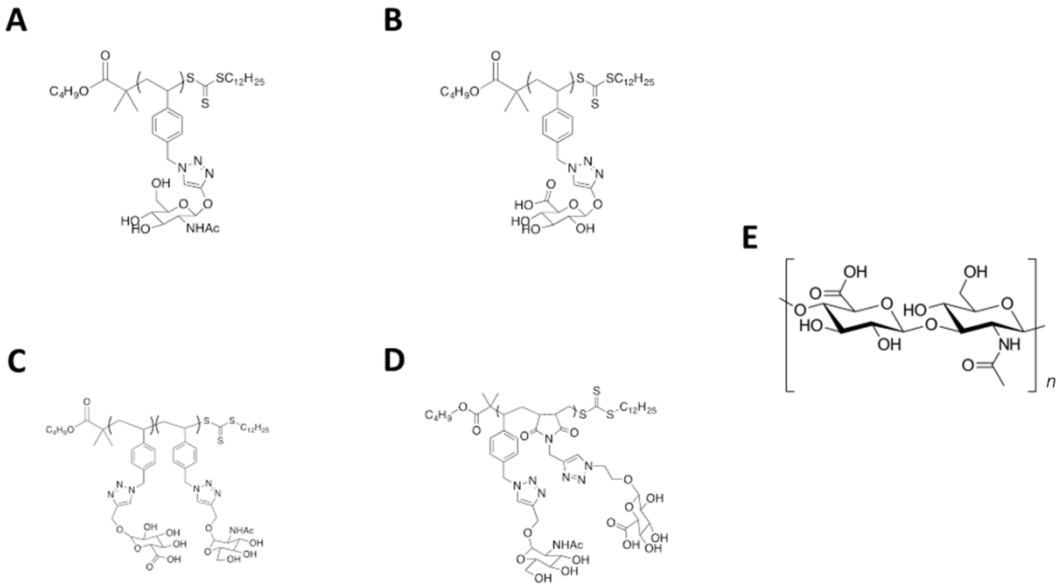

Figure 39: Chemical structure of glycopolymers, PVB-GlcNAc (A) and PVB-GlcA (B) homopolymers, PVB-GlcA-co-VB-GlcNAc (C) and PVB-GlcNAc-alt-PMI-GlcA (D) copolymers, with the repeating HA disaccharide (E).

2. Results

2.1. Cytotoxicity assessment of glycopolymers

Before performing cell studies to investigate the effect of the glycopolymers on cell behaviours and their ability to mimic natural HA, it was necessary to ensure that they were not cytotoxic. LuC4 cells were seeded onto 96-well plates and, following 48 hours incubation, treated with 100 µg/ml, 10 µg/ml, 1 µg/ml, or 0.1 µg/ml of each glycopolymer for 24 hours. The viability of cells was determined using the Live/dead® viability/cytotoxicity kit, this kit was selected in place of simply counting cells as, when counting cells, it can be difficult to determine which cells on the surface are alive and which are dead, the live/dead assay identifies live cells by their intracellular esterase activity. It also provides information on the proportion of dead cells, which is useful information to have when investigating the effect of treatment on cell lines. A final reason

for the use of a fluorescence assay is that it provides a less labour intensive method for collecting data.

Fluorescence intensity was measured at emission 528/20 nm with excitation 485/20 nm and emission: 590/35 nm with excitation 530/25nm, respectively. To calculate the percentage of live and dead cells in each well, the following equations supplied by the manufacturer were used:

Equation 8: Percentage of live cells

$$\%\ Live\ cells = \frac{F(530)_{Sample} - F(530)_{min}}{F(530)_{max} - F(530)_{min}}\ x\ 100\%$$

Equation 9: Percentage of dead cells

$$\%\ Dead\ cells = \frac{F(645)_{Sample} - F(645)_{min}}{F(645)_{max} - F(645)_{min}}\ x\ 100\%$$

Where $F(530)_{sample}$ is the fluorescence signal of the sample at 530 nm, $F(530)_{min}$ is the fluorescence signal at 530 nm of methanol-fixed cells stained with EthD-1, $F(530)_{max}$ is the fluorescence signal at 530 nm of untreated cells stained with calcein, $F(645)_{sample}$ is the fluorescence signal of the sample at 645 nm, $F(645)_{min}$ is the fluorescence signal at 645 nm of methanol-fixed cells stained with calcein, and $F(645)_{max}$ is the fluorescence reading at 645 nm of dead cells stained with EthD-1.

Treatment of LuC4 cells with the alternating copolymer and GlcNAc homopolymer had little effect on the proportion of live cells. However an increase in the number of dead cells for both treatments was seen to increase to around 20%. Treatment with the GlcA homopolymer showed a trend for reduced viability in a dose-dependent manner; a similar trend was not seen with the percentage of dead cells. Treatment of cells with the statistical copolymer resulted in the lowest level of cell viability of around 60%, while cell death was around 30%.

There was no significant difference in cell viability or amount of cell death between any of the four glycopolymer treatments. As such, it was concluded that the HA-based glycopolymers are not significantly cytotoxic.

2.2. Effect of HA-based glycopolymers on sphere formation

The LuC4 cell line used in this work, and in previous experimental chapters, is an immortalised head and neck cancer cell line which contains a subpopulation of cells which exhibit a higher level of CD44 expression. These cells possess stem cell-like properties and are thought to contribute significantly to high rates of secondary tumours and recurrence seen in HNSCC patients.[15,353] A role for CD44/HA induced signalling in the progression of cancer has been established and suggests the importance of this interaction in cell motility, therapeutic resistance, and maintenance of stem cell properties.[354] Specifically, within HNSCC, treatment of cells with HA, through supplementation of cell culture medium, has been shown influence cancer stem cell behaviour. A FACS sorted subpopulation of HNSCC cells, with high CD44 isoform v3 and ALDH1 levels (CD44v3^{high}/ ALDH1^{high}), treated with HA showed an increase in both the number and size of spheres formed in a sphere assay.[244]

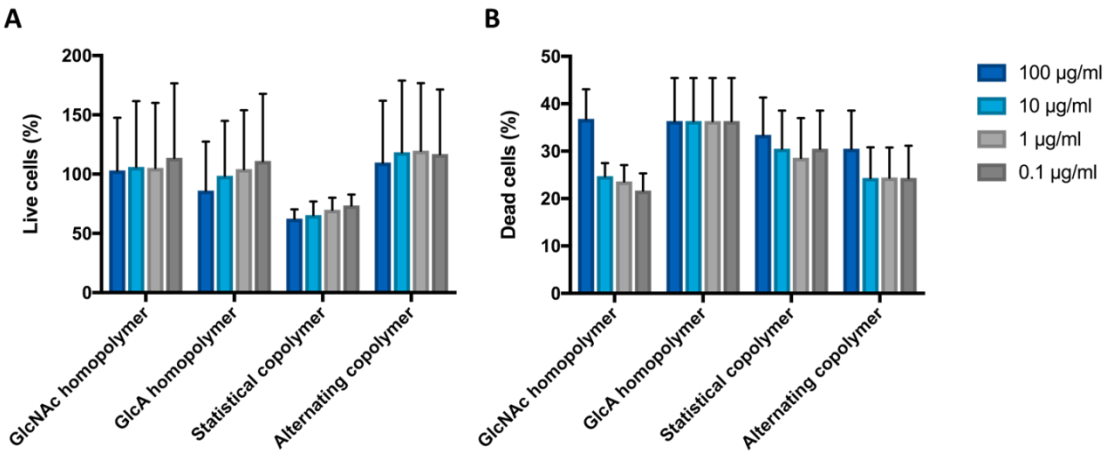

Figure 40: **Effect of glycopolymers on cell viability,** following treatment with HA-based glycopolymers viability was assessed using the Live/Dead viability/cytotoxicity kit. Bar graph shows the average percentage of live (A) and dead (B) LuC4 cells. (n=3), error bars represent standard deviation, two-way ANOVA with Tukey's multiple comparisons.

A similar subpopulation of HNSCC cells, with CSC properties, identified by $CD44^{high}/EpCAM^{low}$ expression profile exists within the LuC4 cell line.[49] Although ALDH1 profile is not used to select for this cell population, it has been shown that at least a fraction of these cells possess ALDH1 enzyme activity and have the capacity to form spheres *in vitro*.[26,49]

As the HA-based glycopolymers did not show cell toxicity we wanted to see if they were able to influence LuC4 CSC properties in a similar way to HA. To asses this a sphere assay was carried out using this $CD44^{high}/EpCAM^{low}$ (EMT) subpopulation of cells. Poly(2-hydroxyethyl methacrylate)-coated plates were used to seed sorted EMT cells in full culture medium supplemented with 1% methylcellulose and 50 µg/ml final concentration of HA or glycopolymer.

Work carried out in the Azevedo laboratory has utilised peptide synthesis to generate small peptides which mimic the natural HA binding motif found in CD44, as well as the more widely expressed link domain sequence, which also binds HA. Surface plasmon resonance was subsequently employed to demonstrate that there are varying degrees of interaction between the synthetic glycopolymers and HA binding sequences. [221] As such we hypothesise that these glycopolymers may be able to alter cell behaviour in a similar way to how HA has been shown to in the literature.

Initially, after 14 days in culture, imaging revealed no real sphere formation under any of the treatment conditions. In some wells, one or two small groups of cells were seen which could represent the early stages of sphere formation (Figure 41).

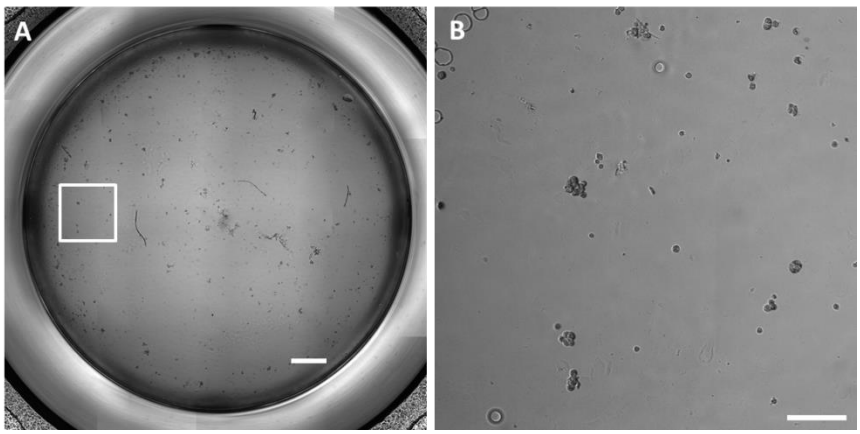

Figure 41: Formation of small cell clusters by sphere assay. Representative image of tissue culture plate wells and LuC4 cells following treatment with 1.5 MDa HA for 14 days (A), and an enlarged image of the selected area (B). Scale bars represent 1 mm and 250 µm, respectively.

Spheres were allowed to form for a further week, to take the total period of time in culture to 21 days. At this time point, an increase in the number of groups of cells was seen, and they tended to be of a larger size (Figure 42). However, the cells within these groups were not highly compacted, and distinct cells could be seen. The morphology of these pre-spheres suggests that a greater period of incubation and treatment would be required to see the formation of fully matured and compacted spheres.

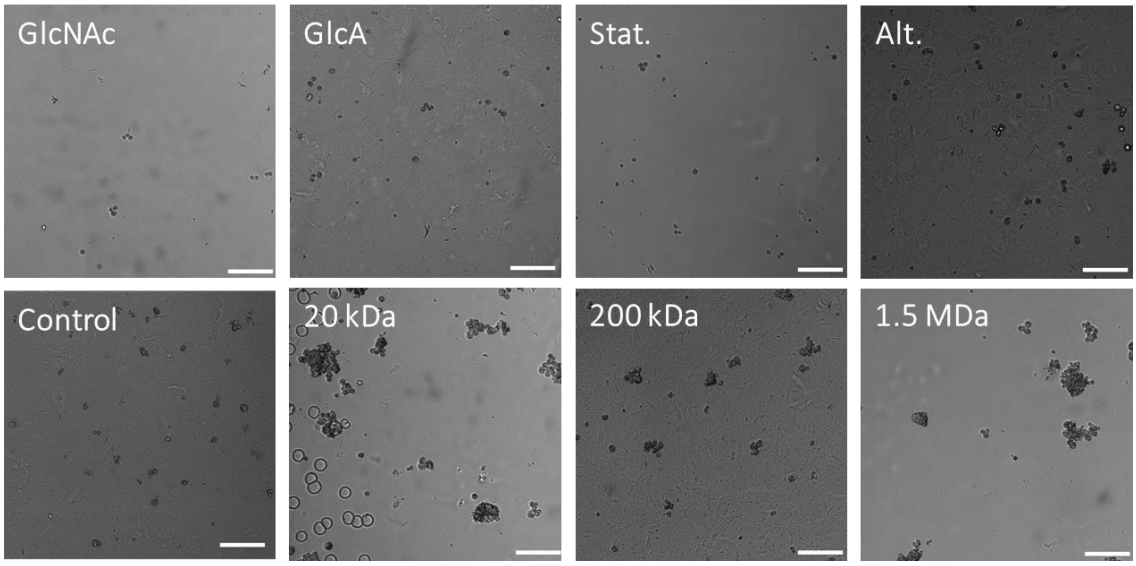

Figure 42: Effect of glycopolymers on LuC4 cell sphere forming ability compared to natural HA. Representative images of LuC4 cells following 21 days in culture under non-adherent conditions. Cells were treated with glycopolymers (top row) or HA with various MW (bottom row), as indicated, with a final concentration of 50 µg/mL. Scale bar represents 250 µm.

As the MW of HA has repeatedly been shown to influence its effects both *in vivo* and *in vitro*, three different molecular weights of HA were used to treat cells with sphere forming potential, 20 kDA, 200 kDa, and 1.5 MDa. Over the course of the 21 days treatment, HA molecular weight did not appear to have a substantial effect on the number of spheres formed. However, a greater average number of 'pre-spheres' was observed when cells were treated with higher HA MW, 200 kDa and 1.5 MDa (Figure 43).

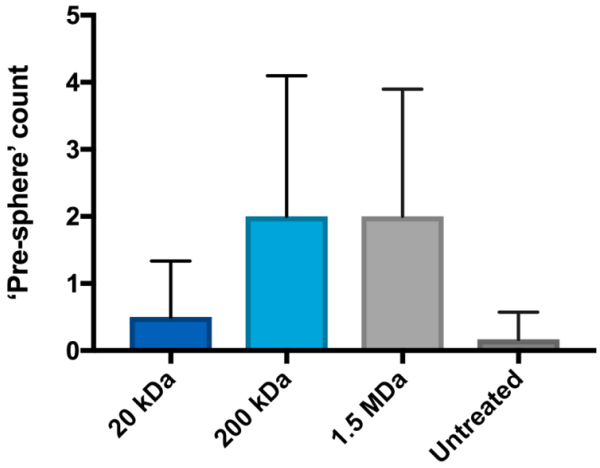

Figure 43: Formation of 'pre-spheres' following treatment with HA. LuC4 cells were cultured under non-adherent conditions and treated with 50 µg/mL HA with a MW of 20 kDa, 200 kDa, or 1.5 MDa. After 21 days the number of 'pre-spheres' were counted. n=3.

3. Discussion

The preliminary experiments presented here demonstrate that treatment of LuC4 cells with HA-based glycopolymers did not affect their viability. Of all the glycopolymers, the statistical copolymer showed the lowest level of cell viability. It was interesting to see that although there was a reduction in cell viability, and an increase in cell death, these values were similar across the range of concentrations used, suggesting that this effect was dose-independent.

To investigate the ability of these glycopolymers to mimic some of the biological functions of HA in the context of head and neck cancer stem cells, a sphere assay was performed. This assay is commonly used to assess the stem-ness of population of cells through determining their ability to form spheres and proliferate in suspension. From this

information, it is possible to calculate the frequency with which stem cells and their progenitors exist in the population of cells being studied.[355]

The clusters of cells that were seen where cells were treated with HA, either with a MW of 200 kDa or 1.5 MDa, and glycopolymers, looked like they could be at the beginning stages of sphere formation. However, it is likely to be misleading to categorise them as spheres in this assay.[355] Mature spheres contain compacted cells with a regular morphology and can have a diameter ranging from around 50-250 μm, while the groups of cells observed in this work were much less condensed and were of a more irregular shape and size. This should be kept in mind throughout the discussion of the trends observed.

As mentioned, existing literature demonstrated the ability of HA treatment to increase sphere formation.[244] However, our results were unable to replicate this convincingly. There a several potential explanations for this. Primarily, it is likely that the duration of the experiment was not sufficiently long to allow maturation of spheres. While sphere formation can be seen in as little as a few days in the case of some cancer cells,[356,357] other cells take much longer before mature spheres are observed. It is possible that the cell aggregates seen are simply due to cell clumping, but a well-established protocol was followed which included passing cells through a strainer to ensure single cell suspension. Additionally, cells were seeded in medium containing 1% methylcellulose, which increases the viscosity of the medium and reduces the amount of cell movement thereby minimising single cells drifting into each other. LuC4 cells have previously been shown to form spheres after 2 weeks of culture,[49] but a higher starting cell density was used, plating twice as many cells per well. This could explain the difference in sphere formation, as it is well established that starting cell concentration can influence the rate of sphere formation.[230]

A trend for increased 'pre-spheres' was seen for the treatment of LuC4 cells with 200 kDa or 1.5 MDa, but not 20 kDa HA (Figure 43). This observation could be indicative of another example of the importance of MW on the effects of HA. To the best of my knowledge the effects of HA molecular weight on sphere formation of CSCs has not been directly compared. Treatment of cells with 500 kDa HA resulted in the upregulation of stem cell genes mediated through interaction with CD44,[358] which supports the idea that high MW

HA is involved in stem cell signalling and promotion of sphere formation previously documented.[244]

Little evidence of the beginnings of sphere formation was observed when cells were treated with the four HA-based glycopolymers, indicating that these glycopolymers are unable to mimic the *in vitro* effects of HA. There are a number of possible reasons why this may be the case. Aside from the polymer backbone, which is more rigid and may have interfered with cell-binding and subsequent signalling, one key difference between the alternating copolymer and natural HA is the absence of a glycosidic bond. This may be important for maintaining the correct conformation of the two monosaccharides for interacting with cell surface receptors to induce signalling. Unpublished data collected by other members of our lab demonstrates that alternating glycopolymer-binding to Pep-1, a HA-binding peptide, is minimal which would also suggest that such glycopolymers in their current format are not yet able to mimic HA binding. It should also be noted that the MW of the glycopolymers is approximately 20 kDa, and when cells were treated with 20 kDa HA minimal effects on pre-sphere number were seen (Figure 43). As such, the lack of effect of the glycopolymers may also be a result of their low MW.

4. Conclusions and outlook

This work demonstrates that HA-based polymers can be used as probes to investigate the behaviour of cancer cells without causing a significant reduction of cell viability, although no effect on sphere formation was seen. Further work to determine the optimal conditions and duration of the sphere assay would be required before any firm conclusions can be drawn from this work.

An important consideration moving forward would be to investigate how glycopolymers are processed by cells. *In vivo*, HA is degraded by hyaluronidases, of which there are six in humans.[63] Their expression and action has been shown to influence cell behaviour. For example, HA fragments produced by the enzymatic action of hyaluronidases can induce activation of metalloproteinases or initiate inflammation.[359,360] Within the literature, glycopolymers have been used to inhibit the function of glycosidases, suggesting that they are resistant to degradation themselves.[350] It would be important to investigate the potential inhibitory effects of HA-based glycopolymers on the ability of hyaluronidases, such as HYAL1, to degrade natural HA. It would be expected that these glycopolymers are

not susceptible to degradation as they lack a glycosidic bond. It is possible that even if glycopolymers alone are not able to influence cell behaviour in the same way as HA, they could still be employed to reduce HA fragmentation by hyaluronidases and act as enzyme inhibitors.

SECTION 4 - CONCLUSIONS

Chapter VI – Conclusions and Future work

This final section of the thesis aims to summarise the work carried out and draw together the key conclusions, with a focus on how this work can be built on through future research.

The work set out in this thesis applies chemical modification of a peptide to create a reagent for forming SAMs that can be used to immobilise a component of the EMC, and subsequently be used for cell culture. A high throughput protocol for selecting candidate peptides for use in this is also established which will inevitably lead to the creation of novel surfaces for probing cell behaviours *in vitro*. Parallel work began to investigate the use of synthetic, HA-based, glycopolymers to manipulate cell properties *in vitro* utilised. With a view to develop a peptide based system that could immobilise these glycopolymers and reduce the need for cell derived products in cell culture systems.

The extracellular environment has a critical role in the regulation of cell behaviour; interactions between the extracellular matrix (ECM) and the cell are responsible for modulation of cell migration, survival, and differentiation. In disease, changes in the localised environment, such as joint tissue in arthritis or the tumour microenvironment, are often evident and have been shown to be responsible for dysregulation of normal cell function. In the case of head and neck cancer (HNC), ECM glycosaminoglycan hyaluronic acid (HA) plays an important role in influencing cell properties. It has been shown to increase the migratory capacity of cells, to upregulate putative stem cell markers, and to enhance behaviour associated with stemness, including contact-independent growth and recapitulate heterogeneity from a single cell.

Immobilisation of HA on surfaces to study its effects on cancer stem cells (CSCs) *in vitro* would be a useful tool. However, the majority of work in the literature utilises chemically modified or cross-linked HA which can interfere with the native characteristics of HA, such as its enzymatic degradation by hyaluronidases. Here, immobilisation of native HA was achieved using self-assembled monolayers (SAMs) of HA-binding peptide, Pep-1, modified to contain a thiol group at its N-terminal. Characterisation of the peptide-HA surface revealed a substrate with distinct properties when compared to HA immobilisation by electrostatic forces with poly-D-lysine. Preparation of these HA

surfaces for tissue culture altered cell migration, but further work to fully establish and exploit HA-cell interactions is required.

The system developed to successfully form peptide SAMs on gold surfaces, using thiolated Pep-1 as a starting point, can easily be applied to a different set of research questions by immobilising a different peptide. Identification of a potential peptide was achieved through combining fluorescence activated cell sorting (FACS), GFP cell lines, and phage display. FACS-isolated $CD44^{high}/EpCAM^{low}$ cells were used as target cells for three rounds of biopanning to select binding peptides from the commercially available New England BioLabs random peptide library. Sequencing the genome of the isolated bacteriophage revealed a 12 amino acid peptide with the sequence TLGGLYQFEYAL. This peptide was seen to have enhanced binding to $CD44^{high}/EpCAM^{low}$ cells compared to $CD44^{high}/EpCAM^{high}$ cells by phage-binding ELISA.

We anticipate that inclusion of a cysteine at the C-terminal will allow the peptide to form a SAM on gold; if this is the case; future research can focus on elucidating potential effects of this peptide *in vitro* and the molecular mechanisms through which the signalling is transduced. There is also scope for develop the peptide-SAM for crude isolation and enrichment of target cells from heterogeneous populations prior to more precise selection techniques, such as FACS.

Research presented in the third chapter started to investigate the ability of HA-based glycopolymers to mimic the biological function of HA. However, additional work is required to fully assess their potential as synthetic HA substitutes or as molecular tools for studying HA's multiple functions.

Over all, the work presented in this thesis has contributed to the development of a peptide-based self-assembly system for the immobilisation of individual components of the ECM and the study of specific cell-ECM interactions *in vitro*. It has also demonstrated the use of phage display for the identification of cell-binding peptide. This peptide has the potential to be modified to incorporate a thiol group and applied to the above self-assembly system.

References

1. Ferlay, J. *et al.* Cancer incidence and mortality worldwide: Sources, methods and major patterns in GLOBOCAN 2012. *Int. J. Cancer* **136,** E359–E386 (2015).
2. Price, G., Roche, M., Crowther, R. & Wright, R. Head and Neck Profiles. (2010). Available at: http://www.ociu.nhs.uk/sph-documents/Head_and_Neck_Profiles.pdf. (Accessed: 19th February 2015)
3. Macmillan Cancer Support. Treatment overview - Understanding -. (2015). Available at: https://www.macmillan.org.uk/information-and-support/head-and-neck-cancers/treating/treatment-decisions/understanding-your-diagnosis/treatment-overview.html. (Accessed: 17th August 2018)
4. Clevers, H. The cancer stem cell: premises, promises and challenges. *Nat. Med.* **17,** 313–9 (2011).
5. Batlle, E. & Clevers, H. Cancer stem cells revisited. *Nat. Med.* **23,** 1124–1134 (2017).
6. Prince, M. E. *et al.* Identification of a subpopulation of cells with cancer stem cell properties in head and neck squamous cell carcinoma. *Proc. Natl. Acad. Sci. U. S. A.* **104,** 973–8 (2007).
7. Locke, M., Heywood, M., Fawell, S. & Mackenzie, I. C. Retention of intrinsic stem cell hierarchies in carcinoma-derived cell lines. *Cancer Res.* **65,** 8944–8950 (2005).
8. Barrandon, Y. & Green, H. *Three clonal types of keratinocyte with different capacities for multiplication*. *Proc. Nati. Acad. Sci. USA* **84,** (1987).
9. Wicha, M. S., Liu, S. & Dontu, G. Cancer Stem Cells: An Old Idea-A Paradigm Shift. *Cancer Res* **66,** 1883–90 (2006).
10. Biddle, A. & Mackenzie, I. C. Cancer stem cells and EMT in carcinoma. *Cancer Metastasis Rev.* 285–293 (2012). doi:10.1007/s10555-012-9345-0
11. Chikamatsu, K. *et al.* Resistance to apoptosis-inducing stimuli in CD44+ head and neck squamous cell carcinoma cells. *Head Neck* **34,** 336–343 (2012).
12. Harper, L. J. *et al.* Normal and malignant epithelial cells with stem-like properties

have an extended G2 cell cycle phase that is associated with apoptotic resistance. *BMC Cancer* **10,** 166 (2010).

13. Tsai, L. L., Yu, C. C., Chang, Y. C., Yu, C. H. & Chou, M. Y. Markedly increased Oct4 and Nanog expression correlates with cisplatin resistance in oral squamous cell carcinoma. *J. Oral Pathol. Med.* **40,** 621–628 (2011).

14. Chikamatsu, K., Takahashi, G., Sakakura, K., Ferrone, S. & Masuyama, K. Immunoregulatory properties of CD44+ cancer stem-like cells in squamous cell carcinoma of the head and neck. *Head Neck* **33,** 208–15 (2011).

15. Sayed, S. I. *et al.* Implications of understanding cancer stem cell (CSC) biology in head and neck squamous cell cancer. *Oral Oncol.* **47,** 237–43 (2011).

16. Arap, W., Pasqualini, R. & Ruoslahti, E. Cancer Treatment by Targeted Drug Delivery to Tumor Vasculature in a Mouse Model Cancer Treatment by Targeted Drug Delivery to Tumor Vasculature in a Mouse Model. **279,** 377–380 (1998).

17. Castaigne, S. *et al.* Effect of gemtuzumab ozogamicin on survival of adult patients with de-novo acute myeloid leukaemia (ALFA-0701): a randomised, open-label, phase 3 study. *Lancet* **379,** 1508–1516 (2012).

18. Rowe, J. M. & Löwenberg, B. Gemtuzumab ozogamicin in acute myeloid leukemia: a remarkable saga about an active drug. *Blood* **121,** 4838–41 (2013).

19. Burnett, A. K. *et al.* Addition of Gemtuzumab Ozogamicin to Induction Chemotherapy Improves Survival in Older Patients With Acute Myeloid Leukemia. *J. Clin. Oncol.* **30,** 3924–3931 (2012).

20. Center for Drug Evaluation and Research. Approved Drugs - FDA Approves Gemtuzumab Ozogamicin for CD33-positive AML. (2017). Available at: https://www.fda.gov/Drugs/InformationOnDrugs/ApprovedDrugs/ucm574518.htm. (Accessed: 18th August 2018)

21. Riechelmann, H. *et al.* Phase I trial with the CD44v6-targeting immunoconjugate bivatuzumab mertansine in head and neck squamous cell carcinoma. *Oral Oncol.* **44,** 823–9 (2008).

22. Heider, K. H., Kuthan, H., Stehle, G. & Munzert, G. CD44v6: A target for antibody-

based cancer therapy. *Cancer Immunol. Immunother.* **53,** 567–579 (2004).

23. Kalluri, R. & Weinberg, R. The basics of epithelial-mesenchymal transition. *J. Clin. Invest.* **119,** (2009).

24. Stone, R. C. *et al.* Epithelial-mesenchymal transition in tissue repair and fibrosis. *Cell Tissue Res.* **365,** 495–506 (2016).

25. Polyak, K. & Weinberg, R. a. Transitions between epithelial and mesenchymal states: acquisition of malignant and stem cell traits. *Nat. Rev. Cancer* **9,** 265–73 (2009).

26. Biddle, A. *et al.* Cancer stem cells in squamous cell carcinoma switch between two distinct phenotypes that are preferentially migratory or proliferative. *Cancer Res.* **71,** 5317–26 (2011).

27. van der Gun, B. T. F. *et al.* EpCAM in carcinogenesis: the good, the bad or the ugly. *Carcinogenesis* **31,** 1913–1921 (2010).

28. Andratschke, M. *et al.* Limited suitability of EpCAM for molecular staging of tumor borders in head and neck cancer. *Anticancer Res.* **26,** 153–158 (2006).

29. Brabletz, T., Jung, A., Spaderna, S., Hlubek, F. & Kirchner, T. Migrating cancer stem cells — an integrated concept of malignant tumour progression. *Nat. Rev. Cancer* **5,** 744–749 (2005).

30. Skvortsova, I. *et al.* Epithelial-to-mesenchymal transition and c-myc expression are the determinants of cetuximab-induced enhancement of squamous cell carcinoma radioresponse. *Radiother. Oncol.* **96,** 108–115 (2010).

31. Hollier, B. G., Evans, K. & Mani, S. a. The epithelial-to-mesenchymal transition and cancer stem cells: a coalition against cancer therapies. *J. Mammary Gland Biol. Neoplasia* **14,** 29–43 (2009).

32. Dave, B., Mittal, V., Tan, N. & Chang, J. Epithelial-mesenchymal transition, cancer stem cells and treatment resistance. *Breast Cancer Res* 1–5 (2012).

33. Screaton, G. R. *et al.* Genomic structure of DNA encoding the lymphocyte homing receptor CD44 reveals at least 12 alternatively spliced exons. **89,** 12160–12164 (1992).

34. Stamenkovic, I., Aruffo, A., Amiot, M. & Seed, B. The hematopoietic and epithelial forms of CD44 are distinct polypeptides with different adhesion potentials for hyaluronate-bearing cells. *EMBO J.* **10,** 343–348 (1991).

35. Mackay, C. R. *et al.* Expression and modulation of CD44 variant isoforms in humans. *J. Cell Biol.* **124,** 71–82 (1994).

36. Jackson, D. G. *et al.* Proteoglycan forms of the lymphocyte homing receptor CD44 are alternatively spliced variants containing the v3 exon. *J. Cell Biol.* **128,** 673–85 (1995).

37. Bennett, K. & Modrell, B. Regulation of CD44 binding to hyaluronan by glycosylation of variably spliced exons. *J. Cell Biol.* **131,** 1623–1633 (1995).

38. Bennett, K. L. *et al.* CD44 Isoforms Containing Exon V3 Are Responsible for the Presentation of Heparin-binding Growth Factor. *J. Cell Biol.* **128,** 687–698 (1995).

39. Hayes, G. M., Chiu, R., Carpenito, C., Dougherty, S. T. & Dougherty, G. J. Identification of sequence motifs responsible for the adhesive interaction between exon v10-containing CD44 isoforms. *J. Biol. Chem.* **277,** 50529–34 (2002).

40. Brown, R. L., Reinke, L. M., Damerow, M. S. & Perez, D. CD44 splice isoform switching in human and mouse epithelium is essential for epithelial-mesenchymal transition and breast cancer progression. **121,** (2011).

41. Günthert, U. *et al.* A New Variant of Glycoprotein CD44 Confers Metastatic Potential to Rat Carcinoma Cells. *Cell* **65,** 13–24 (1991).

42. Wang, S. J., Wong, G., de Heer, A.-M., Xia, W. & Bourguignon, L. Y. W. CD44 variant isoforms in head and neck squamous cell carcinoma progression. *Laryngoscope* **119,** 1518–30 (2009).

43. Wang, S. J., Wreesmann, V. B. & Bourguignon, L. Y. W. ASSOCIATION OF CD44 V3-CONTAINING ISOFORMS WITH TUMOR CELL GROWTH, MIGRATION, MATRIX METALLOPROTEINASE EXPRESSION, AND LYMPH NODE METASTASIS IN HEAD AND NECK CANCER. 550–558 (2007). doi:10.1002/hed

44. Biddle, A., Gammon, L., Fazil, B. & Mackenzie, I. C. CD44 staining of cancer stem-like cells is influenced by down-regulation of CD44 variant isoforms and up-

regulation of the standard CD44 isoform in the population of cells that have undergone epithelial-to-mesenchymal transition. *PLoS One* **8,** e57314 (2013).

45. de Jong, M. C. *et al.* CD44 Expression Predicts Local Recurrence after Radiotherapy in Larynx Cancer. *Clin. Cancer Res.* **16,** 5329–5338 (2010).

46. Donovan, M., Reis, I., Curtis, K., Khan, F. & Franzmann, E. PO-137: Multivariate oral rinse models predict Head and Neck squamous cell carcinoma (HNSCC). in *Radiotherapy and Oncology* **122,** 66 (2017).

47. Hashikata, M. *et al. Snail-induced CD44 high cells in HNSCC with high ABC transporter capacity exhibit potent resistance to cisplatin and docetaxel*. *Int J Clin Exp Pathol* **9,** (2016).

48. Kidwai, F., Costea, D. E., Hutchison, I. & Mackenzie, I. The effects of CD44 down-regulation on stem cell properties of head and neck cancer cell lines. *J. Oral Pathol. Med.* **42,** 682–90 (2013).

49. Shigeishi, H. *et al.* Maintenance of stem cell self-renewal in head and neck cancers requires actions of GSK3β influenced by CD44 and RHAMM. *Stem Cells* **31,** 2073–83 (2013).

50. Tsai, I. Y. Human macrophages adhesion on polysaccharide patterned surfaces. *Soft Matter* **7,** 3599–3606 (2011).

51. Toole, B. P. Hyaluronan-CD44 Interactions in Cancer: Paradoxes and Possibilities. *Clin. Cancer Res.* **15,** 7462–7468 (2009).

52. Bajorath, J., Greenfield, B., Munro, S. B., Day, A. J. & Aruffo, A. Identification of CD44 Residues Important for Hyaluronan Binding and Delineation of the Binding Site. *J. Biol. Chem.* **273,** 338–343 (1998).

53. Wang, S. J. & Bourguignon, L. Y. W. Hyaluronan and the Interaction Between CD44 and Epidermal Growth Factor Receptor in Oncogenic Signaling and Chemotherapy Resistance in Head and Neck Cancer. *Arch. Otolaryngol. Neck Surg.* **132,** 771 (2006).

54. Bourguignon, L. Y. W., Gilad, E., Brightman, A., Diedrich, F. & Singleton, P. Hyaluronan-CD44 Interaction with Leukemia-associated RhoGEF and Epidermal

Growth Factor Receptor Promotes Rho/Ras Co-activation, Phospholipase C-Ca 2 Signaling, and Cytoskeleton Modification in Head and Neck Squamous Cell Carcinoma Cells. *J. Biol. Chem.* **281,** 14026–14040 (2006).

55. Kim, Y. *et al.* CD44-Epidermal Growth Factor Receptor Interaction Mediates Hyaluronic Acid-promoted Cell Motility by Activating Protein Kinase C Signaling Involving Akt, Rac1, Phox, Reactive Oxygen Species, Focal Adhesion Kinase, and MMP-2. *J. Biol. Chem.* **283,** 22513–22528 (2008).

56. Wang, S. J. & Bourguignon, L. Y. W. Hyaluronan-CD44 Promotes Phospholipase C–Mediated Ca 2+ Signaling and Cisplatin Resistance in Head and Neck Cancer. **132,** 19–24 (2006).

57. Torre, C. & Wang, S. hyaluronan-CD44-mediated growth, migration, and cisplatin resistance in head and neck cancer due to inhibition of Rho kinase and PI-3 kinase signaling. *Arch Otolaryngol Head Neck Surg* **136,** 493–501 (2010).

58. Bourguignon, L. Y. W., Singleton, P. a., Diedrich, F., Stern, R. & Gilad, E. CD44 interaction with Na+-H+ exchanger (NHE1) creates acidic microenvironments leading to hyaluronidase-2 and cathepsin B activation and breast tumor cell invasion. *J. Biol. Chem.* **279,** 26991–27007 (2004).

59. Slomiany, M. G. *et al.* Abrogating drug resistance in malignant peripheral nerve sheath tumors by disrupting hyaluronan-CD44 interactions with small hyaluronan oligosaccharides. *Cancer Res.* **69,** 4992–4998 (2009).

60. Thapa, R., Gorski, J. & Bogedin, A. Hyaluronan-mediated ferric oxide nanoparticles causes apoptosis of CD44 expressing head and neck squamous cell carcinoma cells. *Int. J. Cancer Ther. Oncol.* **4,** 424 (2016).

61. Kim, H. *et al.* Hyaluronate and its derivatives for customized biomedical applications. *Biomaterials* **123,** 155–171 (2017).

62. E., S. J. Secondary Structures in Hyaluronan Solutions: Chemical and Biological Implications. *Ciba Foundation Symposium 143 - The Biology of Hyaluronan* (2007). doi:doi:10.1002/9780470513774.ch2

63. Toole, B. P. Hyaluronan: from extracellular glue to pericellular cue. *Nat. Rev.*

Cancer **4,** 528–39 (2004).

64. Silva, A. F., Alves, M. A. & Oliveira, M. S. N. Rheological behaviour of vitreous humour. *Rheol. Acta* **56,** 377–386 (2017).

65. Balazs, E. A. The Physical Properties of Synovial Fluid and the Special Role of Hyaluronic Acid. *Disorders of the Knee* 63–75 (1974).

66. Palmer, J. W. & Meyer, K. Polysaccharide of Vitreous Humor. *J. Biol. Chem.* **107,** 629–634 (1934).

67. Bannuru, R. R., Natov, N. S., Dasi, U. R., Schmid, C. H. & McAlindon, T. E. Therapeutic trajectory following intra-articular hyaluronic acid injection in knee osteoarthritis - meta-analysis. *Osteoarthr. Cartil.* **19,** 611–619 (2011).

68. Kogan, G., Šoltés, L., Stern, R. & Gemeiner, P. Hyaluronic acid: A natural biopolymer with a broad range of biomedical and industrial applications. *Biotechnol. Lett.* **29,** 17–25 (2007).

69. Neuman, M. G., Cohen, L. B. & Nanau, R. M. Hyaluronic acid as a non-invasive biomarker of liver fibrosis. *Clin. Biochem.* **49,** 302–315 (2016).

70. Lokeshwar, V. B. *et al.* Bladder tumor markers for monitoring recurrence and screening comparison of hyaluronic acid-hyaluronidase and BTA-stat tests. *Cancer* **95,** 61–72 (2002).

71. Posey, J. T. *et al.* Evaluation of the Prognostic Potential of Hyaluronic Acid and Hyaluronidase (HYAL1) for Prostate Cancer Evaluation of the Prognostic Potential of Hyaluronic Acid and Hyaluronidase. *Group* **2,** 2638–2644 (2003).

72. Bertrand, D. *et al.* Serum hyaluronan (hyaluronic acid) in breast cancer patients. *Int. J. Cancer* **46,** 388–390 (2006).

73. Franzmann, E. J. *et al.* Expression of tumor markers hyaluronic acid and hyaluronidase (HYAL1) in head and neck tumors. *Int. J. Cancer* **106,** 438–445 (2003).

74. Turley, E. A., Noble, P. W. & Bourguignon, L. Y. W. Signaling properties of hyaluronan receptors. *J. Biol. Chem.* **277,** 4589–4592 (2002).

75. Banerji, S. *et al.* LYVE-1, a new homologue of the CD44 glycoprotein, is a lymph-specific receptor for hyaluronan. *J. Cell Biol.* **144,** 789–801 (1999).

76. Huang, L., Grammatikakis, N., Yoneda, M., Banerjee, S. D. & Toole, B. P. Molecular Characterization of a Novel Intracellular Hyaluronan-binding Protein. *J. Biol. Chem.* **275,** 29829–29839 (2000).

77. West, D. C. & Kumar, S. Hyaluronan and angiogenesis. *Ciba Found. Symp.* **143,** 187-201; discussion 201–7, 281–5 (1989).

78. Litwiniuk, M., Krejner, A., Speyrer, M. S., Gauto, A. R. & Grzela, T. Hyaluronic Acid in Inflammation and Tissue Regeneration. *Wounds a Compend. Clin. Res. Pract.* **28,** 78–88 (2016).

79. Slevin, M., Kumar, S. & Gaffney, J. Angiogenic Oligosaccharides of Hyaluronan Induce Multiple Signaling Pathways Affecting Vascular Endothelial Cell Mitogenic and Wound Healing Responses. *J. Biol. Chem.* **277,** 41046–41059 (2002).

80. Monslow, J., Govindaraju, P. & Puré, E. Hyaluronan - A Functional and Structural Sweet Spot in the Tissue Microenvironment. *Front. Immunol.* **6,** 231 (2015).

81. Vigetti, D. *et al.* Hyaluronan: Biosynthesis and signaling. *Biochim. Biophys. Acta - Gen. Subj.* **1840,** 2452–2459 (2014).

82. Campo, G. M. *et al.* Hyaluronan reduces inflammation in experimental arthritis by modulating TLR-2 and TLR-4 cartilage expression. *BBA - Mol. Basis Dis.* **1812,** 1170–1181 (2011).

83. Wang, C. T., Lin, Y. T., Chiang, B. L., Lin, Y. H. & Hou, S. M. High molecular weight hyaluronic acid down-regulates the gene expression of osteoarthritis-associated cytokines and enzymes in fibroblast-like synoviocytes from patients with early osteoarthritis. *Osteoarthr. Cartil.* 1237–1247 (2006). doi:10.1016/j.joca.2006.05.009

84. Bano, F., Banerji, S., Howarth, M., Jackson, D. G. & Richter, R. P. A single molecule assay to probe monovalent and multivalent bonds between hyaluronan and its key leukocyte receptor CD44 under force. *Sci. Rep.* **6,** 34176- (2016).

85. Altgärde, N. *et al.* Probing the biofunctionality of biotinylated hyaluronan and

chondroitin sulfate by hyaluronidase degradation and aggrecan interaction. *Acta Biomater.* **9,** 8158–8166 (2013).

86. Lih, E., Choi, S. G., Ahn, D. J., Joung, Y. K. & Han, D. K. Optimal conjugation of catechol group onto hyaluronic acid in coronary stent substrate coating for the prevention of restenosis. *J. Tissue Eng.* **7,** 1–11 (2016).

87. Huang, R. *et al.* Conjugation of hyaluronic acid onto surfaces via the interfacial polymerization of dopamine to prevent protein adsorption. *Langmuir* **31,** 12061–12070 (2015).

88. Minsky, B. B., Antoni, C. H. & Boehm, H. Controlled Immobilization Strategies to Probe Short Hyaluronan-Protein Interactions. *Sci. Rep.* **6,** 21608 (2016).

89. Lord, M. S., Pasqui, D., Barbucci, R. & Milthorpe, B. K. Protein adsorption on derivatives of hyaluronic acid and subsequent cellular response. *J. Biomed. Mater. Res. Part A* **91,** 635–646 (2009).

90. Liu, X. *et al.* Grafting hyaluronic acid onto gold surface to achieve low protein fouling in surface plasmon resonance biosensors. *ACS Appl. Mater. Interfaces* **6,** 13034–13042 (2014).

91. Ombelli, M. *et al.* Competitive Protein Adsorption on Polysaccharide and Hyaluronate Modified Surfaces. *Biofouling* **27,** 505–518 (2011).

92. Choi, J. H. *et al.* Adsorption of hyaluronic acid on solid supports: Role of pH and surface chemistry in thin film self-assembly. *J. Colloid Interface Sci.* **448,** 197–207 (2015).

93. Mazumder, M. A. J. Polydimethylsiloxane Substrates with Surfaces Decorated by Immobilized Hyaluronic Acids of Different Molecular Weight for Biomedical Applications. *Arab. J. Sci. Eng.* **42,** 271–280 (2017).

94. Khunmanee, S., Jeong, Y. & Park, H. Crosslinking method of hyaluronic-based hydrogel for biomedical applications. *J. Tissue Eng.* **8,** 204173141772646 (2017).

95. Choi, S. C. *et al.* Modulation of biomechanical properties of hyaluronic acid hydrogels by crosslinking agents. *J. Biomed. Mater. Res. - Part A* **103,** 3072–3080 (2015).

96. Chen, G. *et al.* Photoimmobilization of sulfated hyaluronic acid for antithrombogenicity. *Bioconjug. Chem.* **8,** 730–734 (1997).

97. Keselowsky, B. G., Collard, D. M. & García, A. J. Surface chemistry modulates fibronectin conformation and directs integrin binding and specificity to control cell adhesion. *J. Biomed. Mater. Res.* **66A,** 247–259 (2003).

98. Wertz, C. F. & Santore, M. M. Adsorption and relaxation kinetics of albumin and fibrinogen on hydrophobic surfaces: Single-species and competitive behavior. *Langmuir* **15,** 8884–8894 (1999).

99. Smith, G. P. Filamentous fusion phage: novel expression vectors that display cloned antigens on the virion surface. *Science* **228,** 1315–1317 (1985).

100. Rentero Rebollo, I., Sabisz, M., Baeriswyl, V. & Heinis, C. Identification of target-binding peptide motifs by high-throughput sequencing of phage-selected peptides. *Nucleic Acids Res.* **42,** (2014).

101. Derda, R. *et al.* High-throughput discovery of synthetic surfaces that support proliferation of pluripotent cells. *J. Am. Chem. Soc.* **132,** 1289–1295 (2010).

102. Siegel, D. L., Chang, T. Y., Russell, S. L. & Bunya, V. Y. Isolation of cell surface-specific human monoclonal antibodies using phage display and magnetically-activated cell sorting: Applications in immunohematology. *J. Immunol. Methods* **206,** 73–85 (1997).

103. Park, J. P., Cropek, D. M. & Banta, S. High affinity peptides for the recognition of the heart disease biomarker troponin I identified using phage display. *Biotechnol. Bioeng.* **105,** 678–686 (2010).

104. Rebar, E. J. & Pabo, C. O. Zinc Finger Phage: Affinity Selection of Fingers with New DNA-Binding Specificities. **263,** 6711–673 (1994).

105. Tang, B., Li, Z., Huang, D., Zheng, L. & Li, Q. Screening of a specific peptide binding to VPAC1 receptor from a phage display peptide library. *PLoS One* **8,** e54264 (2013).

106. Hong, F. D. & Clayman, G. L. Isolation of a peptide for targeted drug delivery into human head and neck solid tumors. *Cancer Res.* **60,** 6551–6556 (2000).

107. Rajotte, D. *et al.* Molecular heterogeneity of the vascular endothelium revealed by In vivo Phage Display. *J. Clin. Investig.* **102,** 430–437 (1998).

108. Barbas III, C. F., Burton, D. R., Scott, J. K. & Silverman, G. J. *Phage Display: A Laboratory Manual*. (Cold Spring Harbor Laboratory Press, 2001).

109. Wang, L. F., Du Plessis, D. H., White, J. R., Hyatt, A. D. & Eaton, B. T. Use of a gene-targeted phage display random epitope library to map an antigenic determinant on the bluetongue virus outer capsid protein VP5. *J. Immunol. Methods* **178,** 1–12 (1995).

110. Blüthner, M., Schäfer, C., Schneider, C. & Bautz, F. A. Identification of major linear epitopes on the sp100 nuclear PBC autoantigen by the gene-fragment phage-display technology. *Autoimmunity* **29,** 33–42 (1999).

111. Nilsson, M. *et al.* A fibrinogen-binding protein of Staphylococcus epidermidis. *Infect. Immun.* **66,** 2666–73 (1998).

112. Santini, C. *et al.* Efficient display of an HCV cDNA expression library as C\rterminal fusion to the capsid protein-D of bacteriophage\rlambda. *J. Mol. Biol.* **282,** 125–135 (1998).

113. Tewawong, N., Pitaksajjkul, P., Dekumyoy, P., Ekpo, P. & Ramasoota, P. Mimotope identification using phage displayed random peptide libraries against monoclonal antibodies specific to house dust mite. *Southeast Asian J. Trop. Med. Public Health* **43,** 614–623 (2012).

114. Gómez-Román, V. R. *et al.* Phage-displayed mimotopes recognizing a biologically active anti-HIV-1 gp120 murine monoclonal antibody. *J. Acquir. Immune Defic. Syndr.* **31,** 147–153 (2002).

115. Peng, W. P. *et al.* Identification of a conserved linear B-cell epitope at the N-terminus of the E2 glycoprotein of Classical swine fever virus by phage-displayed random peptide library. *Virus Res.* **135,** 267–272 (2008).

116. Goldstein, J. M. *et al.* Phage Display Analysis of Monoclonal Antibody Binding to Anthrax Toxin Lethal Factor. *Toxins (Basel).* **9,** 221–238 (2017).

117. Yao, Z.-J., Chan, M.-C., Kao, M. C. C. & Chung, M. C. M. Linear epitopes of sperm

whale myoglobin identified by polyclonal antibody screening of random peptide library. *Int. J. Pept. Protein Res.* **48,** 477–485 (1996).

118. Williams, S. C., Badley, R. A., Davis, P. J., Puijk, W. C. & Meloen, R. H. Identification of epitopes within beta lactoglobulin recognised by polyclonal antibodies using phage display and PEPSCAN. *J. Immunol. Methods* **213,** 1–17 (1998).

119. Schellekens, G. A. *et al.* Identification of the core residues of the epitope of a monoclonal antibody raised against glycoprotein D of herpes simplex virus type 1 by screening of a random peptide library. *Eur. J. Immunol.* **24,** 3188–3193 (1994).

120. Fack, F. *et al.* Epitope mapping by phage display: Random versus gene-fragment libraries. *J. Immunol. Methods* **206,** 43–52 (1997).

121. Hebbes, T. R., Turner, C. H., Thorne, A. W. & Crane-Robinson, C. A 'minimal epitope' anti-protein antibody that recognises a single modified amino acid. *Mol. Immunol.* **26,** 865–873 (1989).

122. Hemmer, B. *et al.* Minimal peptide length requirements for CD4+ T cell clones—implications for molecular mimicry and T cell survival. *Int. Immunol.* **12,** 375–383 (2000).

123. Pierschbacher, M. D. & Ruoslahti, E. Cell attachment activity of fibronectin can be duplicated by small synthetic fragments of the molecule. *Nature* **309,** 30 (1984).

124. Zhang, B. & Zhang, Y. Screening and Identification of a Targeting Peptide to Hepatocarcinoma from a Phage Display Peptide Library. *Mol. Med.* **13,** 1 (2007).

125. Abbineni, G., Modali, S., Safiejko-Mroczka, B., Petrenko, V. a. & Mao, C. Evolutionary selection of new breast cancer cell-targeting peptides and phages with the cell-targeting peptides fully displayed on the major coat and their effects on actin dynamics during cell internalization. *Mol. Pharm.* **7,** 1629–1642 (2010).

126. Matsubara, T., Ishikawa, D., Taki, T., Okahata, Y. & Sato, T. Selection of ganglioside GM1-binding peptides by using a phage library. *FEBS Lett.* **456,** 253–256 (1999).

127. Takakusagi, Y. *et al.* Identification of C10 biotinylated camptothecin (CPT-10-B) binding peptides using T7 phage display screen on a QCM device. *Bioorg. Med. Chem.* **15,** 7590–7598 (2007).

128. Kriplani, U. & Kay, B. K. Selecting peptides for use in nanoscale materials using phage-displayed combinatorial peptide libraries. *Curr. Opin. Biotechnol.* **16,** 470–475 (2005).

129. Feng, B. *et al.* A novel affinity ligand for polystyrene surface from a phage display random library and its application in anti-HIV-1 ELISA system. *Biologicals* **37,** 48–54 (2009).

130. Qiang, X. *et al.* Discovery of a polystyrene binding peptide isolated from phage display library and its application in peptide immobilization. *Sci. Rep.* **7,** 2673 (2017).

131. Mummert, M. E., Mohamadzadeh, M., Mummert, D. I., Mizumoto, N. & Takashima, a. Development of a peptide inhibitor of hyaluronan-mediated leukocyte trafficking. *J. Exp. Med.* **192,** 769–779 (2000).

132. Zmolik, J. M. & Mummert, M. E. Pep-1 as a novel probe for the in situ detection of hyaluronan. *J. Histochem. Cytochem.* **53,** 745–751 (2005).

133. Singh, A. *et al.* Enhanced lubrication on tissue and biomaterial surfaces through peptide-mediated binding of hyaluronic acid. *Nat. Mater.* **13,** 988–995 (2014).

134. Mummert, M. E. *et al.* Synthesis and surface expression of hyaluronan by dendritic cells and its potential role in antigen presentation. *J. Immunol.* **169,** 4322–31 (2002).

135. Koide, A. *et al.* Accelerating phage-display library selection by reversible and site-specific biotinylation. *Protein Eng. Des. Sel.* **22,** 685–690 (2009).

136. Arne, G., Berit, M. & Per, O. Immunochemical studies on antigen preparations from staphylococcus aureus. *Acta Pathol. Microbiol. Scand.* **61,** 588–596 (1964).

137. Koolpe, M., Burgess, R., Dail, M. & Pasquale, E. B. EphB receptor-binding peptides identified by phage display enable design of an antagonist with ephrin-like affinity. *J. Biol. Chem.* **280,** 17301–17311 (2005).

138. Lee, C. M. Y., Iorno, N., Sierro, F. & Christ, D. Selection of human antibody fragments by phage display. *Nat. Protoc.* **2,** 3001–3008 (2007).

139. Marks, J. D. *et al.* Human Antibody Fragments specific for human blood group

antigens from a phage display library. *Nat. Biotechnol.* **11,** 159–1564 (1993).

140. Portolano, S., McLachlan, S. M. & Rapoport, B. High affinity, thyroid-specific human autoantibodies displayed on the surface of filamentous phage use V genes similar to other autoantibodies. *J. Immunol.* **151,** 2839–2851 (1993).

141. Giordano, R., Cardó-Vila, M., Lahdenranta, J., Pasqualini, R. & Arap, W. Biopanning and rapid analysis of selective interactive ligands. *Nat. Med.* 1249–1253 (2001).

142. Jia, W. D. *et al.* A novel peptide that selectively binds highly metastatic hepatocellular carcinoma cell surface is related to invasion and metastasis. *Cancer Lett.* **247,** 234–242 (2007).

143. Gray, B. P. & Brown, K. C. Combinatorial peptide libraries: Mining for cell-binding peptides. *Chem. Rev.* **114,** 1020–1081 (2014).

144. Yao, V. J. *et al.* Targeting pancreatic islets with phage display assisted by laser pressure catapult microdissection. *Am. J. Pathol.* **166,** 625–636 (2005).

145. Joyce, J. A. *et al.* Stage-specific vascular markers revealed by phage display in a mouse model of pancreatic islet tumorigenesis. *Cancer Cell* **4,** 393–403 (2003).

146. Arap, W., Kolonin, M. & Trepel, M. Steps toward mapping the human vasculature by phage display. *Nat. Med.* **8,** 121–127 (2002).

147. Krag, D. N. *et al.* Selection of tumor-binding ligands in cancer patients with phage display libraries. *Cancer Res.* **66,** 7724–7733 (2006).

148. Derda, R. *et al.* Diversity of phage-displayed libraries of peptides during panning and amplification. *Molecules* **16,** 1776–1803 (2011).

149. Williams, B. R. & Sharon, J. Polyclonal anti-colorectal cancer Fab phage display library selected in one round using density gradient centrifugation to separate antigen-bound and free phage. *Immunol. Lett.* **81,** 141–148 (2002).

150. Chen, L. *et al.* Polyclonal Fab phage display libraries with a high percentage of diverse clones to Cryptosporidium parvum glycoproteins. *Int. J. Parasitol.* **33,** 281–291 (2003).

151. 'T Hoen, P. A. C. *et al.* Phage display screening without repetitious selection rounds.

Anal. Biochem. **421,** 622–631 (2012).

152. Derda, R., Tang, S. K. Y. & Whitesides, G. M. Uniform Amplification of Phage with Different Growth Characteristics in Individual Compartments Consisting of Monodisperse Droplets. *Angew. Chemie Int. Ed. English* **49,** 5301–5304 (2010).

153. Vodnik, M., Zager, U., Strukelj, B. & Lunder, M. Phage display: Selecting straws instead of a needle from a haystack. *Molecules* **16,** 790–817 (2011).

154. Felici, F., Castagnoli, L., Musacchio, A., Jappelli, R. & Cesareni, G. Selection of antibody ligands from a large library of oligopeptides expressed on a multivalent exposition vector. *J. Mol. Biol.* **222,** 301–310 (1991).

155. Barbas III, C. F., Kang, A. S., Lerner, R. A. & Benkovict, S. J. Assembly of combinatorial antibody libraries on phage surfaces: The gene III site. *Proc. Natl. Acad. Sci. USA* **88,** 7978–7982 (1991).

156. O'Connell, D., Becerril, B., Roy-Burman, A., Daws, M. & Marks, J. D. Phage versus phagemid libraries for generation of human monoclonal antibodies. *J. Mol. Biol.* **321,** 49–56 (2002).

157. Vaughan, T. J. *et al.* Human Antibodies With Sub-Nanomolar Affinities Isolated From A Large Non-Immunized Phage Display Library. *Nat. Biotechnol.* **14,** 309–314 (1996).

158. Barbas, C. F., Bain, J. D., Hoekstra, D. M. & Lerner, R. a. Semisynthetic combinatorial antibody libraries: a chemical solution to the diversity problem. *Proc. Natl. Acad. Sci. U. S. A.* **89,** 4457–61 (1992).

159. Braunagel, M. in *Recombinant Antibodies for Cancer Therapy: Methods and Protocols* (eds. Welschof, M. & Krauss, J.) 123–132 (Humana Press, 2003). doi:10.1385/1-59259-334-8:123

160. Zwick, M. *et al.* Identification and characterization of a peptide that specifically binds the human, broadly neutralizing anti-human immunodeficiency virus type 1 antibody b12. *J. Virol.* **75,** 6692–6699 (2001).

161. Pande, J. *et al.* Functional effects of caloxin 1c2, a novel engineered selective inhibitor of plasma membrane Ca2+-pump isoform 4, on coronary artery. *J. Cell.*

Mol. Med. **12,** 1049–1060 (2008).

162. Demartis, A. *et al.* Polypharmacy through Phage Display: Selection of Glucagon and GLP-1 Receptor Co-agonists from a Phage-Displayed Peptide Library. *Sci. Rep.* **8,** 1–9 (2018).

163. Sugahara, K. N. *et al.* Tissue-Penetrating Delivery of Compounds and Nanoparticles into Tumors. *Cancer Cell* **16,** 510–520 (2009).

164. Teesalu, T., Sugahara, K. N., Kotamraju, V. R. & Ruoslahti, E. C-end rule peptides mediate neuropilin-1-dependent cell, vascular, and tissue penetration. *Proc. Natl. Acad. Sci.* **106,** 16157–16162 (2009).

165. Sutherland, R., Buchegger, F., Schreyer, M., Vacca, A. & Mach, J. P. Penetration and Binding of Radiolabeled Anti-Carcinoembryonic Antigen Monoclonal Antibodies and Their Antigen Binding Fragments in Human Colon Multicellular Tumor Spheroids. *Cancer Res.* **47,** 1627–1633 (1987).

166. Fujimori, K., Covell, D. G., Fletcher, J. E. & Weinstein, J. N. Modeling analysis of the global and microscopic distribution of immunoglobulin G, $F(ab')_2$, and Fab in tumors. *Cancer Res.* **49,** 5656–5663 (1989).

167. Juweid, M. *et al.* Micropharmacology of Monoclonal-Antibodies in Solid Tumors - Direct Experimental Evidence for a Binding-Site Barrier. *Cancer Res.* **52,** 5144–5153 (1992).

168. Cardote, T. A. F. & Ciulli, A. Cyclic and Macrocyclic Peptides as Chemical Tools to Recognise Protein Surfaces and Probe Protein-Protein Interactions. *ChemMedChem* **11,** 787–794 (2016).

169. Giebel, L. B. *et al.* Screening of Cyclic Peptide Phage Libraries Identifies Ligands That Bind Streptavidin with High Affinities. *Biochemistry* **34,** 15430–15435 (1995).

170. Kolvunen, E., Wang, B. & Ruoslahti, E. Phage libraries displaying cyclic peptides with different ring sizes: Ligand specificities of the rgd-directed integrine. *Bio/Technology* **13,** 265–270 (1995).

171. Nicol, C. G. *et al.* Use of in vivo phage display to engineer novel adenoviruses for targeted delivery to the cardiac vasculature. *FEBS Lett.* **583,** 2100–2107 (2009).

172. Holliger, P. & Hudson, P. J. Engineered antibody fragments and the rise of single domains. *Nat. Biotechnol.* **23,** 1126–1136 (2005).

173. Chapman, A. P. PEGylated antibodies and antibody fragments for improved therapy: A review. *Adv. Drug Deliv. Rev.* **54,** 531–545 (2002).

174. Toporkiewicz, M. Toward a magic or imaginary bullet ? Ligands for drug targeting to cancer cells : principles , hopes , and challenges. 1399–1414 (2015).

175. Rautio, J., Meanwell, N. A., Di, L. & Hageman, M. J. The expanding role of prodrugs in contemporary drug design and development. *Nat. Rev. Drug Discov.* **17,** 559–587 (2018).

176. Larocca, D. *et al.* Targeting Bacteriophage to Mammalian Cell Surface Receptors for Gene Delivery. **9,** 2393–2399 (1998).

177. Kamada, H. *et al.* Creation of novel cell-penetrating peptides for intracellular drug delivery using systematic phage display technology originated from Tat transduction domain. *Biol Pharm Bull* **30,** 218–223 (2007).

178. Cao, Q. *et al.* Phage diplay peptide probes for imaging early response to bevacizumab treatment. **41,** 1103–1112 (2012).

179. Gilad, Y. *et al.* Dual-drug RGD conjugates provide enhanced cytotoxicity to melanoma and non-small lung cancer cells. *Biopolymers* **106,** 160–171 (2016).

180. Willuda, J. *et al.* Preclinical Antitumor Efficacy of BAY 1129980—a Novel Auristatin-Based Anti-C4.4A (LYPD3) Antibody–Drug Conjugate for the Treatment of Non–Small Cell Lung Cancer. *Mol. Cancer Ther.* **16,** 893–904 (2017).

181. Svensen, N., Walton, J. G. A. & Bradley, M. Peptides for cell-selective drug delivery. *Trends Pharmacol. Sci.* **33,** 186–192 (2012).

182. Miller, S. M. *et al.* Comparison of the proteolytic susceptibilities of Homologous L-Amino Acid, D-Amino Acid, and N-Substituted Glycine PEptide and Peptoid Oligomers. *Drug Dev. reasrch* **35,** 20–32 (1995).

183. Jespers, L. S., Roberts, A., Mahler, S. M., Winter, G. & Hoogenboom, H. R. Guiding the selection of human antibodies from phage display repertoires to a single epitope of an antigen. *Bio/Technology* **12,** 899–903 (1994).

184. Philippidis, A. The Top 15 Best-Selling Drugs of 2016. *Genetic Engineering & Biotechnology News* (2017). Available at: https://www.genengnews.com/the-lists/the-top-15-best-selling-drugs-of-2016/77900868. (Accessed: 31st July 2018)

185. Tang, C., Chen, S., Qian, H. & Huang, W. Interleukin-23: As a drug target for autoimmune inflammatory diseases. *Immunology* **135,** 112–124 (2012).

186. Wu, C.-H., Kuo, Y.-H., Hong, R.-L. & Wu, H.-C. α-Enolase–binding peptide enhances drug delivery efficiency and therapeutic efficacy against colorectal cancer. *Sci. Transl. Med.* **7,** 290ra91 (2015).

187. Bertoldo, D. *et al.* Phage Selection of Peptide Macrocycles against β-Catenin to Interfere with Wnt Signaling. *ChemMedChem* **11,** 834–839 (2016).

188. *Self-Assembling Biomaterials Molecular Design, Characterization and Application in Biology and Medicine*. (Woodhead Publishing, 2018).

189. Jadhav, S. A. Self-assembled monolayers (SAMs) of Carboxylic acids: an overview. *Cent. Eur. J. Chem.* **9,** 369–378 (2011).

190. Bekmurzayeva, A., Duncanson, W. J., Azevedo, H. S. & Kanayeva, D. Surface modification of stainless steel for biomedical applications: Revisiting a century-old material. *Mater. Sci. Eng. C* (2018). doi:10.1016/j.msec.2018.08.049

191. Tosatti, S., Michel, R., Textor, M. & Spencer, N. D. Self-Assembled Monolayers of Dodecyl and Hydroxy-dodecyl Phosphates on Both Smooth and Rough Titanium and Titanium Oxide Surfaces. *Langmuir* **18,** 3537–3548 (2002).

192. Wang, J., Wu, F., Watkinson, M., Zhu, J. & Krause, S. "Click" Patterning of Self-Assembled Monolayers on Hydrogen-Terminated Silicon Surfaces and Their Characterization Using Light-Addressable Potentiometric Sensors. *Langmuir* **31,** 9646–9654 (2015).

193. Cabanas-Danés, J. *et al.* A fluorogenic monolayer to detect the co-immobilization of peptides that combine cartilage targeting and regeneration. *J. Mater. Chem. B* **1,** 1903 (2013).

194. Arima, Y. & Iwata, H. Effect of wettability and surface functional groups on protein adsorption and cell adhesion using well-defined mixed self-assembled monolayers.

J. Mater. Chem. **17,** 4079–4087 (2007).

195. Dowling, D. P., Miller, I. S., Ardhaoui, M. & Gallagher, W. M. Effect of Surface Wettability and Topography on the Adhesion of Osteosarcoma Cells on Plasma-modified Polystyrene. *J. Biomater. Appl.* **26,** 327–347 (2011).

196. Yan, H. *et al.* Self-assembled monolayers with different chemical group substrates for the study of MCF-7 breast cancer cell line behavior. *Biomed. Mater.* **8,** 035008 (2013).

197. Ren, Y. J. *et al.* In vitro behavior of neural stem cells in response to different chemical functional groups. *Biomaterials* **30,** 1036–1044 (2009).

198. Keselowsky, B. G., Collard, D. M. & Garcia, A. J. Integrin binding specificity regulates biomaterial surface chemistry effects on cell differentiation. *Proc. Natl. Acad. Sci.* **102,** 5953–5957 (2005).

199. Valamehr, B. *et al.* Hydrophobic surfaces for enhanced differentiation of embryonic stem cell-derived embryoid bodies Results. *Proc. Natl. Acad. Sci.* **105,** 14459–14464 (2008).

200. Roberts, C. *et al.* Using mixed self-assembled monolayers presenting RGD and (EG)3OH groups to characterize long-term attachment of bovine capillary endothelial cells to surfaces. *J. Am. Chem. Soc.* **120,** 6548–6555 (1998).

201. Orner, B. P., Derda, R., Lewis, R. L., Thomson, J. A. & Kiessling, L. L. Arrays for the combinatorial exploration of cell adhesion. *J. Am. Chem. Soc.* **126,** 10808–10809 (2004).

202. Derda, R. *et al.* High-throughput discovery of synthetic surfaces that support proliferation of pluripotent cells. *J. Am. Chem. Soc.* **132,** 1289–1295 (2010).

203. Reubinoff, B. E., Pera, M. F., Fong, C. Y., Trounson, A. & Bongso, A. Embryonic stem cell lines from human blastocysts: somatic differentiation in vitro. *Nat. Biotechnol.* **18,** 399–404 (2000).

204. Alom Ruiz, S. & Chen, C. S. Microcontact printing: A tool to pattern. *Soft Matter* **3,** 168–177 (2007).

205. Mrksich, M., Dike, L. E., Tien, J., Ingber, D. E. & Whitesides, G. M. Using

microcontact printing to pattern the attachment of mammalian cells to self-assembled monolayers of alkanethiolates on transparent films of gold and silver. *Exp. Cell Res.* **235,** 305–313 (1997).

206. Chen, C. S., Mrksich, M., Huang, S., Whitesides, G. M. & Ingber, D. E. Micropatterned surfaces for control of cell shape, position, and function. *Biotechnol. Prog.* **14,** 356–363 (1998).

207. Martinez-Rivas, A., González-Quijano, G. K., Proa-Coronado, S., Séverac, C. & Dague, E. Methods of micropatterning and manipulation of cells for biomedical applications. *Micromachines* **8,** (2017).

208. Strulson, M. K., Johnson, D. M. & Maurer, J. A. Increased Stability of Glycol-Terminated Self-Assembled Monolayers for Long-Term Patterned Cell Culture. *Langmuir* **28,** 4318–4324 (2012).

209. Choi, S. & Chae, J. Reusable biosensors via in situ electrochemical surface regeneration in microfluidic applications. *Biosens. Bioelectron.* **25,** 527–531 (2009).

210. Gobi, K. V., Iwasaka, H. & Miura, N. Self-assembled PEG monolayer based SPR immunosensor for label-free detection of insulin. *Biosens. Bioelectron.* **22,** 1382–1389 (2007).

211. Johnson, D. M. & Maurer, J. A. Recycling and reusing patterned self-assembled monolayers for cell culture. *Chem. Commun.* **47,** 520–522 (2011).

212. Jiang, D. *et al.* Regulation of lung injury and repair by Toll-like receptors and hyaluronan. *Nat. Med.* **11,** 1173–1179 (2005).

213. Rudrabhatla, S. R., Mahaffey, C. L. & Mummert, M. E. Tumor microenvironment modulates hyaluronan expression: The lactate effect. *J. Invest. Dermatol.* **126,** 1378–1387 (2006).

214. Merrifield, R. B. Solid Phase Peptide Synthesis. I. The Synthesis of a Tetrapeptide. *J. Am. Chem. Soc.* **85,** 2149–2154 (1963).

215. Bürgi, T. Properties of the gold-sulphur interface: from self-assembled monolayers to clusters. *Nanoscale* **7,** 15553–15567 (2015).

216. Ho, C. S. *et al.* Electrospray ionisation mass spectrometry: principles and clinical applications. *Clin. Biochem. Rev.* **24,** 3–12 (2003).

217. Collis, L. *et al.* Rapid hyaluronan uptake is associated with enhanced motility: Implications for an intracellular mode of action. *FEBS Lett.* **440,** 444–449 (1998).

218. Díez-Pascual, A. M. & Shuttleworth, P. S. Layer-by-layer assembly of biopolyelectrolytes onto thermo/pH-responsive micro/nano-gels. *Materials (Basel).* **7,** 7472–7512 (2014).

219. Shen, W.-C. & Ryser, H. J. P. Poly (L-lysine) and poly (D-lysine) conjugates of methotrexate: different inhibitory effect on drug resistant cells. *Mol. Pharmacol.* **16,** 614–622 (1979).

220. Khademhosseini, A. *et al.* Layer-by-layer deposition of hyaluronic acid and poly-L-lysine for patterned cell co-cultures. *Biomaterials* **25,** 3583–3592 (2004).

221. Collis, D. W. P. Hyaluronan (HA) glycopolymers and self-assembling HA-binding peptides : a synthetic toolbox for probing HA-peptide / protein interactions and creating supramolecular HA biomaterials. (2018).

222. Yigit, M. V & Medarova, Z. In vivo and ex vivo applications of gold nanoparticles for biomedical SERS imagingi. *Am J Nucl Med Mol Imaging* **2,** 232–241 (2012).

223. Biolin Scientific AB. QSensor QSX 301 Gold. 1 Available at: https://cdn2.hubspot.net/hubfs/516902/Pdf/QSense/Extranet/Marketing materials/Brochures for printing/Product Brochures/Sensor spec sheet QSX301Gold.pdf?t=1534142155943. (Accessed: 15th August 2018)

224. Love, J. C., Estroff, L. A., Kriebel, J. K., Nuzzo, R. G. & Whitesides, G. M. *Self-assembled monolayers of thiolates on metals as a form of nanotechnology*. *Chemical Reviews* **105,** (2005).

225. Qin, D., Xia, Y. & Whitesides, G. M. Soft lithography for micro- and nanoscale patterning. *Nat. Protoc.* **5,** 491–502 (2010).

226. Sauerbrey, G. Verwendung von Schwingquarzen zur Wägung dünner Schichten und zur Mikrowägung. *Zeitschrift für Phys.* **155,** 206–222 (1959).

227. Setúbal, M. F. *et al. Effects of Cetuximab and Erlotinib on the behaviour of cancer*

stem cells in head and neck squamous cell carcinoma. *Oncotarget* **9,** (2018).

228. Fluorescence SpectraViewer - UK. Available at: https://www.thermofisher.com/uk/en/home/life-science/cell-analysis/labeling-chemistry/fluorescence-spectraviewer.html. (Accessed: 14th September 2018)

229. 3,3′,5,5′-Tetramethylbenzidine ≥98% (TLC) | Sigma-Aldrich. Available at: https://www.sigmaaldrich.com/catalog/product/sigma/t2885?lang=en&region=GB. (Accessed: 14th September 2018)

230. Pastrana, E., Silva-Vargas, V. & Doetsch, F. Eyes wide open: a critical review of sphere-formation as an assay for stem cells. *Cell Stem Cell* **8,** 486–98 (2011).

231. Orner, B. P., Derda, R., Lewis, R. L., Thomson, J. A. & Kiessling, L. L. Arrays for the Combinatorial Exploration of Cell Adhesion. *J. Am. Chem. Soc.* **126,** 10808–10809 (2004).

232. Gugutkov, D., Altankov, G., Carlos Rodríguez Hernández, J., Monleó Pradas, M. & Salmeró Sánchez, M. Fibronectin activity on substrates with controlled ÀÀOH density. (2009). doi:10.1002/jbm.a.32374

233. Ballester-Beltrán, J. *et al.* Effect of topological cues on material-driven fibronectin fibrillogenesis and cell differentiation. in *Journal of Materials Science: Materials in Medicine* (2012). doi:10.1007/s10856-011-4532-z

234. Corvaglia, V., Marega, R., De Leo, F., Michiels, C. & Bonifazi, D. Unleashing Cancer Cells on Surfaces Exposing Motogenic IGDQ Peptides. *Small* **12,** 321–329 (2016).

235. Zhang, Z. & Christopher, G. F. The nonlinear viscoelasticity of hyaluronic acid and its role in joint lubrication. *Soft Matter* **11,** 2596–2603 (2015).

236. Collins, M. N. & Birkinshaw, C. Hyaluronic acid based scaffolds for tissue engineering - A review. *Carbohydr. Polym.* **92,** 1262–1279 (2013).

237. Kim, H. D. & Valentini, R. F. Retention and activity of BMP-2 in hyaluronic acid-based scaffolds in vitro. *J. Biomed. Mater. Res. An Off. J. Soc. Biomater. Japanese Soc. Biomater. Aust. Soc. Biomater. Korean Soc. Biomater.* **59,** 573–584 (2002).

238. Leach, J. B., Bivens, K. A., Patrick, C. W. J. & Schmidt, C. E. Photocrosslinked hyaluronic acid hydrogels: Natural, biodegradable tissue engineering scaffolds.

Biotechnol. Bioeng. **82,** 578–589 (2003).

239. Miralles, G. *et al.* Sodium alginate sponges with or without sodium hyaluronate: In vitro engineering of cartilage. *J. Biomed. Mater. Res.* **57,** 268–278 (2001).

240. Yoo, H. S., Lee, E. A., Yoon, J. J. & Park, T. G. Hyaluronic acid modified biodegradable scaffolds for cartilage tissue engineering. *Biomaterials* **26,** 1925–1933 (2005).

241. Knudson, W., Biswas, C., Li, X. Q., Nemec, R. E. & Toole, B. P. The role and regulation of tumour-associated hyaluronan. *Ciba Found. Symp.* **143,** 150-169,281-285 (1989).

242. Toole, B. P. & Slomiany, M. G. Hyaluronan, CD44 and Emmrin: Partners in cancer cell chemoresistance. **11,** 110–121 (2009).

243. Bourguignon, L. Y. W., Wong, G., Earle, C. & Chen, L. Hyaluronan-CD44v3 interaction with Oct4-Sox2-Nanog promotes miR-302 expression leading to self-renewal, clonal formation, and cisplatin resistance in cancer stem cells from head and neck squamous cell carcinoma. *J. Biol. Chem.* **287,** 32800–24 (2012).

244. Bourguignon, L. Y. W., Wong, G. & Shiina, M. Up-regulation of histone methyltransferase, DOT1L, by matrix hyaluronan promotes MicroRNA-10 expression leading to tumor cell invasion and chemoresistance in cancer stem cells from head and neck squamous cell carcinoma. *J. Biol. Chem.* **291,** 10571–10585 (2016).

245. Martins, I. M., Reis, R. L. & Azevedo, H. S. Phage display technology in biomaterials engineering: Progress and opportunities for applications in regenerative medicine. *ACS Chem. Biol.* **11,** 2962–2980 (2016).

246. Mummert, M. & Mummert, D. Functional Roles of Hyaluronan in B16-F10 Melanoma Growth and Experimental Metastasis in Mice1. *Mol. Cancer Ther.* **2,** 295–300 (2003).

247. Singh, A., Li, P., Beachley, V., McDonnell, P. & Elisseeff, J. H. A hyaluronic acid-binding contact lens with enhanced water retention. *Contact Lens Anterior Eye* **38,** 79–84 (2015).

248. Marx, K. A. Quartz crystal microbalance: A useful tool for studying thin polymer

films and complex biomolecular systems at the solution - Surface interface. *Biomacromolecules* **4,** 1099–1120 (2003).

249. Picart, C. *et al.* Buildup mechanism for poly(L-lysine)/hyaluronic acid films onto a solid surface. *Langmuir* **17,** 7414–7424 (2001).

250. Niepel, M. S. *et al.* Cross-linking multilayers of poly- l -lysine and hyaluronic acid: Effect on mesenchymal stem cell behavior. *Int. J. Artif. Organs* **41,** 223–235 (2018).

251. Cowman, M. K., Lee, H.-G., Schwertfeger, K. L., McCarthy, J. B. & Turley, E. A. The Content and Size of Hyaluronan in Biological Fluids and Tissues. *Front. Immunol.* **6,** 261 (2015).

252. Schmaus, A. *et al.* Accumulation of small hyaluronan oligosaccharides in tumour interstitial fluid correlates with lymphatic invasion and lymph node metastasis. *Br. J. Cancer* **111,** 559–567 (2014).

253. Termeer, C. C. *et al.* Oligosaccharides of Hyaluronan Are Potent Activators of Dendritic Cells. *J. Immunol.* **165,** 1863–1870 (2000).

254. Asari, A., Kanemitsu, T. & Kurihara, H. Oral administration of high molecular weight hyaluronan (900 kDa) controls immune system via Toll-like receptor 4 in the intestinal epithelium. *J. Biol. Chem.* **285,** 24751–8 (2010).

255. Johannsmann, D. Viscoelastic, mechanical, and dielectric measurements on complex samples with the quartz crystal microbalance. *Phys. Chem. Chem. Phys.* **10,** 4516–4534 (2008).

256. Q-sense. Quartz crystal microbalance with dissipation. *Tech. Note* **27,** 2 (2011).

257. Rodahl, M. & Kasemo, B. A simple setup to simultaneously measure the resonant frequency and the absolute dissipation factor of a quartz crystal microbalance. *Rev. Sci. Instrum.* **67,** 3238–3241 (1996).

258. Van Beek, M., Jones, L. & Sheardown, H. Hyaluronic acid containing hydrogels for the reduction of protein adsorption. *Biomaterials* **29,** 780–789 (2008).

259. Liang, J., Jiang, D. & Noble, P. W. Hyaluronan as a therapeutic target in human diseases. *Adv. Drug Deliv. Rev.* **97,** 186–203 (2016).

260. Brunner, D. *et al.* Serum-free Cell Culture: The Serum-free Media Interactive Online Database. *ALTEX Altern. to Anim. Exp.* **27,** 53–62 (2010).

261. Lee, J.-J., Kwon, J.-H., Park, Y. K., Kwon, O. & Yoon, T.-W. The effects of various hormones and growth factors on the growth of human insulin-producing cell line in serum-free medium. *Experimantal Mol. Med.* **29,** 209–216 (1997).

262. Lerman, M. J., Lembong, J., Muramoto, S., Gillen, G. & Fisher, J. P. The Evolution of Polystyrene as a Cell Culture Material. *Tissue Eng. Part B Rev.* **24,** 359–372 (2018).

263. Verdanova, M., Sauerova, P., Hempel, U. & Kalbacova, M. H. Initial cell adhesion of three cell types in the presence and absence of serum proteins. *Histochem. Cell Biol.* **148,** 273–288 (2017).

264. Kim, Y. & Kumar, S. CD44-Mediated Adhesion to Hyaluronic Acid Contributes to Mechanosensing and Invasive Motility. *Mol. Cancer Res.* (2014). doi:10.1158/1541-7786.MCR-13-0629

265. Gupta, A. *et al.* Promising noninvasive cellular phenotype in prostate cancer cells knockdown of matrix metalloproteinase 9. *Sci. World J.* (2013). doi:10.1155/2013/493689

266. Bourguignon, L. Y. W., Wong, G., Earle, C. & Chen, L. Hyaluronan-CD44v3 interaction with Oct4-Sox2-Nanog promotes miR-302 expression leading to self-renewal, clonal formation, and cisplatin resistance in cancer stem cells from head and neck squamous cell carcinoma. *J. Biol. Chem.* (2012). doi:10.1074/jbc.M111.308528

267. Nyegaard, S., Christensen, B. & Rasmussen, J. T. An optimized method for accurate quantification of cell migration using human small intestine cells. *Metab. Eng. Commun.* **3,** 76–83 (2016).

268. Staton, C. A., Reed, M. W. R. & Brown, N. J. A critical analysis of current in vitro and in vivo angiogenesis assays. *Int. J. Exp. Pathol.* **90,** 195–221 (2009).

269. Hilaire, M. R. *et al.* Blue fluorescent amino acid for biological spectroscopy and microscopy. *Proc. Natl. Acad. Sci. U. S. A.* **114,** 6005–6009 (2017).

270. Thomas, L., Byers, R., Vink, J. & Stamenkovic, I. CD44H regulations tumor cell

migration on hyaluronate-coated substrate. *J. Cell Biol.* **118,** 971–977 (1992).

271. Jourdainne, L. *et al.* Dynamics of poly(L-lysine) in hyaluronic acid/poly(L-lysine)multilayer films studied by fluorescence recovery after pattern photobleaching. *Langmuir* **24,** 7842–7847 (2008).

272. Picart, C. *et al.* Molecular basis for the explanation of the exponential growth of polyelectrolyte multilayers. *Proc. Natl. Acad. Sci.* **99,** 12531–12535 (2002).

273. Csucs, G., Michel, R., Lussi, J. W., Textor, M. & Danuser, G. Microcontact printing of novel co-polymers in combination with proteins for cell-biological applications. *Biomaterials* **24,** 1713–1720 (2003).

274. Tolstyka, Z. P. *et al.* Chemoselective immobilization of proteins by microcontact printing and bio-orthogonal click reactions. *Chembiochem* **14,** 2464–71 (2013).

275. Zhang, W., Xue, C. Y. & Yang, K. L. A method of printing uniform protein lines by using flat PDMS stamps. *J. Colloid Interface Sci.* (2011). doi:10.1016/j.jcis.2010.09.029

276. Elloumi-Hannachi, I., Maeda, M., Yamato, M. & Okano, T. Portable microcontact printing device for cell culture. *Biomaterials* (2010). doi:10.1016/j.biomaterials.2010.08.019

277. Elloumi Hannachi, I. *et al.* Fabrication of transferable micropatterned-co-cultured cell sheets with microcontact printing. *Biomaterials* (2009). doi:10.1016/j.biomaterials.2009.06.033

278. Polio, S. R. & Smith, M. L. Patterned Hydrogels for Simplified Measurement of Cell Traction Forces. *Methods Cell Biol.* **121,** 17–31 (2014).

279. Toyota, T., Wakamoto, Y., Hayashi, K. & Ohnum, K. in *Innovations in Biotechnology* (InTech, 2012). doi:10.5772/30653

280. Joo, S. *et al.* Effects of ECM protein micropatterns on the migration and differentiation of adult neural stem cells. *Sci. Rep.* (2015). doi:10.1038/srep13043

281. Ström, A., Larsson, A. & Okay, O. Preparation and physical properties of hyaluronic acid-based cryogels. *J. Appl. Polym. Sci.* **132,** 1–11 (2015).

282. Delapierre, F. D. *et al.* High throughput micropatterning of interspersed cell arrays using capillary assembly. *Biofabrication* (2017). doi:10.1088/1758-5090/aa5852

283. Pawitan, J. A. Prospect of stem cell conditioned medium in regenerative medicine. *Biomed Res. Int.* **2014,** 965849 (2014).

284. Fosgerau, K. & Hoffmann, T. Peptide therapeutics: current status and future directions. *Drug Discov. Today* **20,** 122–128 (2015).

285. Zhou, M. *et al.* Self-assembled peptide-based hydrogels as scaffolds for anchorage-dependent cells. *Biomaterials* **30,** 2523–2530 (2009).

286. Dasgupta, A., Mondal, H. & Das, D. Peptide hydrogels. *RSC Adv.* **3,** 9117–9149 (2013).

287. Lau, J. L. & Dunn, M. K. Therapeutic peptides: Historical perspectives, current development trends, and future directions. *Bioorg. Med. Chem.* **26,** 2700–2707 (2018).

288. Madsbad, S. Review of head-to-head comparisons of glucagon-like peptide-1 receptor agonists. *Diabetes, Obes. Metab.* **18,** 317–332 (2016).

289. Brooks, H., Lebleu, B. & Vivès, E. Tat peptide-mediated cellular delivery: back to basics. *Adv. Drug Deliv. Rev.* **57,** 559–577 (2005).

290. Genové, E., Shen, C., Zhang, S. & Semino, C. E. The effect of functionalized self-assembling peptide scaffolds on human aortic endothelial cell function. *Biomaterials* **26,** 3341–3351 (2005).

291. Pihlanto, A. Antioxidative peptides derived from milk proteins. *Int. Dairy J.* **16,** 1306–1314 (2006).

292. Belkin, A. M. & Stepp, M. A. Integrins as receptors for laminins. *Microsc. Res. Tech.* **51,** 280–301 (2000).

293. Tuckwell, D. & Humphries, M. Integrin–collagen binding. *Semin. Cell Dev. Biol.* **7,** 649–657 (1996).

294. Pankov, R. & Yamada, K. M. Fibronectin at a glance. *J. Cell Sci.* **115,** 3861–3 (2002).

295. Huettner, N., Dargaville, T. R. & Forget, A. Discovering Cell-Adhesion Peptides in

Tissue Engineering: Beyond RGD. *Trends Biotechnol.* **36,** 372–383 (2018).

296. Schense, J. C., Bloch, J., Aebischer, P. & Hubbell, J. A. Enzymatic incorporation of bioactive peptides into fibrin matrices enhances neurite extension. *Nat. Biotechnol.* **18,** 415–419 (2000).

297. Li, X. *et al.* Short laminin peptide for improved neural stem cell growth. *Stem Cells Transl. Med.* **3,** 662–70 (2014).

298. Joshi, S. *et al.* The Rational Design of Therapeutic Peptides for Aminopeptidase N using a Substrate-Based Approach. *Sci. Rep.* **7,** 1424 (2017).

299. Hao, J. *et al.* Identification and rational redesign of peptide ligands to CRIP1, a novel biomarker for cancers. *PLoS Comput. Biol.* **4,** e1000138 (2008).

300. Xie, H. *et al.* Combining Peptide and DNA for Protein Assay: CRIP1 Detection for Breast Cancer Staging. *ACS Appl. Mater. Interfaces* **6,** 459–463 (2014).

301. Mi, Z. *et al.* Identification of a synovial fibroblast-specific protein transduction domain for delivery of apoptotic agents to hyperplastic synovium. *Mol. Ther.* **8,** 295–305 (2003).

302. Pi, Y. *et al.* Targeted delivery of non-viral vectors to cartilage in vivo using a chondrocyte-homing peptide identified by phage display. *Biomaterials* **32,** 6324–6332 (2011).

303. Hudziak, R. M. *et al.* p185HER2 monoclonal antibody has antiproliferative effects in vitro and sensitizes human breast tumor cells to tumor necrosis factor. *Mol. Cell. Biol.* **9,** 1165–72 (1989).

304. Garnock-Jones, K. P., Keating, G. M. & Scott, L. J. Trastuzumab. *Drugs* **70,** 215–239 (2010).

305. Ponta, H., Sherman, L. & Herrlich, P. a. CD44: from adhesion molecules to signalling regulators. *Nat. Rev. Mol. Cell Biol.* **4,** 33–45 (2003).

306. Tijink, B. M. *et al.* A Phase I Dose Escalation Study with Anti-CD44v6 Bivatuzumab Mertansine in Patients with Incurable Squamous Cell Carcinoma of the Head and Neck or Esophagus. *Clin. Cancer Res.* **12,** 6064–6072 (2006).

307. Clay, M. *et al.* Single marker identification of head and neck squamous cell carcinoma cancer stem cells with aldehyde dehyrdrogenase. *Head Neck* **32,** 1195–1201 (2010).

308. Chen, Y.-C. *et al.* Inhibition of tumorigenicity and enhancement of radiochemosensitivity in head and neck squamous cell cancer-derived ALDH1-positive cells by knockdown of Bmi-1. *Oral Oncol.* **46,** 158–165 (2010).

309. La Fleur, L., Johansson, A.-C. & Roberg, K. A CD44high/EGFRlow Subpopulation within Head and Neck Cancer Cell Lines Shows an Epithelial-Mesenchymal Transition Phenotype and Resistance to Treatment. *PLoS One* **7,** e44071 (2012).

310. Hakami, A. R., Ball, J. K. & Tarr, A. W. Non-ionic detergents facilitate non-specific binding of M13 bacteriophage to polystyrene surfaces. *J. Virol. Methods* **221,** 1–8 (2015).

311. TUPScan in SAROTUP suite. Available at: http://immunet.cn/sarotup/cgi-bin/TUPScan.pl. (Accessed: 8th September 2018)

312. Cheung, C. S. F. *et al.* A new approach to quantification of mAb aggregates using peptide affinity probes. *Sci. Rep.* **7,** 42497 (2017).

313. Yu, D. *et al.* Targeting Jurkat T Lymphocyte Leukemia Cells by an Engineered Interferon-Alpha Hybrid Molecule. *Cell. Physiol. Biochem.* **42,** 519–529 (2017).

314. Litvinov, S. V. *et al.* Epithelial Cell Adhesion Molecule (Ep-CAM) Modulates Cell–Cell Interactions Mediated by Classic Cadherins. *J. Cell Biol.* **139,** 1337–1348 (1997).

315. Mazia, D. Adhesion of cells to surfaces coated with polylysine. Applications to electron microscopy. *J. Cell Biol.* **66,** 198–200 (1975).

316. Miltenyi, S., Müller, W., Weichel, W. & Radbruch, A. High gradient magnetic cell separation with MACS. *Cytometry* **11,** 231–238 (1990).

317. Miltenyi Biotech. *StraightFrom ™ Whole Blood CD326 (EpCAM) MicroBeads human*. **326,** (2017).

318. The History of Dynabeads® and Biomagnetic Separation - UK. (2018). Available at: https://www.thermofisher.com/uk/en/home/brands/product-brand/dynal/the-

history-of-dynabeads.html. (Accessed: 8th September 2018)

319. Stemcell Technologies. EasySep™ Cell Separation. (2018). Available at: https://www.stemcell.com/products/brands/easysep-cell-separation.html#section-easysep-human. (Accessed: 20th August 2018)

320. Cusano, A. M. *et al.* Integration of binding peptide selection and multifunctional particles as tool-box for capture of soluble proteins in serum. *J. R. Soc. Interface* **11,** (2014).

321. McMullen, K. P., Chalmers, J. J., Lang, J. C., Kumar, P. & Jatana, K. R. Circulating tumor cells in head and neck cancer: A review. *World J. Otorhinolaryngol. - head neck Surg.* **2,** 109–116 (2016).

322. Saucedo-Zeni, N. *et al.* A novel method for the in vivo isolation of circulating tumor cells from peripheral blood of cancer patients using a functionalized and structured medical wire. *Int. J. Oncol.* **41,** 1241–50 (2012).

323. Gallerani, G., Cocchi, C., Bocchini, M., Piccinini, F. & Fabbri, F. Characterization of Tumor Cells Using a Medical Wire for Capturing Circulating Tumor Cells: A 3D Approach Based on Immunofluorescence and DNA FISH. *J. Vis. Exp.* 1–8 (2017). doi:10.3791/56936

324. Rugo, H., Brammer, M., Zhang, F. & Lalla, D. Effect of Trastuzumab on Health-Related Quality of Life in Patients With HER2-Positive Metastatic Breast Cancer: Data From Three Clinical Trials. *Clin. Breast Cancer* **10,** 288–293 (2010).

325. Stangelberger, A. *et al.* Targeted chemotherapy with cytotoxic bombesin analogue AN-215 inhibits growth of experimental human prostate cancers. *Int. J. Cancer* **118,** 222–229 (2006).

326. Baudino, T. Targeted Cancer Therapy: The Next Generation of Cancer Treatment. *Curr. Drug Discov. Technol.* **12,** 3–20 (2015).

327. Rao, W. *et al.* Chitosan-Decorated Doxorubicin-Encapsulated Nanoparticle Targets and Eliminates Tumor Reinitiating Cancer Stem-like Cells. *ACS Nano* **9,** 5725–5740 (2015).

328. Cwirla, S. E. *et al.* Peptide agonist of the thrombopoietin receptor as potent as the

natural cytokine. *Science* **276,** 1696–1699 (1997).

329. Baldwin, M. A. Protein identification by mass spectrometry: issues to be considered. *Mol. Cell. Proteomics* **3,** 1–9 (2004).

330. Kolker, E., Higdon, R. & Hogan, J. M. Protein identification and expression analysis using mass spectrometry. *Trends Microbiol.* **14,** 229–235 (2006).

331. Gold, M. H. Use of hyaluronic acid fillers for the treatment of the aging face. *Clin. Interv. Aging* **2,** 369–76 (2007).

332. Masuko, K., Murata, M., Yudoh, K., Kato, T. & Nakamura, H. Anti-inflammatory effects of hyaluronan in arthritis therapy: Not just for viscosity. *Int. J. Gen. Med.* **2,** 77–81 (2009).

333. Fan, X., Zhao, X., Qu, X. & Fang, J. *pH sensitive polymeric complex of cisplatin with hyaluronic acid exhibits tumor-targeted delivery and improved in vivoantitumor effect*. *International Journal of Pharmaceutics* (Elsevier B.V., 2015). doi:10.1016/j.ijpharm.2015.10.066

334. Itano, N. & Kimata, K. Mammalian Hyaluronan Synthases. *IUBMB Life* **54,** 195–199 (2002).

335. Camenisch, T. D. *et al.* Disruption of hyaluronan synthase-2 abrogates normal cardiac morphogenesis and hyaluronan-mediated transformation of epithelium to mesenchyme. *J. Clin. Invest.* **106,** 349–60 (2000).

336. Kobayashi, N. *et al.* Hyaluronan deficiency in tumor stroma impairs macrophage trafficking and tumor neovascularization. *Cancer Res.* **70,** 7073–83 (2010).

337. Bai, K.-J. *et al.* The Role of Hyaluronan Synthase 3 in Ventilator-induced Lung Injury. *Am. J. Respir. Crit. Care Med.* **172,** 92–98 (2005).

338. Itano, N. *et al.* Three Isoforms of Mammalian Hyaluronan Synthases Have Distinct Enzymatic Properties. *J. Biol. Chem.* **274,** 25085–25092 (1999).

339. Fallacara, A., Baldini, E., Manfredini, S. & Vertuani, S. Hyaluronic Acid in the Third Millennium. *Polymers (Basel).* **10,** 701 (2018).

340. Boeriu, C. G., Springer, J., Kooy, F. K., van den Broek, L. A. M. & Eggink, G.

Production Methods for Hyaluronan. *Int. J. Carbohydr. Chem.* 2013, 1–14 (2013).

341. Liu, L., Liu, Y., Li, J., Du, G. & Chen, J. Microbial production of hyaluronic acid: current state, challenges, and perspectives. *Microb. Cell Fact.* 10, 99 (2011).

342. Sheng, J. Z. *et al.* Use of induction promoters to regulate hyaluronan synthase and UDP-glucose-6-dehydrogenase of *Streptococcus zooepidemicus* expression in *Lactococcus lactis* : a case study of the regulation mechanism of hyaluronic acid polymer. *J. Appl. Microbiol.* 107, 136–144 (2009).

343. Jing, W. & De Angelis, P. L. Dissection of the two transferase activities of the Pasteurella multocida hyaluronan synthase: Two active sites exist in one polypeptide. *Glycobiology* 10, 883–889 (2000).

344. Jing, W. & DeAngelis, P. L. Synchronized Chemoenzymatic Synthesis of Monodisperse Hyaluronan Polymers. *J. Biol. Chem.* 279, 42345–42349 (2004).

345. Sze, J. H., Brownlie, J. C. & Love, C. A. Biotechnological production of hyaluronic acid: a mini review. *3 Biotech* 6, 67 (2016).

346. Wong, C.-H. Mimics of Complex Carbohydrates Recognized by Receptors. *Acc. Chem. Res.* 32, 376–385 (1999).

347. Kuo, T. Y., Chien, L. A., Chang, Y. C., Liou, S. Y. & Chang, C. C. Synthetic mimics of carbohydrate-based anticancer vaccines: Preparation of carbohydrate polymers bearing unimolecular trivalent carbohydrate ligands by controlled living radical polymerization. *RSC Adv.* (2014). doi:10.1039/c4ra04907a

348. Kiessling, L. L. & Grim, J. C. Glycopolymer probes of signal transduction. *Chem. Soc. Rev.* 42, 4476 (2013).

349. Iyer, S., Rele, S., Grasa, G., Nolan, S. & Chaikof, E. L. Synthesis of a hyaluronan neoglycopolymer by ring-opening metathesis polymerizationElectronic supplementary information (ESI) available: spectral data for compound 11, glycomonomer 14 and glycopolymer [A]. See http://www.rsc.org/suppdata/cc/b3/b301734f/. *Chem. Commun.* 1518 (2003). doi:10.1039/b301734f

350. Sletten, E. T., Loka, R. S., Yu, F. & Nguyen, H. M. Glycosidase Inhibition by

Multivalent Presentation of Heparan Sulfate Saccharides on Bottlebrush Polymers. *Biomacromolecules* **18,** 3387–3399 (2017).

351. *Global Hyaluronic Acid (HA) Raw Material Market 2017-2025: FDA-Approved Hyaluronic Acid-Based Viscosupplements Such as ORTHOVISC and MONOVISC is Expected to Boost Usage Over the Next 8 Years - Research and Markets*. (2017).

352. Kolb, H. C., Finn, M. G. & Sharpless, K. B. Click Chemistry: Diverse Chemical Function from a Few Good Reactions. *Angew. Chemie Int. Ed.* **40,** 2004–2021 (2001).

353. Shiina, M. & Bourguignon, L. Y. W. Selective Activation of Cancer Stem Cells by Size-Specific Hyaluronan in Head and Neck Cancer. *Int. J. Cell Biol.* **2015,** 1–10 (2015).

354. Wang, S. J. & Bourguignon, L. Y. W. Role of hyaluronan-mediated CD44 signaling in head and neck squamous cell carcinoma progression and chemoresistance. *Am. J. Pathol.* **178,** 956–63 (2011).

355. Johnson, S., Chen, H. & Lo, P.-K. In vitro Tumorsphere Formation Assays. *Bio-protocol* **3,** (2013).

356. Cao, L. *et al.* Sphere-forming cell subpopulations with cancer stem cell properties in human hepatoma cell lines. *BMC Gastroenterol.* **11,** 71 (2011).

357. Lo, P.-K. *et al.* CD49f and CD61 identify Her2/neu-induced mammary tumor-initiating cells that are potentially derived from luminal progenitors and maintained by the integrin-TGFβ signaling. *Oncogene* **31,** 2614–26 (2012).

358. Bourguignon, L. Y. W., Wong, G., Earle, C. & Chen, L. Hyaluronan-CD44v3 interaction with Oct4-Sox2-Nanog promotes miR-302 expression leading to self-renewal, clonal formation, and cisplatin resistance in cancer stem cells from head and neck squamous cell carcinoma. *J. Biol. Chem.* **287,** 32800–32824 (2012).

359. Horton, M. R., Shapiro, S., Bao, C., Lowenstein, C. J. & Noble, P. W. Induction and regulation of macrophage metalloelastase by hyaluronan fragments in mouse macrophages. *J. Immunol.* **162,** 4171–6 (1999).

360. Ohno, S., Im, H.-J., Knudson, C. B. & Knudson, W. Hyaluronan oligosaccharides induce matrix metalloproteinase 13 via transcriptional activation of NFkappaB and

p38 MAP kinase in articular chondrocytes. *J. Biol. Chem.* **281,** 17952–60 (2006).